Design and development of a 3D-printed electrochemical sensor for the detection of *Pseudomonas aeruginosa*

A thesis submitted in fulfilment of the requirements for the degree of

Doctor of Engineering in Medical Devices

Caitlin McLean BEng (Hons)

Supervisors:

Dr. Lynn Dennany

Dr. James Windmill

Centre for Doctoral Training in Medical Devices & Health Technologies

Department of Biomedical Engineering

University of Strathclyde 2022

This thesis is the result of the author's original research. It has been composed by the author and has not been previously submitted for examination which has led to the award of a degree.

Signed: 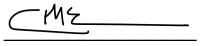

Date: 9th August 2022

Acknowledgements

I would like to extend my deepest gratitude to the following, without whom this thesis would not exist:

Lynn, for always being there, and for creating such a supportive environment within your research team.

James, for your invaluable help and advice. Talking with you put my mind at ease.

Mr Dow, Mr Gallagher, Mr Abercrombie, and Ms Bell, for nurturing my passion for science.

Gemma, for all our conversations. Our almost daily check-ins have kept me sane, as has studying alongside you for the past eight years.

Kelly, for keeping our lab running even when it seemed impossible, and forever assisting everyone in the group with their work. Your upbeat attitude has made all the difference, especially in the past few months.

Ben, Andy, Julien, Rolan and Chris, for helping me in the labs and answering my many questions. Without your help, my progress would have been truly glacial.

Callum, for your kindness and valuable contribution to the project.

My parents, for your unwavering support throughout my education.

My family; the McLeans and the McCluckies, for showing an interest in my work and keeping my feet on the ground. I am lucky to have you all.

Scott, for everything.

Abstract

Pseudomonas aeruginosa (*P. aeruginosa*) is a frequent cause of nosocomial infection, which can lead to significant morbidity and mortality. Its early detection is vital for effective treatment before the bacterium can develop antibiotic resistance. Current detection methods are often time consuming, costly, or require experienced personnel. There is a clear need for the development of a rapid and sensitive sensing platform for the detection of *P. aeruginosa*. Additive manufacturing may be the key to overcoming the issues faced by current detection methods. Methods such as digital light processing (DLP) are cost effective, produce little to no waste, and facilitate expeditious prototyping. This work details the initial stages of developing a 3D printed electrochemical sensor for the detection of *P. aeruginosa.* The initial sensor design incorporated multi-walled carbon nanotubes (MWCNT) and was successful in detecting pyocyanin (PyoC), a *P. aeruginosa* virulence factor, at clinically relevant concentrations. This study achieved a linear response across the clinically relevant range of 0 – 100 μM, with a limit of detection (LOD) of 2.5 μM. PyoC detection was also achieved in human serum. Further sensor designs were then explored, considering facile manufacture and operation. The goal was to produce a point-of-care sensor that can detect analytes rapidly and sensitively, with no need for sample pretreatment. As well as printing MWCNT composites using DLP, carbon black (CB) resins were successfully photopolymerised onto glassy carbon (GC) electrodes for their initial assessment. These electrodes were used to study the electrochemical detection of gentamicin (GN). A linear response was achieved from 25 – 200 μg/mL. The insights gleaned in the exploration of conductive, photopolymerisable resins are valuable in terms of expanding rapid, cost-effective electrode manufacture. Overall, these studies

provide proof of concept regarding 3D printed electrochemical sensors and explore the feasibility of utilising conductive additives to successfully manufacture electrodes.

Publications and Presentations

McLean, C., Tiller, B., Mansour, R., Brown, K., Windmill, J., Dennany, L. (2022) Characterising the response of novel 3D printed CNT electrodes to the virulence factor pyocyanin. Journal of Electroanalytical Chemistry 909, 116149. ISSN 1572-6657.

This paper is presented within Chapter 3 of this thesis.

Lynn Dennany and James Windmill undertook the initial conceptualisation of this research and oversaw the supervision of the research team. Caitlin McLean and Kelly Brown conducted the research investigation, with Kelly Brown carrying out the work described in Section 3.4.4. All authors contributed to the interpretation of data, preparation, review and editing of the presented research.

McLean, C., Brown, K., Windmill, J., Dennany, L. (2022) Innovations in point-of-care electrochemical detection of *Pseudomonas Aeruginosa*. Journal of Electroanalytical Chemistry. *Under editorial review as of April 2022.*

This paper is presented within Chapter 1 of this thesis.

RSC 7th Analytical Biosciences ECRM, University of Strathclyde, 5-6 March 2020. *Poster Presentation*.

RSC Twitter Poster Conference, Online Meeting, 3 March 2020. *Poster Presentation.*

BioMedEng19, Imperial College London, 5-6 September 2019. *Poster Presentation.*

Electrochem 19, University of Strathclyde, 26-28 August 2019. *Poster Presentation.*

Abbreviations

3D	Three-dimensional
PyoC	Pyocyanin
PyoV	Pyoverdine
SEM	Scanning electron microscope
HCAI	Healthcare-associated infection
P. aeruginosa	Pseudomonas aeruginosa
SWV	Square wave voltammetry
RSD	Relative standard deviation
ROS	Reactive oxygen species
PCR	Polymerase chain reaction
QS	Quorum sensing
LOD	Limit of detection
DNA	Deoxyribonucleic acid
RNA	Ribonucleic acid
ΔE_p	Peak-to-peak separation
AMR	Antimicrobial resistance
NP	Nanoparticle
HOMO	Highest occupied molecular orbital
LUMO	Lowest unoccupied molecular orbital
ESA	Electrochemical sensor array
$OH^{\cdot}$	Hydroxyl radical
O_{2^-}	Superoxide

H_2O_2	Hydrogen peroxide
AM	Additive Manufacturing
CAD	Computer Aided Design
CAM-LEM	Computer Aided Manufacturing of Laminated Engineering Materials
CB	Carbon black
CBAM	Composite Based Additive Manufacturing
CDLP	Continuous Digital Light Processing
CE	Counter electrode
CV	Cyclic voltammetry
CVD	Chemical Vapour Deposition
DED	Directed Energy Deposition
DIW	Direct Ink Writing
DLP	Digital Light Processing
DMLS	Direct Metal Laser Sintering
DPV	Differential pulse voltammetry
E	Potential
FDM	Fused Deposition Modelling
GC	Glassy carbon
GN	Gentamicin
GO	Graphene oxide
LOM	Laminated Object Manufacturing
MW	Molecular weight
PBF	Powder Bed Fusion

PEGDA	Poly(ethylene glycol) diacrylate
PSL	Plastic Sheet Lamination
RE	Reference electrode
SDL	Selective Deposition Lamination
SLA	Stereolithography
SLCOM	Selective Lamination Composite Object Manufacturing
SLM	Selective Laser Melting
SLS	Selective Laser Sintering
SPE	Screen-printed electrode
SW/MWCNT	Single-/Multi-walled carbon nanotube
UAM	Ultrasonic Additive Manufacturing
UV	Ultraviolet
WE	Working electrode

Table of Contents

Chapter 3 Experimental Methods

Chapter 4 Characterising the Response of Novel 3D printed CNT Electrodes to the Virulence Factor Pyocyanin

CHAPTER ONE

INTRODUCTION AND LITERATURE REVIEW

1.1. Nosocomial Infection

Nosocomial, or healthcare-associated infections (HCAIs) are defined by the World Health Organisation (WHO) as: "An infection acquired in hospital by a patient who was admitted for a reason other than that infection" [1, 2] or "An infection occurring in a patient in a hospital or other health care facility in whom the infection was not present or incubating at the time of admission, [including] infections acquired in the hospital but appearing after discharge [or] occupational infections among staff of the facility". [3] HCAIs are prevalent; the WHO has evaluated that around 15 % of hospitalised patients will suffer from a HCAI. [4] High income countries see an incidence of 3.5 – 12 % and middle- and low-income countries, an incidence of 5.7 – 19.1 %. [5] With an estimated 1.4 million people suffering from HCAI-related complications globally at any one time, and 8.9 million HCAIs estimated to occur annually within European hospitals and long-term care facilities (LTCFs), HCAIs can be considered a global health crisis. [6] Additionally, HCAIs are the cause of 4 – 56 % of all deaths in neonates. [5] Patients in intensive care are particularly susceptible, as their immune system is compromised and infection risk is higher; a study on the Extended Prevalence of Infection in Intensive Care (EPIC II) stated that incidence in the intensive care unit (ICU) may reach as high as 51 %. [7] Prolonged hospital stays and erroneous treatment with broad-spectrum antibiotics also heighten HCAI risk. [5]

HCAIs extend hospitalisation, which is the most significant contributor to the considerable economic burden they cause. [8-10] Use of additional hospital resources and equipment create an imbalance within the healthcare system, which sees funds going towards treating potentially preventable conditions. [4] Coello *et al*. demonstrated that,

for patients with surgical wound infections, hospitalisation length was increased by circa 8.2 days. [11] During hospital stays, patients are at risk of developing HCAIs due to factors such as proximity to hospital staff and infected patients, as well as lack of hygiene and deficient waste disposal techniques. Lengthy hospital stays may result in disability and increased antimicrobial resistance (AMR), leading to a higher death rate. HCAIs are a leading cause of mortality. [12] Figure 1.1 highlights the burden of some of the most prevalent HCAIs. [5, 13-22]

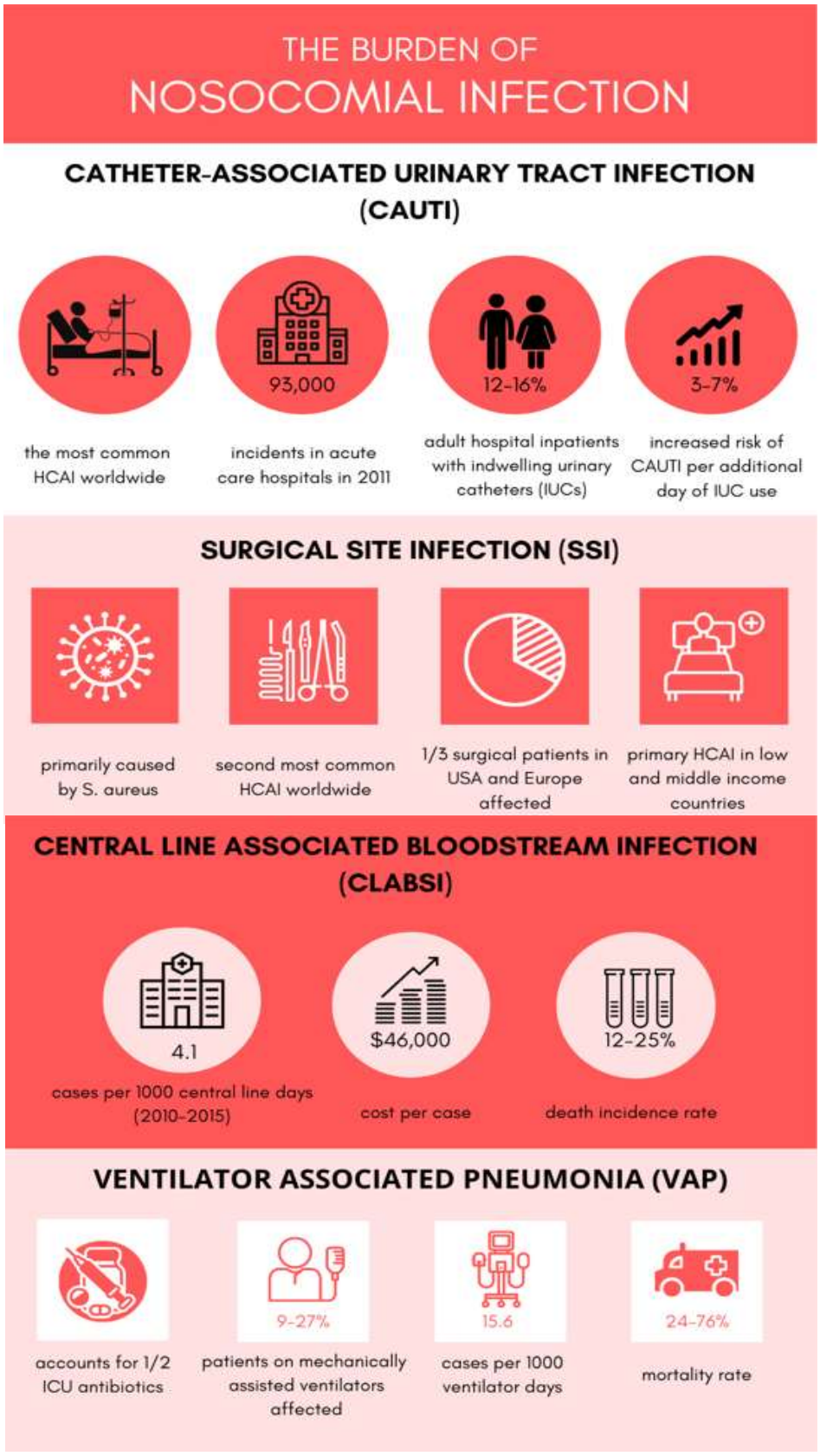

Figure 1.1: Morbidity and mortality regarding the most prevalent nosocomial infections

Nosocomial pathogens comprise bacteria, viruses, protozoans and fungal parasites, though bacteria are most prevalent, constituting approximately 90 % of infections. [5, 22] Common agents contributing to HCAIs include enterococci, *Streptococcus spp*., *S. aureus*, *Klebsiella pneumonia (K. pneumonia)*, *Escherichia coli (E. coli)* and *Pseudomonas aeruginosa (P. aeruginosa)*. [23] *P. aeruginosa, S. aureus* and *E. coli* have a particularly prominent role. [24] Gram-negative bacteria such as *Pseudomonas spp*. thrive in a clinical environment as they tend to be isolated in water. Thus, there is a risk that they may colonise a patient's digestive tract. Multi-resistant *Klebsiella* and *P. aeruginosa* are prevalent in clinical environments; especially in developing countries due to reduced availability of, or funding for, costly second-line antibiotics. [25]

Previously effective drugs are becoming ineffectual as more drug-resistant organisms develop. [26] Resistance has increased largely due to prolonged or incorrect use of antibiotics, as well as self-medication. [5] Antibiotic use causes selection and exchange of genetic resistance elements, which increasingly results in the emergence of multidrug resistant strains of bacteria. Microorganisms which are sensitive to the drug become suppressed, whilst resistant strains thrive and are likely to spread within a hospital setting. There are several strains of staphylococci, enterococci, pneumococci, and tuberculosis which have now developed a resistance to many or all once-effective antimicrobials. [2] High worldwide incidence rates of HCAIs are caused by bacteria with a high resistance, such as methicillin-resistant *Staphylococcus aureus* (MRSA) or multidrug-resistant Gram-negative bacteria. Urli *et al*. studied 178 patients admitted to the ICU for 48 hours or more and found that *S. aureus* and *P. aeruginosa* were amongst the most frequently isolated pathogens, with 68 % of *S. aureus* displaying methicillin-resistance and 76 % of *P. aeruginosa* exhibiting antibiotic resistance.

These were also the most frequently isolated bacteria in cases of late onset pneumonia, (*S. aureus*, 44 %; *P. aeruginosa*, 37 %). AMR was higher than predicted in 75 % of isolated strains. [27]

This review aims to compare a number of electrochemical sensors for the detection of *P. aeruginosa*, by exploiting the redox activity associated with one of its virulence factors, pyocyanin (PyoC). A comprehensive overview of different sensor types is provided, along with their benefits and limitations regarding point-of-care PyoC detection. The potential for new research within this field is also explored.

1.2. Pseudomonas aeruginosa

P. aeruginosa is an opportunistic pathogen which frequently causes severe nosocomial infection, resulting in high mortality rates. [28-36] It is the fourth most common bacteria responsible for hospital acquired infections in Europe. [37] From 2016 – 2017, such infections cost the NHS in the region of £2.1 billion. [38] The most prevalent bacterial strains are highlighted in Table 1.1.

Table 1.1: Ten most frequently isolated bacteria (of 604 studied) in long-term care facilities (LTCFs). [37]

Bacteria	Frequency of isolation (%)
Escherichia coli	34.4
Staphylococcus aureus	10.2
Proteus mirabilis	8.1
Pseudomonas aeruginosa	**6.8**
Klebsiella pneumoniae	6.7
Clostridium difficile	5.0
Enterococcus faecalis	3.1
Providencia species	2.5
Morganella species	1.5
Acinetobacter baumannii	1.3

The gram-negative bacterium tends to find success amongst patients whose immune systems are compromised [39] and is considered the most perturbing bacteria in cystic fibrosis (CF) lung infections, as well as blood stream and chronic surgical/burn wound infections. Amongst CF patients, 80 % will suffer a *P. aeruginosa* infection at some point in their lives. [40] These infections tend to be highly inflammatory as they progress, leading to death in over 90 % of infected CF patients. [41] Immune compromised patients are at high risk of developing sepsis, ventilator associated pneumonia (VAP), urinary tract infection (UTI) and surgical site infection (SSI), to which *P. aeruginosa* is a key contributor. [42] In these cases, mortality rates may reach as high as 76 %, depending on which pathogens are prevalent. [40] The presence of *P. aeruginosa* is known to

contribute to the delay of healing in chronic wounds. Wolcott *et al.* and Hogsberg *et al.* stated that for patients receiving split thickness skin grafts to treat chronic leg ulcers, *P. aeruginosa* presence acted as a predictor of skin graft outcome. [43, 44]

Increasingly, *P. aeruginosa* has displayed inherited and acquired resistances to many antibiotics. [28, 31-34] Efforts have been made by the Centres for Disease Control and Prevention (CDC) and the Infectious Diseases Society of America (IDSA) to stem the spread of drug-resistant pathogens via diagnosis and monitoring, with an aim to minimise the spread of antibiotic resistant strains. [45] Early *P. aeruginosa* detection is vital for successful treatment, whilst the bacteria can still be treated successfully with antibiotics, though this has proven difficult due to a lack of sensitive detection methods at this stage. [46, 47]

As previously stated, *P. aeruginosa* is a gram-negative bacterium, whose outer membrane contains Protein F (OprF), which behaves as a porin, reducing permeability and endowing the microbe with a high antibiotic resistance. [48] This is in contrast with gram-positive bacteria, which are multi-layered and more susceptible to antibiotics. To facilitate movement and display chemotaxis, *P. aeruginosa* utilises a single flagellum, which also attaches to host tissues and promotes invasion during the early stages of infection. [49] Type IV pili, [50] polar filaments comprised of homopolymers from pilin, [51] endow *P. aeruginosa* with the ability to bind to mucosal surfaces and epithelial cells. Figure 1.2 (a) shows a scanning electron microscope (SEM) image of *P. aeruginosa*, whilst Figure 1.2 (b) depicts a computer-generated image of *P. aeruginosa*, based on SEM imaging.

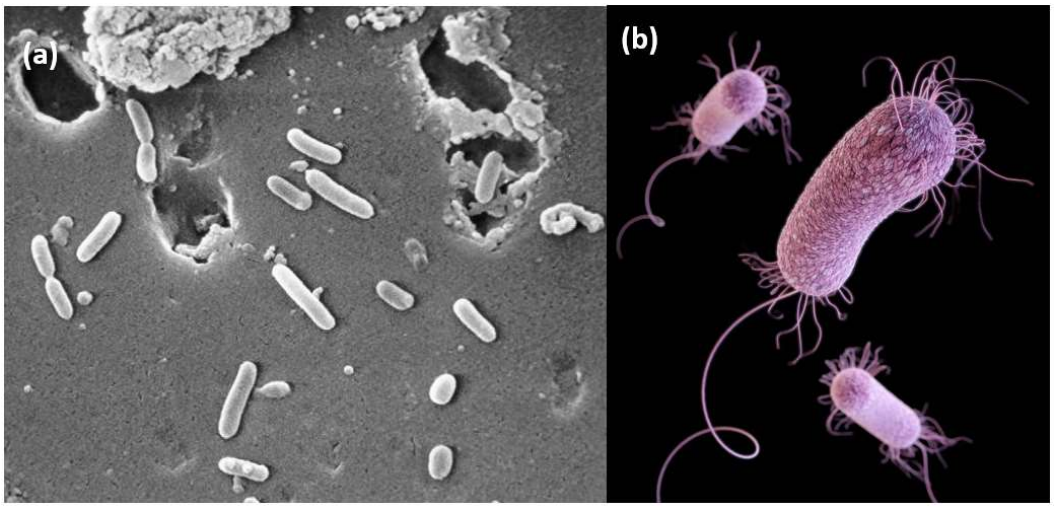

Figure 1.2: SEM image of P. aeruginosa [52] (b) 3D computer-generated image of P. aeruginosa bacteria [53] P. aeruginosa is characterised as a rod-shaped, monoflagellated bacterium of 1 - 5 µm in length and 0.5 - 1.0 µm in width. [54]

1.2.1. *P. aeruginosa* biofilms

Biofilms have been defined as a mucilaginous accumulation of bacteria, suspended in an extracellular polymeric substance (EPS) matrix. [55-57] Often, biofilms will irreversibly attach to a surface, with particular success at a solid-liquid interface. [55] Their tenacity within a clinical environment derives from the use of implantable medical devices, which are associated with 60 – 70 % of HCAIs. [58] Antibiotic treatment of biofilm infections can reverse symptoms which are caused by the expulsion of planktonic cells but cannot kill the biofilm itself. [59] Therefore, symptoms are capable of recurring, rendering surgical intervention necessary. [60]

Biofilms may be readily produced by *P. aeruginosa*, greatly contributing to its pathogenicity. [61] Whilst other bacteria establish biofilms through cell division, [57] *P. aeruginosa* form microcolonies, using type IV pili to facilitate congregation. [62-64] The immune response of the host is subdued, furthering the progression of infection and

limiting antibiotic efficacy. [60] PyoC is also known to be linked to biofilm formation. [65, 66]

1.2.2. Pyocyanin

PyoC is the redox-active virulence factor produced by *P. aeruginosa,* which also acts as a quorum sensing (QS) molecule for the pathogen. QS describes the process by which bacteria control gene expression, via cell-to-cell communication, in response to fluctuations in cell-population density. [67, 68] Chemical signalling molecules, known as autoinducers, are produced and released by QS bacteria, and accumulate as a function of cell density. [67] The bacteria can then monitor the number of autoinducers being produced, and alter gene expression accordingly. [68] QS enables individual bacteria to carry out a range of functions, such as virulence and biofilm formation. [69]

Several studies have confirmed the exclusive secretion of PyoC by *P. aeruginosa,* which uniquely carries the protein-encoding genes required for its synthesis. [70-74]

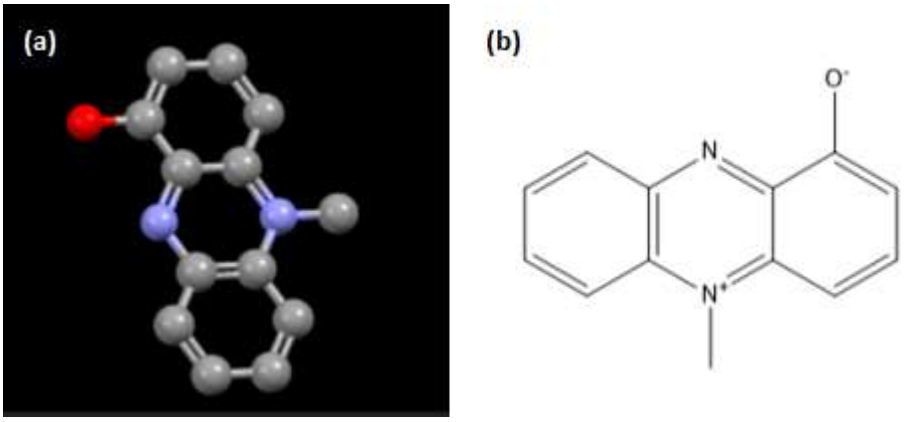

Figure 1.3: (a) 3D and (b) 2D representations of pyocyanin.

PyoC has the molecular formula $C_{13}H_{10}N_2O$ and may exist in one of three states: oxidised, monovalently reduced or divalently reduced. [75] The redox activity of PyoC endows it with the ability to act as an electron shuttle, disrupting the redox homeostasis of host cells by relieving them of electrons which are then donated to oxygen (O_2), causing generation of reactive oxygen species (ROS) such as superoxide (O_2-) and hydrogen peroxide (H_2O_2). This results in cell damage and death. [76] Whilst PyoC has oxidative effects on other organisms such as *E.coli*, *P. aeruginosa* itself appears immune to this, due to limited redox-cycling. [77]

QS, which occurs during wound colonisation, allows the bacteria to intuitively control gene expression, thus controlling virulence. Bacterial virulence is increased, and host physiology is damaged, contributing to an increased risk of infection. It has been reported that QS results in PyoC being synthesised by 96 – 98 % of *P. aeruginosa* strains. [78, 79] All *P. aeruginosa* isolates studied by Sismaet *et al*. produced measurable concentrations of PyoC, with increasing severity of symptoms and cases of comorbidity as PyoC concentrations rose. [34] Reimer *et al*. stated that *P. aeruginosa* pulmonary infections may produce sputum samples containing up to 130 μM of PyoC, whilst this value can be in the mM range for ear infection secretions. [80] PyoC shows promise as a diagnostic biomarker for *P. aeruginosa* infection, enabling rapid identification of nosocomial infections involving the pathogen. [71-73, 81]

Biosynthesis and redox activity

PyoC is known to be extremely pathogenic, causing inflammatory physiological effects to host tissue which leads to infection amplification and comorbidity. [34, 82] Sharp *et al.* highlighted the progression of infection as follows: [65, 78, 83, 84]

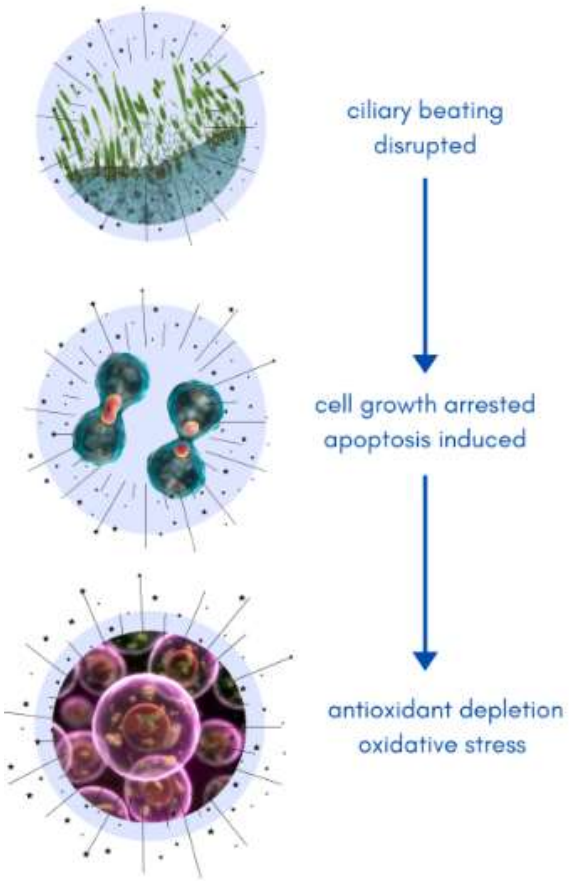

Figure 1.4: Progression of P. aeruginosa infection.

Ciliary dysfunction impairs mucociliary clearance, a vital line of defence for the lungs, [85] and causes chronic nose, ear, sinus and chest problems. [86-88] Low concentrations of PyoC induce cellular senescence, with apoptosis occurring at higher concentrations. Inhibition of cell growth and replication impedes tissue repair and advances morbidity and mortality. [84] Antioxidant depletion results in the formation of free radicals, which, in turn, leads to oxidative stress. [89] Furthermore, the immune response of the host is attenuated and the switch from acute to chronic infection is promoted. [90]

Oxidative Stress

Oxidative stress is defined as an imbalance between free radical production and antioxidant defences. [89] The term 'free radical' references any chemical species with a single unpaired electron in its outer valence shell. [91] An imbalance infers increased chemical activity, which may lead to tissue injury. [89] The instability of free radicals leads to their high reactivity. They tend to react with nonradicals, as they are much more abundant within the human body. Possible targets include all biological macromolecules, proteins, lipids, nucleic acids, and carbohydrates. [91]

When a radical reacts with a nonradical, a free radical chain reaction is initiated. New radicals are formed, which may go on to react with other macromolecules. Prominent examples of this are protein damage and lipid peroxidation. The hydroxyl radical ($OH^{\cdot}$) is understood as the most potent oxidant and displays an extremely short half-life. It can attack most biological molecules and initiate the propagation of free radical chain reactions. Oxygen may accept an electron to form O_2-, which in itself is not particularly reactive. Its oxidative potential is weak; it is much more successful at reducing iron complexes (e.g., cytochrome C). However, it can dismutase to form H_2O_2, [84] a means by which PyoC has induced oxidative stress in both epithelial [92] and endothelial cells. [93]

Mohamed *et al.* studied the effects of oxidative stress on *P. aeruginosa* in mice. The susceptibility of *P. aeruginosa* to various antibiotics was altered upon exposure to H_2O_2, with minimum inhibitory concentrations (MICs) either increasing or decreasing. QS genes were found to be expressed at a significantly lower level in H_2O_2-stressed

cells. Overall, exposure to oxidative stress reduced *P. aeruginosa* pathogenicity in the host. [94] Previous studies had reported an increase in *P. aeruginosa* host virulence in response to oxidative stress; [65, 95] however, this was likely due to experimental differences. [94] It is also important to consider that bacterial defences may be increased by low levels of oxidative stress, whilst increasing levels can markedly damage bacterial cells, due to excessive ROS production, according to the hierarchical oxidative stress model. [96]

PyoC has been shown to contribute to the unusual tenacity of *P. aeruginosa* infections. [65] PyoC-associated ROS have been linked to cellular phenomena which enhance *P. aeruginosa's* capacity for survival. [97] *P. aeruginosa* pathology is also increased by weakening of host defences, via depression of mucociliary transport [98, 99] and the initiation of bronchoconstriction if nebulized into the airways. [100]

Considerable antioxidant defence mechanisms are in place which act to protect the body from free radical attack. Gutteridge described an antioxidant as "any substance that, when present at low concentrations, compared with those of the oxidizable substrate, considerably delays or inhibits oxidation of the substrate." Catalase, dismutase and peroxidase enzymes are key cellular antioxidant defences. [101] Furthermore, the ability of mitochondrial cytochrome oxidase to act as a catalyst in the electron transport chain (ETC) without the release of ROS greatly decreases potential for intracellular production of free radicals. [102]

PyoC biosynthesis

PyoC is biosynthesized from phenazine-1-carboxylate, as described in Scheme 1.1. 5-methyl-phenazine-1-carboxylate is an unstable intermediate, whose reactive nature

facilitates the two-step conversion of phenazine-1-carboxylate to PyoC. This process is regulated by PhzM and PhzS , which are protein-encoding genes. [103, 104]

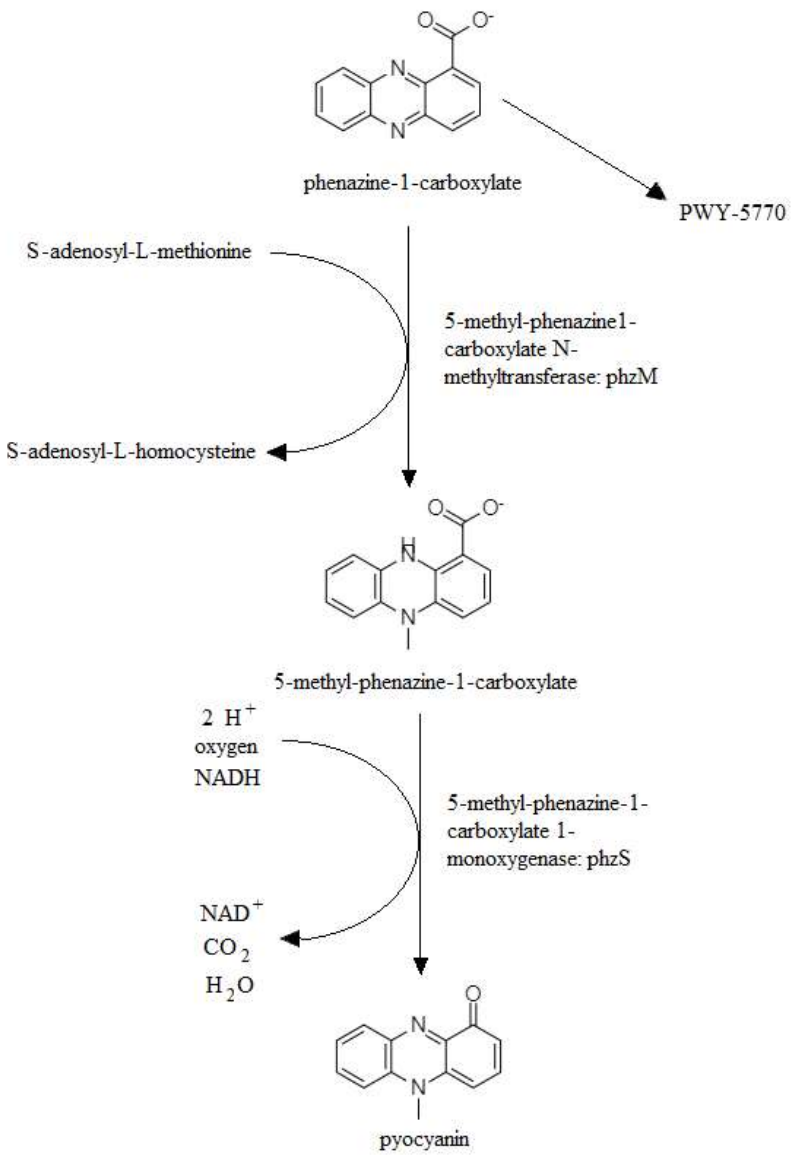

Scheme 1.1: Pyocyanin biosynthesis pathway. Adapted from Fulcher, 2010. [103]

The toxicity of PyoC can be largely attributed to its redox activity, which causes depletion of cellular antioxidants such as NADH and glutathione. [105] It also modifies cytosolic concentration of calcium, causing disruption of ion transport regulation,

ciliary beating, and mucus secretion by airway epithelial cells. [106] The mechanisms by which PyoC initiates pathogenesis are variable. It may inhibit nitric oxide synthase [107-109] or form a complex to interact with endothelium-derived relaxing factor or nitric oxide (NO). NO is vital for blood flow and blood pressure control, as well as immune function. [110] PyoC also inhibits epidermal cell growth [111] and lymphocyte proliferation, [112] has antibiotic properties against other microorganisms, [113] and influences the acquisition of iron by pseudomonads. [114]

P. aeruginosa-derived phenazines may also prompt alveolar macrophages to produce interleukin-8 (IL-8) and leukotriene B4. These are known as neutrophil chemotaxins; they populate the airways with neutrophils, inciting an inflammatory response and neutrophil-mediated tissue damage. [115, 116] Phenazines are thought to boast such a broad range of biological activity due to their ability to undergo redox cycling in the presence of molecular oxygen and reducing agents. This causes a build-up of toxic O_2- and H_2O_2 and ultimately leads to oxidative cell injury or death. [117-119] PyoC can also act synergistically with pyochelin, a siderophore, and with transferrin cleaved by *P. aeruginosa* or neutrophil-secreted proteases in infected lungs. This catalyses the formation of $OH^{\cdot}$, a highly cytotoxic agent which causes damage to pulmonary endothelial cells. [117, 119]

1.3. Detection methods

1.3.1. Introduction

Given the swift progression of *P. aeruginosa* infections, rapid detection *in situ* is vital for efficacy of treatment. Current bacterial identification methods usually take 24 hours or more; whilst newer molecular and biochemical identification methods

improve upon this delay, they require a sufficient number of cells for investigation, thus requiring an incubation period of several hours. [120] Some clinics may be able to utilise polymerase chain reaction (PCR) identification, which can give quantitative results and takes less time (1 hour +). This technique requires extensive preparation of samples, as well as expensive reagents, which contribute to its limited clinical availability. [121] Processing also takes several hours, deeming this technique inadequate regarding a point-of-care clinical setting. [61] Absorbance and spectroscopic methods provide robust results; however, their operation is complicated. PyoC must be extracted from samples using chloroform and then purified, which requires trained technicians and the use of hazardous solvents. The need for extensive sample preparation also contributes to longer detection times. [121] Liquid chromatography-mass spectrometry (LC-MS) can produce quantitatively reliable results; however, expansive instrumentation is required, as is supernatant extraction from the growth medium. [47] Microbiological colony identification is also common, though it has low sensitivity and requires the use of costly equipment and reagents. Additionally, the process is laborious, increasing time and labour costs. [122] Automated instrumentation techniques call for plate culture preparation to obtain a bacterial colony. This incurs a lead time of a minimum 18 – 24 hours. [123, 124] Currently, there is a clear need for the development of a simple, sensitive PyoC detection method. Results must be achieved rapidly and in a cost-effective manner, without any need for pretreatment or sample incubation.

Electrochemical methods may help to bridge this gap (See Table 1.2). Increasingly, the electroactive nature of PyoC has been exploited to enable electrochemical detection methods which do not require sensor functionalisation. [121] Various studies have utilised PyoC as a *P. aeruginosa* biomarker due to its redox activity. [34, 61, 78, 81, 104, 121, 125-130] Its excellent electrochemical activity, due to its substituted phenazine structure, makes the toxin especially applicable for detection using cyclic voltammetry (CV). [131] The electrochemical signals produced may also be amplified using redox activation (altering environmental parameters such as pH, causing the analyte to be dominant in its redox active form), or redox cycling, which would enable ultrasensitive detection of diagnostic biomarkers. [132] Figure 1.5 provides an overview of the current infection detection pathway, which can be compared to that which may be achieved with electrochemical sensing (Figure 1.6).

Table 1.2: Summary of electrochemical methods for the detection of P. aeruginosa

Detection Method(s)	Electrode Material	Target Analyte(s)	Detection Range	Limit of Detection	Ref
SWV	Carbon	PyoC	0.6 - 41.3 µM	N/A	34
SWV	Carbon	PyoC	N/A	N/A	61
CV, SWV	Agar hydrogel & Au/Ag nanoalloy-modified carbon	PyoC	0.12 - 25 µM	0.04 µM	104
SWV	Carbon	PyoC, PyoV	0.01 - 0.1 µM, 5 - 50 µM	2.12 µA/µM, 1.09 nA/µM	126
EC-SERS, CV, SWV	Au	PyoC	100 µM, 500 µM	N/A	127
CV	Au	PyoC	2 - 100 µM	2 µM	81
CV, DPV, EIS	Au NP-modified graphite	PyoV	0.5 - 100 µM	66.90 µM	140
CV, DPV, EIS	Au NP-modified graphite	PyoV	1 – 100 μML^{-1}	333.33 nML^{-1}	141
CV	Carbon	2-AA	0 - 60 mM	7.6 mM	142
CV, SWV	CS/AuNP-, T-Macro-modified carbon	PyoC	1 - 100 µM, 0.75 - 25 µM	1.6 µM, 0.75 µM	130
Amperometry	Au	*P. aeruginosa*	N/A	N/A	153
Impedance measurements	Au	*P. aeruginosa*	10^2 - 10^5 CFU/mL	N/A	154
CV	Au	PAP	0 - 50 µM	10 pM	143

SWV	Carbon	PyoC, 5-MCA, OHPHZ	0 - 200 µM	N/A	144
SWV, CV	Transparent carbon	PyoC, 5-MCA, OHPHZ	1- 250 µM	N/A	145
CV	Polyaniline/AuNPs decorated ITO	PyoC	1.9 - 238 µM	500 nM	128, 129
CV	AuNP-modified chromium/ITO	*P. aeruginosa*	10 - 10^5 CFU/mL	10 CFU/mL	161
CV	AuNPs/rGO	PyoC	1 - 100 µM	0.27 µM (PBS), 1.34 µM (saliva), 2.3 µM (urine)	162
CV, DPV	Super P/AuNP-modified Cu-ZrMOF	*P. aeruginosa*	10-10^6 CFU mL^{-1}	2 CFU mL^{-1}	164
CV, SWV	Ti/Au-modified nanograss	PyoC	0 - 25 µM	172 nM	125
CV, LSV	CCLP/Au CP-modified GC	HQ, H_2O_2, IgG HRP	10^1 - 10^7 CFU/mL	9×10^2 CFU/mL	166
CV, SWV	PA/CNT	PyoC	0.10 - 100 μML^{-1}	0.10 μML^{-1}	167
SWV	Streptavidin-HRP-modified Au	16S rRNA	0.3 - 600 pg/µL	0.012 pg/µL	191
SWV	Au	PyoC, PCA	0 - 10 µM, 0 - 300 µM	2.6 µM	192
SWV	Pt	PyoC	0 - 200 µM	0.6 µM	193
SECM	Pt	PyoC	N/A	N/A	194
EIS	Au-modified Si	PA01	N/A	N/A	198
EIS	Stainless steel	PA01	N/A	N/A	199

SWV	PA01-modified PG	RA-13	N/A	N/A	200
CV, EIS	NH2/AgNP-modified GC	*P. aeruginosa*	10^2 - 10^7 CFU/mL	N/A	205
CV, amperometry	Nanozyme/AuNP-modified carbon	*P. aeruginosa*	60.0 - 6.0 × 10^7 CFU/mL	60.0 CFU/mL	207
CV, EIS	PA/Apt/CNCNF-modified GC	*P. aeruginosa*	10^1 - 10^7 CFU/mL	1 CFU/mL	208

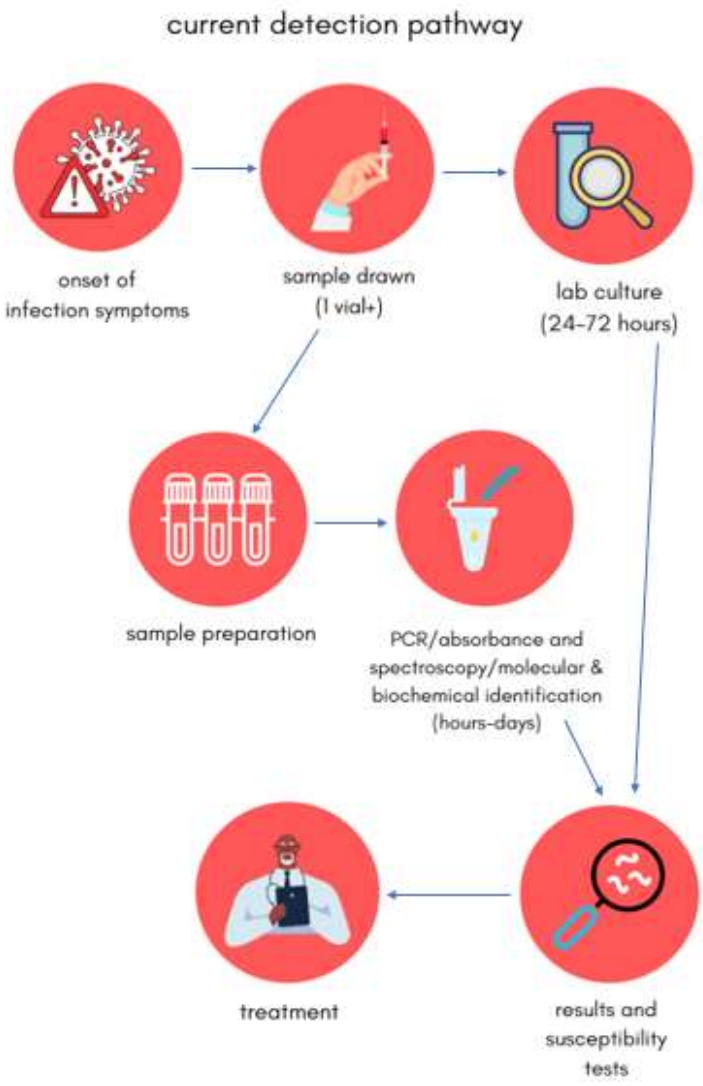

Figure 1.5: An overview of the current HCAI diagnostic pathway.

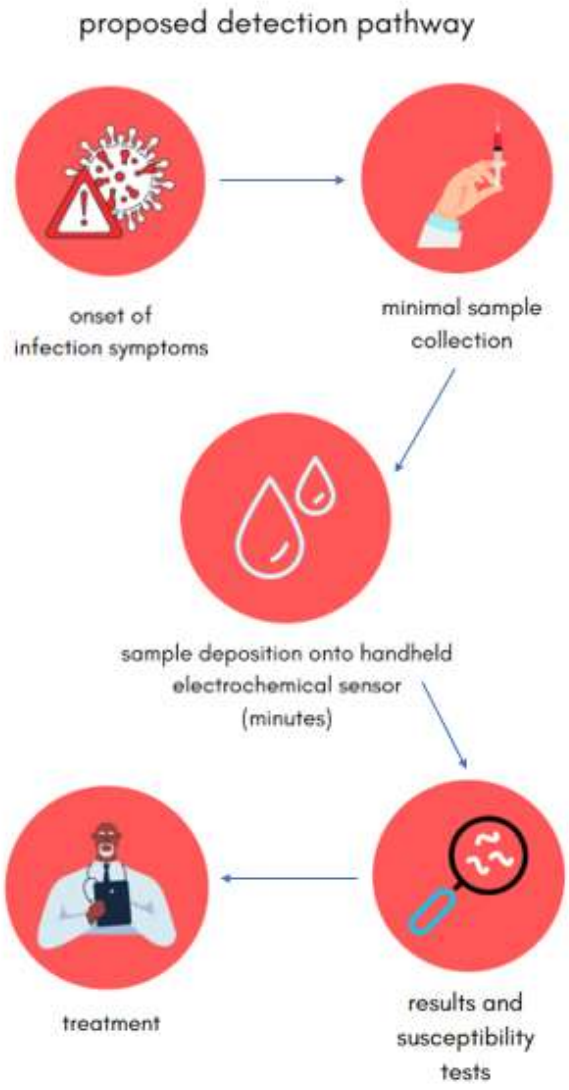

Figure 1.6: A proposed, expedited diagnostic pathway facilitated by electrochemical detection.

Thus, the study of electrochemical biosensors is increasing in popularity. These sensors are cheap to produce, simple to operate and can be extremely sensitive. Their portability and speed of operation renders them applicable for incorporation into point-of-care devices. This enables real-time diagnosis and monitoring without the need for pretreatment. [39]

1.3.2. Screen-printed electrodes

Screen-printed electrodes (SPEs) are an attractive and increasingly prevalent option for low-cost, disposable biosensors. Their manufacture involves the layered deposition of ink onto a solid substrate, through a screen shaped to the required geometry. Often, SPEs will feature a three-electrode configuration (working (WE), reference (RE) and counter (CE) electrodes) which lends itself to electrochemical analysis. Inks may be commercial or self-produced and can include a wide selection of materials, including catalysts. [133, 134] The expansion of nanomaterials in recent years has allowed the electrochemical properties of SPEs to consistently advance. [135]

Though limited to flat substrates, there are many advantages to the screen-printing process. Designs are flexible; electrode area, thickness and composition are easy to control and adjust. Good reproducibility allows for statistically valid experimental results. [134, 136] Given their bulk manufacture, SPEs can be produced cheaply and at high rates. Their simple operation negates the need for pretreatment or highly skilled personnel and allows for real-time, point-of-care testing. [135] These capabilities lend themselves well to the detection of *P. aeruginosa,* commonly through recognition of PyoC. [34, 61, 81, 104, 126, 127]

Carbon SPEs

Various studies have utilised carbon WEs and CEs in conjunction with silver (Ag) REs to detect PyoC using square wave voltammetry (SWV). [34, 61, 104, 126] SWV techniques boast rapidity, [126] although Cernat *et al.* (2019) also utilized CV for electrode characterization. [104] Sismaet *et al.* have successfully detected PyoC from clinical isolates taken from CF patients and HCAI patients, as well as fluid and biofilm samples

from wound patients. [34, 61] Their methods have potential for point-of-care *Pseudomonas* screening, with their PyoC probe displaying 71 % sensitivity and 57 % specificity when compared with 16S rRNA sequencing. Further work is required, however, to comprehend the clinical implications of false positive and false negative tests. [61] PyoC was detected by Cernat *et al*. in real samples with spiked analyte, using modified SPEs with an agar hydrogel and Au/Ag nanoalloy. They obtained a linear range of 0.12 – 25 µM, with a limit of detection (LOD) of 0.04 µM (signal-to-noise ratio (SNR) = 3). PyoC detection in whole blood was possible within 5 – 10 minutes from sample collection. [104]

Screen printing also allows for innovation regarding print surfaces. Ciui *et al*. screen-printed electrodes onto gloves to allow for simple operation and speed, with a detection time of approximately 4 minutes.

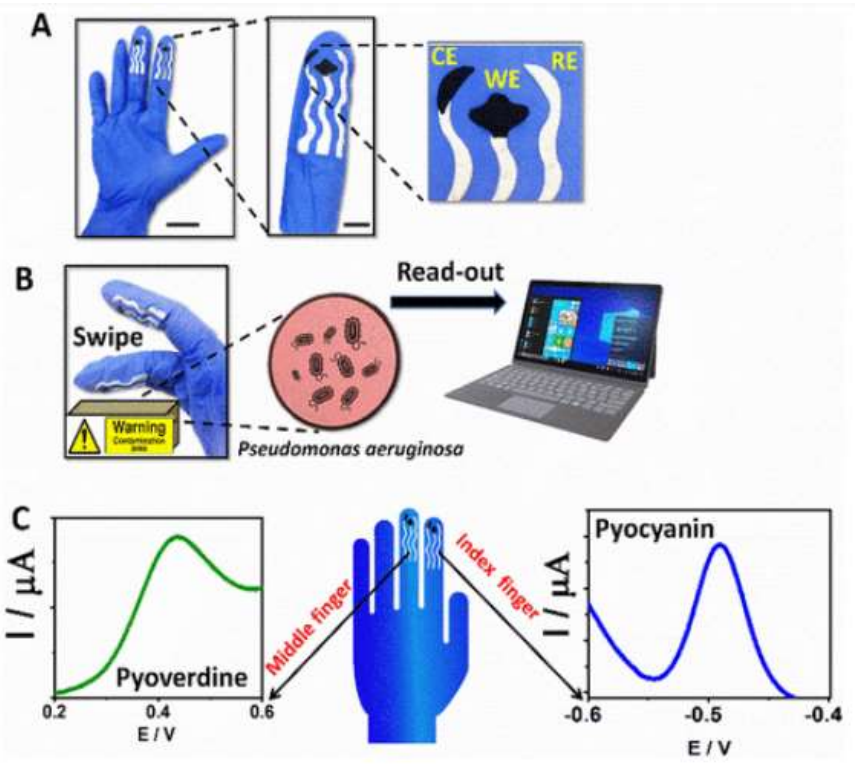

Figure 1.7: (A) Screen-printed sensing glove (left, scale bar: 3 cm) and electrode configuration (right, scale bar: 1 cm). (B) On-glove swiping approach for obtaining P. aeruginosa residues from surfaces. (C) PyoV and PyoC detection from the middle and index finger sensing platforms respectively. Reprinted with permissions from American Chemical Society [126]

Electrodes were highly sensitive (2.12 µA/µM), with an R^2 value of 0.935, and were stable over 14 days, with a relative standard deviation (RSD) value of 4.14 % (n=5). Translating this innovative technology into a clinical setting will involve the integration of handheld, wireless instrumentation. [126]

Gold SPEs

Commercial screen-printed gold (Au) electrode chips (Au WE, Au RE, Ag CE) have been used to detect PyoC using CV. These studies reported adequate biomarker detection, with relatively high sensitivity. [81, 127] However, it is important to note that the use of Au can be limited by amalgam formation, which alters the structure at the electrode surface. [137] The necessary cleaning procedures can also be time consuming

and involve hazardous chemicals, rendering them unsuitable for a clinical environment. [138]

One significant advantage of Au-based electrodes is the ability to combine electrochemical techniques with that of surface enhanced Raman spectroscopy (SERS), which can be performed on metallic surfaces such as Au and Ag. Do *et al*. confirmed that PyoC detection was possible during early stages of infection and that EC-SERS could be applied to the detection of other *P. aeruginosa* bacterial biomarkers. [127] Alatraktchi *et al*. obtained an R^2 value of 0.991 for PyoC quantification on Au electrodes, with its detection in human saliva displaying a standard deviation of 2.5 % ± 1 % (n=5) from the PyoC concentration added to samples. A detection window between 0.58 V and 0.82 V was identified as being free from the interference of other redox-active compounds. A LOD of 2 μM was achieved outwith any interfering compounds. [81]

Graphite SPEs

Graphite-based SPEs have also been utilised for the detection of pyoverdine (PyoV) and 2-aminoacetophenone (2-AA), a chemical compound produced by multiple strains of *P. aeruginosa,* [139] using CV and differential pulse voltammetry (DPV). [140-142] These materials offer an advantage in terms of cost and potential range over other metallic surfaces such as Au or Ag. Gandouzi *et al*. succeeded in detecting PyoV using surface-modified graphite SPEs. [140, 141] Detection was achieved with linearity for a concentration range of 1 – 100 $\mu M L^{-1}$ (correlation coefficient, R = 0.995, RSD = 4.916 %). The LOD was found to be 333.33 $nM L^{-1}$. [141] Recovery tests were also performed for PyoV detection in real samples (tap water, human serum, saliva). Recoveries for

25 µM/L PyoV ranged from 98.41 % to 100.55 % for tap water; 98.83 % to 101.88 % for human serum and 96.5 % to 102.12 % for saliva, all of which lie within the acceptable tolerance range, suggesting reliable methodology. RSD values ranged from 1.9 % to 4.1 %. [140, 141] Metters *et al*. discussed the merits of graphite SPEs for point-of-care electrochemical detection as well as their economic benefits. They were able to use carbon-based SPEs to detect 2-AA, with a detection limit of 7.6 mM. This study provided proof of concept that 2-AA can be detected with electrochemical techniques. [142]

The utilization of SPEs for electrochemical sensing is a valuable area of research. Their capacity for cheap mass production, simple operation, and the fact that pretreatment steps are not required, render them a viable technology for further development. [135] The adaptability of SPEs currently allows for the detection of many analytes and will be the key to expanding their applications in future. For example, the incorporation of biomaterials with SPEs can greatly increase sensitivity and selectivity and is an area of research which is constantly expanding. The incorporation of unique materials will contribute significantly to the field, and broaden possible applications. [133] The electrochemical properties of SPEs are continually improving, due to advances in nanomaterials; this is likewise an ongoing area of growth. [135] Also notable is the potential for SPEs to be incorporated into portable and miniaturized devices; given the enduring need for electronics miniaturization, it can be assumed that new applications will develop in this field. [133, 134]

1.3.3. Arrays

The development of electrode arrays has increased in popularity in recent years. [130, 143-147] These are sensors which contain at least two WEs [148] and they are utilised across a range of fields, including environmental, food and clinical analysis. Biosensors are one of the primary sensor types used in arrays, although they may also contain multiple sensor types. [149] In the case of electrochemical sensor arrays (ESAs), multiple sensors allow for simultaneous detection of more than one species. [150] The analytic capabilities of electrode arrays are considered competitive with quantitative chromatographic techniques. Stefan *et al*. have summarised the primary electrochemical sensors used in sensor array construction. [149] The main aspects of array development are design, calibration, and convolution. [151] Design informs quality; especially regarding *in-vivo* clinical analysis. [152] In this sense, geometry and potentiostatic control are significant design factors. As the construction of ESAs has developed, it has become possible to glean chemical fingerprints for complex matrices. [149] The use of arrays is often preferred to chromatographic techniques, as there is no need for onerous sampling processes or high-quality materials. Their use increases rapidity of flow analysis [149] and generally, they offer valuable spatial and rapid temporal resolution. [148] ESAs are known to provide superior precision, particularly regarding clinical analysis. [149] However, high standards must be met to ensure satisfactory calibration, and it is necessary to record many measurements on known samples prior to employment in point-of-care systems. [151]

In a clinical setting, ESAs show promise as highly sensitive alternatives to PCR detection assays. [153] Sheybani *et al*. achieved bacterial detection levels of five orders

of magnitude lower than similar sensors, with an array which monitored local pH and bacterial cell attachment within wounds. This Au-based dual sensor array eliminated the need for biorecognition elements, external solutions, pre- and post- sample processing, and visual assessment of the wound. Arrays were stable over time and gave accurate, real-time results for initial testing within wound infection models. [154] The effectiveness of ESAs has also been illustrated in human clinical fluid samples. Liao *et al*. achieved species-specific detection of bacterial pathogens in uropathogens isolates and clinical urine specimens. The array consisted of sixteen sensors containing Au WE, CE and RE, with each WE containing a capture probe specific to a urinary pathogen, including a *P. aeruginosa* probe.

Capture probes acted to fix the target to the sensor, whilst detector probes allowed for target recognition on the sensor surface. Over 90 % of clinical microbiology library uropathogens were recognised by these probes. Results were acquired within 45 minutes from sample collection, without the need for labelling or target amplification. Notably, this was the first study to describe bacterial pathogen detection in human fluid samples using an ESA. Given the potential for miniaturisation, electrochemical sensors may prove to be more cost effective and user friendly than current clinical sensors. [153]

Baldrich *et al*. were able to detect N-(3-oxo)-dodecanoyl-L-homoserine lactone (oxo-C12-HSL), an acyl homoserine lactone (AHL) produced by *P. aeruginosa*, in artificial saliva as well as spiked cultures and *P. aeruginosa* supernatants, using Au microelectrode arrays. AHLs were detected indirectly, via beta-galactosidase (β-gal) activity, which is AHL-induced. CV scans resulted in detection limits as low as 2 pM, in 20 µL sample volumes. Measurements took seconds following a 2-hour assay. [143]

Transparent carbon ultramicroelectrode arrays (T-CUAs) have been utilised in various studies to detect *P. aeruginosa*-derived phenazine metabolites. [144, 145, 147] These arrays have excellent conductivity; they are inert and highly biocompatible and boast rapid response times, amplified current responses, high SNR and low LODs. [130, 145-147, 155] T-CUAs have been used by Simoska *et al*. to monitor PYO, 5-methylphenazine-1-carboxylic acid (5-MCA), and 1-hydroxyphenazine (OHPHZ). [144, 145] Elliott *et al*. successfully utilised T-CUAs to electrochemically detect PyoC, with LODs as low as 1.0 ± 0.3 μM for 1.54 T-CUA with an LDR of 1-100 μM.

The merits of sensor arrays are many and can largely be attributed to their versatility. Utilising two or more electrodes makes it possible to detect multiple targets simultaneously, since each electrode is individually addressable. [148] Individual sensors can be modified, for example with nanoparticles (NPs) or biorecognition elements, to optimise their functionality. [130] Spatio-temporal analysis of analytes is also possible, as multiple sensors can be used for 'mapping'. [148] A broad range of electrochemical sensors may be utilised; particularly common are amperometric sensors, gas sensors, ion-selective and membrane electrodes. [149]

However, conscientious array design is vital to performance. Careful consideration of the target medium is necessary for addressing which matrix should be used. Polymer-based matrices are favoured over carbon-based, though they have relatively low construction reproducibility. [149] Where ultramicroelectrodes are utilised, often arrays will be designed to function in parallel to enhance SNR, since their ability to produce extremely low currents – in the picoamp (pA) range – may lead to noise limitations. [146, 156-159] Despite this, their use enables higher current densities and low limits of detection. [146]

1.3.4. Surface modification

Electrochemical sensors may be surface modified, often using NPs, to improve specificity and selectivity. [141] Gold NPs (AuNPs) are often utilised for surface modification and contribute to high sensitivity and signal amplification. [128, 140, 141, 160, 161] Elkhawaga *et al.* utilised ultrasensitive polyaniline (PANI)/Au NPs/indium tin oxide (ITO) modified sensors for rapid detection of PyoC in clinical isolates. A linear range was obtained from 238 μM to 1.9 μM, with a LOD of 500 nM. PyoC detection by SWV showed 100 % agreement with the molecular method regarding sensitivity and specificity, against other methods such as SPE and automated methods. High selectivity was also achieved for traces of PyoC in the presence of interferences such as vitamin C, uric acid, and glucose. Khalifa *et al*. utilised the same sensors for successful PyoC detection in corneal ulcer samples. [128, 129] Reduced graphene oxide (rGO) SPEs were modified with AuNPs by Rashid *et al.* for the detection of PyoC via DPV. Under ideal conditions, a favourable linear range was achieved, with LODs of 0.27 μM, 1.34 μM and 2.3 μM for PyoC detection in PBS, human saliva and urine, respectively. [162] Zhang *et al*. used Super P/AuNPs treated Au electrodes to quantify *P. aeruginosa*. The use of metal-organic framework (MoF) allowed for signal amplification, with the added advantage of a large surface area, as well as the ability to control its structure and aperture. [163] A zirconium series metal-organic framework (ZrMOF) was also utilised, which gave the advantage of being able to immobilise metal ions and biological ligands.

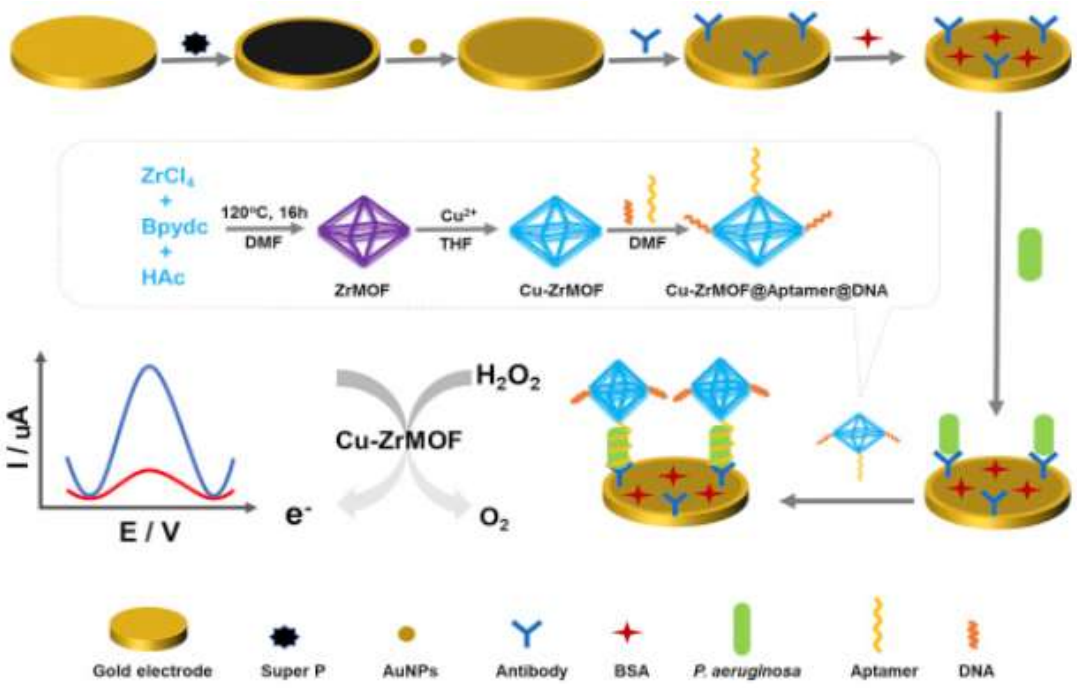

Scheme 1.2: Electrochemical detection of P. aeruginosa via Super P/AuNPs treated Au electrodes. Reprinted with permission from Elsevier 2019 [164]

Results could be obtained in 120 minutes, with a linearity range of 10-10^6 CFU/mL and LOD of 2 CFU/mL (SNR=3). Sensors also displayed good reproducibility and specificity, highlighting the potential advantages of MOFs for electrode surface modification. [164]

The conjugation of an electrochemical active molecule (EAM) and a specific antibody on redox-active AuNPs (raAuNPs) was utilised by Lee *et al*. This resulted in the enhancement of signals received by individual bacterium by six orders of magnitude at optimum conditions, since each AuNP contains thousands of EAMs. The self-assembled layer of EAMs had good electrode coverage, which prevented direct solution contact; thus, electrode fouling was minimised. [161] Background noise from interferences can also be reduced. [165] The resulting biosensor had high sensitivity, with a dynamic range of 10 – 10^5 CFU/mL and a detection limit of 10 CFU/mL. It showed

considerable potential as an electrochemical biosensor for pathogenic bacterial cell detection in blood plasma. [161]

Chitosan gold NPs (CS/AuNP) and planar transparent macroelectrodes (T-Macro) were used by Elliott *et al*. to modify the surface of T-CUAs. Treatment with CS/AuNP elicited a LOD of 1.6 ± 0.2 μM and LDR of 1 – 100 μM; T-Macro modification gave a LOD of 0.75 ± 0.09 μM and LDR of 0.75 – 25 μM. It was concluded that these parameters were sufficient for PyoC detection in a range of *in vitro* and *in vivo* cellular environments. [130] High sensitivity was achieved by Gandouzi *et al*., who deposited graphene-AuNPs composite film onto graphite-based SPEs for utilisation in PyoV detection. Electrodes exhibited a linear range of 1 – 100 μM/L and a LOD of 0.33 μM/L and were stable long-term with good reproducibility. DPV scans produced a signal which was six times higher after surface modification. [141] AuNPs decorated graphene/graphite-modified SPEs were then used to detect PyoV with high sensitivity in tap water, human serum, and saliva. The sensor had linearity from 0.5 to 100 μM and a LOD of 66.90 nM (SNR = 3) when tested in PyoV solutions. In PyoV spiked saliva, serum and tap water, recoveries were 96.75 %, 98.83 % and 100.55 % respectively, thus validifying practical applications for the sensor. [140]

Successful wound monitoring was documented by Sheybani *et al*., who used electrochemical sensor arrays to observe *P. aeruginosa* growth. Arrays were based on sensors with Au WE, Ag RE and Pt CE, and stability was improved with the addition of biocompatible polymeric coatings (chitosan and Nafion) which act to promote the attachment of bacterial cells and prevent non-specific cell and protein fouling. These advantages could allow for the long-term operation of in situ sensor arrays in areas of low resources. [154]

Cernat *et al*. developed a thermosensitive polymer-based electrochemical sensor, modified with a Au/Ag nanoalloy, for the detection of PyoC. The sensor displayed a linear range of 0.12 – 25 μM and LOD of 0.04 μM (SNR = 3). Sensors were effective in spiked real samples and required no pretreatment, except a dilution step. PyoC detection with high recovery in whole blood was possible within 5 – 10 minutes of sample collection. [104]

Nanograss topography was etched onto the surface of electrodes in a study by Alatraktchi *et al*., with 200 nm Au deposited on top. Compared to a standard Au electrode, the addition of nanograss increased the surface area by 3.9 times. This enables enhanced electron transfer which leads to a low LOD. A higher current is also permitted for the same WE footprint, which allows for an improved SNR and higher sensitivity. PyoC was detected in spiked hypertonic saline samples, with an R^2 value of 0.9901 and a LOD of 172 nM. When tested on airway samples from CF patients, the sensor identified *P. aeruginosa* within 60 seconds, with no need for sample pretreatment. [125] Krithiga *et al*. also modified the surface of glassy carbon (GC) electrodes to increase their surface area. Calcium cross-linked pectin-gold nanoparticles (CCLP-AuNPs) were deposited onto GC electrodes, with anti Ps drop-casted on top. A further layer of Au tagged anti rabbit horseradish peroxidase (IgG-HRP) was then added. The CCLP-AuNPs acted to increase the electrode's surface area, further immobilising the antibody, and thus improving response. The immunosensor was used to detect *P. aeruginosa* in water, and displayed good sensitivity, with a detection limit of 9×10^2 CFU/mL, and high reproducibility. However, preparing the electrochemical immunosensor assay and fabricating the

electrodes involved many steps, with the need for drying and incubation increasing production time. [166]

Inkjet-printed polyacrylamide-coated carbon nanotube (PA/CNT) electrodes were developed in a proof-of-concept study by Jarošová *et al.* to detect PyoC in wound fluid simulant. Electrode fabrication involved a multi-step, layered process. The initial conductive geometry was printed onto Kapton substrate using Ag. Onto this, a CNT electrode layer was printed, followed by a UV-curable dielectric ink which acted as an insulating layer. To prevent electrode fouling, the electrodes were then coated with polyacrylamide (PA) hydrogel. Electrodes were flexible and disposable and were linear over the range 0.10 to 100 μM L^{-1} (R^2 = 0.9992), with a LOD of 0.10 μM L^{-1} (S/N = 3). This was a vital study regarding the exploration of printing materials and processes for the fabrication of effective electrochemical sensors.[167]

The use of immunosensors to monitor water is appealing, since current methods such as PCR lack rapidity and can be expensive, as well as requiring complex pretreatment. Bekir *et al*. developed an immunosensor which utilised the immobilisation of purified polyclonal anti *P. aeruginosa* antibodies on a poly(pyrrole-3-carboxylic acid)-modified SPCE. Immobilised antibodies are increasingly being integrated into biosensors for the recognition and capture of specific bacteria, offering unparalleled specificity. [168-175] The immunosensor successfully and sensitively detected *P. aeruginosa* in groundwater solution. [176]

Surface modification is an advantageous tool for the improvement of electrochemical electrode performance, regarding both specificity and sensitivity. Metal NPs are often employed to augment electrochemical reactions, by means of their catalytic activity.

Their superior conductivity facilitates improved communication between protein redox centres and the electrode surface. Better detection limits can also be achieved due to the high surface area of NPs compared with bulk metal surfaces. Improved selectivity and detectability is possible, although this may involve the use of complex and costly equipment. [161] AuNPs have shown particular merit for surface modification, displaying a plethora of assets, including impressive biocompatibility, catalytic activity, and electron transfer rate. [141, 177] Gandouzi *et al*. demonstrated the synergetic effect of utilising two nanostructures (Au and graphene), resulting in improved electrocatalytic efficiency for the electrochemical oxidation of PyoV, compared to bare SPEs. [141] Future work in this area will involve further discovery of viable surface modifiers, for optimal target analyte detection.

1.3.5. Biorecognition elements and aptasensors

Biorecognition elements are utilised to furnish a biosensor with analyte specificity, consequently increasing selectivity, sensitivity, and reproducibility. Careful consideration of which biorecognition element to use is necessary, since its specificity relies on a strong affinity to the target analyte. [178] Naturally occurring elements, such as antibodies, enzymes (or, in the case of aptasensors, DNA or RNA aptamers) [179] may be used, as well as synthetic elements such as nanostructures. [178] The blood glucose biosensor is the current gold standard and has become a vital monitoring tool for those with diabetes. [178, 180] Despite its simplicity, it is highly sensitive, selective, reproducible, and cost efficient. [178, 181]

Amperometric detection of redox signals can be achieved if detector probes are coupled to oxidoreductase reporter enzymes. [182, 183] Applying a fixed potential between

the WE and RE, a current is generated by enzyme-catalysed redox activity, which can then be measured and analysed. [184-186] Current amplitude is affected by how many target-probe-reporter enzyme complexes are affixed to the sensor. Again, electrochemical methods have an advantage over techniques such as PCR, as they can detect target nucleic acids directly in clinical specimens, since the initial step in the process is nucleic hybridisation and not enzyme-based target amplification. [153]

Electrochemical DNA sensor structure comprises a recognition layer, which contains oligonucleotide probes, and an electrochemical signal transducer. [153] Often, they are formed using 'sandwich' hybridisation of target nucleic acids by capture and detector probes. [187-190] Liao *et al*. used capture probes to affix the bacterial 16S rRNA target to the surface of the sensor; detection was achieved by hybridisation to both the biotin-modified capture probe attached to the surface of the sensor, and to a second, fluorescein-modified detector probe. [153] Stem-loop structured probes were employed by Liu *et al*. in their fabrication of a DNA biosensor for *P. aeruginosa* 16S ribosomal RNA (rRNA) detection. Probes were modified to include a thiol and a biotin and were immobilised onto a Au electrode. In the absence of the target, probes were 'closed', with the hybridisation of the target allowing them to 'open', triggering a reaction at the electrode surface between the biotin and streptavidin-horseradish peroxidase (HRP). Electrochemical techniques can then be employed for analyte detection. The biosensor performed well, boasting stability and selectivity, with a detection limit of 0.012 pg/μL. However, it must be noted that, in this case, sensor fabrication and hybridisation is a relatively lengthy process. [191]

P. aeruginosa is often employed for biofilm monitoring, as its electroactive phenazine products can be easily monitored. [192] ESAs have been utilised for the monitoring of *P.*

aeruginosa products [192, 193] and QS mechanisms, [194] and biofilm formation at the electrode surface has been monitored using voltammetric [195-197] and impedance [198, 199] techniques. Robb *et al*. modified pyrolytic graphite (PG) electrodes with *P. aeruginosa* PA01 to monitor the dispersion of PA01 biofilm. [200] Previously, an electrochemical assay was detected to observe antimicrobial peptide (AMP) exposure-induced alginate disruption and it was found that it was related to anti-biofilm activity. [201] This was improved upon by similarly immobilizing *P. aeruginosa* PA01 onto the electrode and monitoring the response to anti-biofilm compound RA-13. [200]

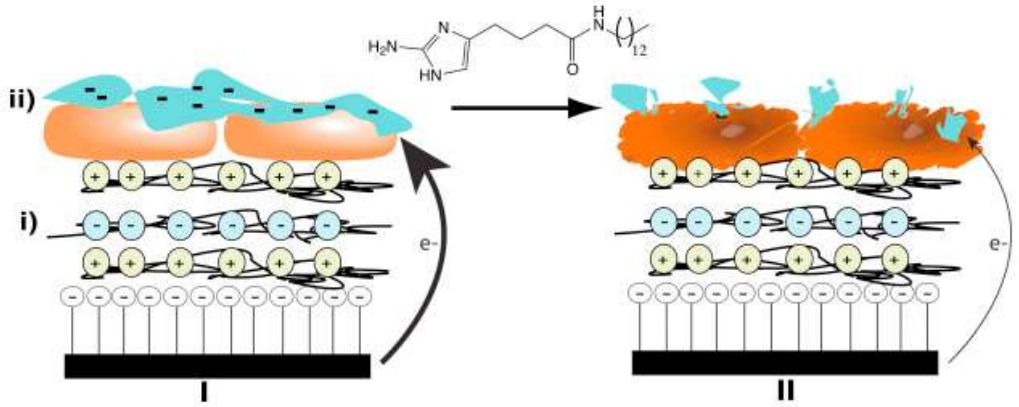

Scheme 1.3: Overview of the P. aeruginosa electrochemical assay. Formation of the electrode using (i) layer by layer cationic (yellow) and anionic (blue) polymers and (ii) P. aeruginosa PA01 (orange) that can produce biofilm (aqua) Reprinted with permission from Elsevier 2018 [200]

P. aeruginosa immobilisation improves simplicity of the assay, since electroactive phenazines (such as PyoC) are produced, which are easy to measure with electrochemical methods. [192, 193, 201-204] Overall, the assay was shown to be capable of distinguishing anti-biofilm compound activity in real time. [200]

Roushani *et al*. described the first impedimetric aptasensor for ultrasensitive *P. aeruginosa* detection. After modifying the surface of a GC electrode with AuNPs, the NH2-aptamer was covalently attached. [205] Covalent bonding is achieved by the

aptamer amino group, which ensures attachment. [196] Electrode modification influences the intensity of the electrochemical signal and the biological molecule stabilisation. Use of AuNPs improved electrochemical signal due to an increase in surface area; electron transfer was also significantly accelerated. The aptasensor was tested in blood serum samples under optimum conditions, and results were confirmed by PCR. A linear range was achieved with a R^2 value of 0.9984 and inter-electrode repeatability was acceptable, with an RSD value of 4.75 %. The sensor also had the advantage of relatively low cost and high sensitivity when compared to other sensors. Thus, clinical diagnosis of *P. aeruginosa* was deemed possible. [205] Aptamers can also be employed as mediators, as demonstrated by Das *et al*. in their fabrication of an innovative nanozyme sensor for *P. aeruginosa* detection. The term 'nanozyme' describes a nanomaterial which exhibits characteristics of an enzyme. [206] The peroxidase-like nanozyme activity of AuNPs was inhibited by the adsorption of F23, an aptamer specific to *P. aeruginosa*. Given the high affinity of F23 for *P. aeruginosa*, the aptamer parts from the surface of the AuNPs in the presence of the pathogen. This re-enables the peroxidase-like activity of the AuNPs, resulting in the oxidation of 3,3′,5,5′-tetramethylbenzidine (TMB), which can then be electrochemically detected. Amperometry techniques saw a detection limit of 60.0 CFU/mL in water. [207] Sarabaegi *et al.* describe the use of hollow carbon nanocapsules-based nitrogen-doped carbon nanofibers (CNCNF) to facilitate aptamer immobilisation onto the surface of a GC electrode. Desirable electrochemical performance was attributed to the high distribution of N-doped nanocapsules in solution, which was achieved via electrospinning. The resulting aptasensors were utilised for impedimetric detection of *P. aeruginosa*. A linear range of 10^1 – 10^7 $CFUmL^{-1}$ was achieved under optimal

conditions, with a LOD of 1 $CFUmL^{-1}$. In spiked serum samples, recoveries between 99.80 % and 106.00 % were achieved, indicating the potential for desirable performance in clinical samples.[208]

There are various advantages and disadvantages to each type of biorecognition element, which must be considered in sensor design. Natural biorecognition elements, such as antibodies and enzymes, boast good selectivity and reusability, but suffer when it comes to reproducibility. This is likely due to variable success regarding the attachment of the biorecognition element during manufacture. [178] New antibody discovery is also limited since the process is lengthy and costly. [209, 210] Synthetic biorecognition elements have virtually the opposite characteristics. Molecularly imprinted polymers (MIPs) are known to have good reproducibility, but lack selectivity. Pseudo-natural biorecognition elements also exist; they are a combination of natural subunits and synthetic supramolecular structures - for example nucleic acids and aptamers. Generally, these elements provide good sensitivity and reproducibility; though they are costly and can exhibit non-specific binding. [178] Pseudo-natural biorecognition elements have an extensive range of applications, with the exception of nucleic acid recognition elements, whose only optimal target are nucleic acids. [211-214]

Biosensors are a constantly growing area of research. [178, 181-183, 186, 210-218] To enable their optimisation, it is essential that biorecognition elements are well understood; Morales *et al.* discussed the need for a comprehensive guide to biorecognition element selection and characterisation. Future work in this field will involve improving biosensor reusability and reproducibility as well as expanding the range of biorecognition elements available to researchers. [178]

1.4 Conclusion and Research Aims

P. aeruginosa is a prevalent cause of nosocomial infection, causing substantial morbidity and mortality and displaying antibiotic resistance. [28-36] Current detection methods require extensive preparation and/or highly trained personnel and are unable to detect the pathogen in a timely manner. [47, 61, 121-124] A range of studies have spoken to utilising the electrochemically active virulence factors secreted by *P. aeruginosa* to detect it as early as possible, allowing for more effective treatment. Research in this area has proven the efficacy of electrochemical detection, as well as its desirable sensitivity. It is fast becoming clear that this is a viable option for rapid diagnostics since these methods can be executed in seconds and eliminate the need for pretreatment. Future research in this area will involve optimising detection methods and creating portable testing equipment that could be utilised in a clinical environment. Sensitive point-of-care testing would provide a significant advancement towards a reduction in morbidity and mortality, by allowing treatment before the pathogen is able to advance and develop resistance.

This project aims to develop a 3D printed electrochemical sensor for the detection of *P. aeruginosa*. Ideally, this device will be suitable for point-of-care infection diagnostics, and capable of rapid and sensitive analyte detection. The initial focus will be upon the design of a printed sensing platform, using multi-walled carbon nanotubes (MWCNTs) as the conductive element within the 3D printing resin. Further iterations of this design will be explored, with a focus cheap and facile manufacture. Finally, the effectiveness of a carbon black (CB) PEGDA material for electrochemical detection will be explored, using CB-modified GC electrodes.

1.5. References

1. G. Ducel, *WHO/BAC/79.1*, 2002.
2. World Health Organisation, *WHO/CDS/CSR/EPH/2002.12*, 2002.
3. A. S. Benenson, *Control of Communicable Diseases in Man*, American Public Health Society, 1970.
4. World Health Organization, *The burden of health care-associated infection worldwide: A summary*, 2010.
5. H. A. Khan, F. K. Baig and R. Mehboob, *Asian Pacific Journal of Tropical Biomedicine*, 2017, **7**, 478-482.
6. European Centre for Disease Prevention and Control, *Infographic: Healthcare-associated infections – a threat to patient safety in Europe*, 2018.
7. J. L. Vincent, J. Rello, J. Marshall, E. Silva, A. Anzueto, M. C. D., R. Moreno, J. Lipman, C. Gomersall, Y. Sakr and K. Reinhart, *Journal of the American Medical Association*, 2009, **302**, 2323-2329.
8. R. Plowman, *European communicable disease bulletin*, 2000, **5**, 49-50.
9. D. Pittet, D. Tarara and R. P. Wenzel, *Journal of the American Medical Association*, 1994, **271**, 1598-1601.
10. D. S. Wakefield, C. M. Helms, R. M. Massanari, M. Mori and M. Pfaller, *American Journal of Infection Control*, 1988, **16**, 185-192.
11. R. Coello, H. Glenister, J. Fereres, C. Bartlett, D. Leigh, J. Sedgwick and E. M. Cooke, *The Journal of Hospital Infection*, 1993, **25**, 239-250.
12. S. Ponce-de-Leon, *Journal of Hospital Infection*, 1991, **18**, 376-381.
13. Centers for Disease Control and Prevention, Urinary Tract Infection (Catheter-Associated Urinary Tract Infection [CAUTI] and Non-Catheter-Associated Urinary Tract Infection [UTI]) Events).
14. J. W. Warren, *Infectious Disease Clinics of North America*, 1997, **11**, 609-622.
15. M. McGuckin, *The Patient Survival Guide: 8 Simple Solutions to Prevent Hospital and Healthcare Associated Infections*, demosHEALTH, 2012.
16. E. Lo, L. E. Nicolle, S. E. Coffin, C. Gould, L. L. Maragakis, J. Meddings, D. A. Pegues, A. M. Pettis, S. Saint and D. S. Yokoe, *Infection Control and Hospital Epidemiology*, 2014, **35**, 464-479.
17. D. J. Anderson, *Infectious Disease Clinics of North America*, 2011, **25**, 135-153.
18. World Health Organisation, Global guidelines on the prevention of surgical site infection).
19. Y. Haddadin and H. Regunath, Central Line Associated Blood Stream Infections (CLABSI)).
20. J. L. Vincent, D. J. Bihari, H. A. Bruining, J. White, M. H. Nicolas-Chanoin, M. Wolff, R. C. Spencer and M. Hemmer, *Journal of the American Medical Association*, 1995, **274**, 639-644.
21. M. P. Charles, A. Kali, J. M. Easow, N. M. Joseph, M. Ravishankar, S. Srinivasan, S. Kumar and S. Umadevi, *The Australasian Medical Journal*, 2014, **7**, 334-344.

22. S. Gatermann, F. R., W. Handrick, L. Lietritz, K. G. Naber and A. Podbielski, *MIQ 02: Urinary Tract Infections: Quality standards for microbiological infections*, 2005, 8-21.
23. H. A. Khan, A. Ahmad and R. Mehboob, *Asian Pacific Journal of Tropical Biomedicine*, 2015, **5**, 505-509.
24. T. C. Horan, M. Andrus and M. A. Dudeck, *American Journal of Infection Control*, 2008, **36**.
25. Proceedings of the 3rd Decennial International Conference on Nosocomial Infections, *International Conference on Nosocomial Infections*, 1990, **30**.
26. P. K. Singh, *World Health Organisation*, 2016.
27. T. Urli, G. Perone, A. Acquarolo, S. Zappa, B. Antonini and A. Candiani, *Journal of Hospital Infection*, 2002, **52**, 130-135.
28. S. L. Chua, J. K. H. Yam, P. Hao, S. S. Adav, M. M. Salido, Y. Liu, M. Givskov, S. K. Sze, T. Tolker-Nielsen and L. Yang, *Nature Communications*, 2016, **7**, 10750.
29. P. Deschaght, S. Van Daele, F. De Baets and M. Vaneechoutte, *Journal of Cystic Fibrosis*, 2011, **10**, 293-297.
30. A. A. Khan and C. E. Cerniglia, *Applied and Environmental Microbiology*, 1994, **60**, 3739-3745.
31. A. Mohanty, M. H. Kathawala, J. Zhang, W. N. Chen, J. S. Loo, S. Kjelleberg, L. Yang and B. Cao, *Biotechnology and Bioengineering*, 2014, **111**, 858-865.
32. M. D. Obritsch, D. N. Fish, R. MacLaren and R. Jung, *Antimicrobial Agents and Chemotherapy*, 2004, **48**, 4606-4610.
33. V. H. Tam, K. T. Chang, K. Abdelraouf, C. G. Brioso, M. Ameka, L. A. McCaskey, J. S. Weston, J. P. Caeiro and K. W. Garey, *Antimicrobial Agents and Chemotherapy*, 2010, **54**, 1160-1164.
34. H. J. Sismaet, A. J. Pinto and E. D. Goluch, *Biosensors and Bioelectronics*, 2017, **97**, 65-69.
35. L. M. Ringen and C. H. Drake, *Journal of Bacteriology*, 1952, **64**, 841-845.
36. T. S. Walker, H. P. Bais, E. Deziel, H. P. Schweizer, L. G. Rahme, R. Fall and J. M. Vivanco, *Plant Physiology*, 2004, **134**, 320-331.
37. K. Latour, P. Kinross, M. L. Moro, F. Fitzpatrick, E. Ricchizzi, T. Dillane, J. Griškevičienė and B. Jans, *European Centre for Disease Prevention and Control*, 2013, 47.
38. J. F. Guest, T. Keating, D. Gould and N. Wigglesworth, *BMJ Open*, 2020, **10**, e033367.
39. F. A. Alatraktchi, H. K. Johansen, S. Molin and W. E. Svendsen, *Nanomedicine (Lond)*, 2016, **11**, 2185-2195.
40. R. L. Gibson, J. L. Burns and B. W. Ramsey, *American Journal of Respiratory and Critical Care Medicine*, 2003, **168**, 918-951.
41. O. Bukelman, N. Amara, R. Mashiach, P. Krief, M. M. Meijler and L. Alfonta, *Chemical Communications*, 2009, 2836-2838.
42. Corona-Nakamura, A.L., M. G. Miranda-Novales, B. Leanos-Miranda, L. Portillo-Gomez, A. Hernandez-Chavez and J. Anthor-Rendon, *Archives of Medical Research*, 2001, **32**, 238-242.

43. R. D. Wolcott, J. D. Hanson, E. J. Rees, L. D. Koenig, C. D. Phillips, R. A. Wolcott, S. B. Cox and J. S. White, *Wound Repair and Regeneration*, 2016, **24**, 163-174.
44. T. Hogsberg, T. Bjarnsholt, J. S. Thomsen and K. Kirketerp-Moller, *PLoS One*, 2011, **6**.
45. H. W. Boucher, G. H. Talbot, J. S. Bradley, J. E. Edwards, D. Gilbert, L. B. Rice, M. Scheld, B. Spellberg and J. Bartlett, *Clinical Infectious Diseases*, 2009, **48**, 1-12.
46. F. Alatraktchi, *PLoS One*, 2018, **13**.
47. J. Oziat, S. Elsen, R. M. Owens, G. G. Malliaras and P. Mailley, *Conference Proceedings IEEE Engineering in Medicine and Biology Society*, 2015, **2015**, 7522-7525.
48. V. A. Stanisich and M. H. Richmond, *Genetics and Biochemistry of Pseudomonas*, 1975, 163-190.
49. C. Delden, *Pseudomonas*, 2004, 1-7.
50. J. Lederberg, M. Alexander , B. Bloom , D. Hopwood, R. Hull , B. Iglewski, A. Laskin, S. Oliver, M. Schaechter and W. Summers, in *Encyclopedia of Microbiology*, Encyclopedia of Microbiology, San Diego, Second edn., 2000, vol. 3, pp. 876-891.
51. R. B. Fick, *Pseudomonas aeruginosa, the opportunist : pathogenesis and disease*, Boca Raton : CRC Press, [1993] ©1993, 1993.
52. J. Carr, P. Aeruginosa SEM Image - CDC Public Health Image Library).
53. J. Oosthuizen, Multidrug-resistant Pseudomona Aeruginosa - CDC Public Health Image Library).
54. N. A. Bhawsar and M. Singh, *International Journal of Advanced Research*, 2014, **2**, 778-783.
55. R. Donlan, *Emerging Infectious Disease journal*, 2002, **8**, 881.
56. T. Rasamiravaka, Q. Labtani, P. Duez and M. El Jaziri, *BioMed Research International*, 2015, **2015**, 759348.
57. M. Chicurel, *Nature*, 2000, **408**, 284-286.
58. J. D. Bryers, *Biotechnology and Bioengineering*, 2008, **100**, 1-18.
59. T. J. Marrie, J. Nelligan and J. W. Costerton, *Circulation*, 1982, **66**, 1339-1341.
60. J. W. Costerton, Z. Lewandowski, D. E. Caldwell, D. R. Korber and H. M. Lappin-Scott, *Annual Review of Microbiology*, 1995, **49**, 711-745.
61. H. J. Sismaet, A. Banerjee, S. McNish, Y. Choi, M. Torralba, S. Lucas, A. Chan, V. K. Shanmugam and E. D. Goluch, *Wound Repair and Regeneration*, 2016, **24**, 366-372.
62. G. A. O'Toole and R. Kolter, *Molecular Microbiology*, 1998, **30**, 295-304.
63. A. J. Merz, M. So and M. P. Sheetz, *Nature*, 2000, **407**, 98-102.
64. T. Tolker-Nielsen, U. C. Brinch, P. C. Ragas, J. B. Andersen, C. S. Jacobsen and S. Molin, *Journal of Bacteriology*, 2000, **182**, 6482-6489.
65. G. W. Lau, D. J. Hassett, H. Ran and F. Kong, *Trends in Molecular Medicine*, 2004, **10**, 599-606.
66. N. A. Whitehead, A. M. Barnard, H. Slater, N. J. Simpson and G. P. Salmond, *FEMS Microbiology Reviews*, 2001, **25**, 365-404.
67. M. B. Miller and B. L. Bassler, *Annual Review of Microbiology*, 2001, **55**, 165-199.

68. S. T. Rutherford and B. L. Bassler, *Cold Spring Harbor Perspectives in Medicine*, 2012, **2**.
69. W. J. Windsor, *American Society for Microbiology*, 2020.
70. H. K. Johansen, S. M. Moskowitz, O. Ciofu, T. Pressler and N. Hoiby, *Journal of Cystic Fibrosis*, 2008, **7**, 391-397.
71. L. E. Dietrich, A. Price-Whelan, A. Petersen, M. Whiteley and D. K. Newman, *Molecular Microbiology*, 2006, **61**, 1308-1321.
72. K. Kanthakumar, G. Taylor, K. W. Tsang, D. R. Cundell, A. Rutman, S. Smith, P. K. Jeffery, P. J. Cole and R. Wilson, *Infection and Immunity*, 1993, **61**, 2848.
73. L. R. Usher, R. A. Lawson, I. Geary, C. J. Taylor, C. D. Bingle, G. W. Taylor and M. K. Whyte, *The Journal of Immunology*, 2002, **168**, 1861-1868.
74. G. M. Denning, S. S. Iyer, K. J. Reszka, Y. O'Malley, G. T. Rasmussen and B. E. Britigan, *The American Journal of Physiology-Lung Cellular and Molecular Physiology*, 2003, **285**, L584-592.
75. Chemical Entities of Biological Interest, CHEBI:8653 - Pyocyanine, (accessed 30/1/20).
76. T. Das, S. K. Kutty, N. Kumar and M. Manefield, *PLoS One*, 2013, **8**, e58299.
77. D. J. Hassett, L. Charniga, K. Bean, D. E. Ohman and M. S. Cohen, *Infection and Immunity*, 1992, **60**, 328-336.
78. D. Sharp, P. Gladstone, R. B. Smith, S. Forsythe and J. Davis, *Bioelectrochemistry*, 2010, **77**, 114-119.
79. E. A. Reyes, M. J. Bale, W. H. Cannon and J. M. Matsen, *Journal of Clinical Microbiology*, 1981, **13**, 456-458.
80. A. Reimer, B. Edvaller and B. Johansson, *Acta Oto-Laryngologica Supplementum*, 2000, **543**, 86-88.
81. F. A. a. Alatraktchi, S. B. Andersen, H. K. Johansen, S. Molin and W. E. Svendsen, *Sensors (Basel, Switzerland)*, 2016, **16**, 408.
82. S. Hall, C. McDermott, S. Anoopkumar-Dukie, A. J. McFarland, A. Forbes, A. V. Perkins, A. K. Davey, R. Chess-Williams, M. J. Kiefel, D. Arora and G. D. Grant, *Toxins*, 2016, **8**, 236.
83. Y. Q. O'Malley, K. J. Reszka, D. R. Spitz, G. M. Denning and B. E. Britigan, *American Journal of Physiology-Lung Cellular and Molecular Physiology*, 2004, **287**, L94-L103.
84. M. Muller, *Free Radical Biology and Medicine*, 2006, **41**, 1670-1677.
85. X. M. Bustamante-Marin and L. E. Ostrowski, *Cold Spring Harbor Perspectives in Biology*, 2017, **9**, a028241.
86. B. Thomas, A. Rutman and C. Callaghan, *European Respiratory Journal*, 2009, **34**, 401.
87. A. Bush, R. Chodhari, N. Collins, F. Copeland, P. Hall, J. Harcourt, M. Hariri, C. Hogg, J. Lucas, H. M. Mitchison, C. O'Callaghan and G. Phillips, *Archives of Disease in Childhood*, 2007, **92**, 1136.
88. P. G. Noone, M. W. Leigh, A. Sannuti, S. L. Minnix, J. L. Carson, M. Hazucha, M. A. Zariwala and M. R. Knowles, *American Journal of Respiratory and Critical Care Medicine*, 2004, **169**, 459-467.
89. B. Halliwell, *Lancet*, 1994, **344**, 721-724.

90. M. Kesarwani, R. Hazan, J. He, Y. Que, Y. Apidianakis, B. Lesic, G. Xiao, V. Dekimpe, S. Milot, E. Deziel, F. Lépine and L. G. Rahme, *PLOS Pathogens*, 2011, **7**, e1002192.
91. J. Betteridge, *Metabolism*, 2000, **49**, 3-8.
92. Y. Q. O'Malley, M. Y. Abdalla, M. L. McCormick, K. J. Reszka, G. M. Denning and B. E. Britigan, *American Journal of Physiology-Lung Cellular and Molecular Physiology*, 2003, **284**, L420-L430.
93. M. Muller, *Free Radical Biology and Medicine*, 2002, **33**, 1527-1533.
94. F. A. Mohamed, G. H. Shaker and M. M. Askoura, *Current Microbiology*, 2020, **77**, 479-490.
95. W. Lau Gee, H. Ran, F. Kong, J. Hassett Daniel and D. Mavrodi, *Infection and Immunity*, 2004, **72**, 4275-4278.
96. T. Xia, M. Kovochich, J. Brant, M. Hotze, J. Sempf, T. Oberley, C. Sioutas, J. I. Yeh, M. R. Wiesner and A. E. Nel, *Nano Letters*, 2006, **6**, 1794-1807.
97. K. J. Reszka, G. M. Denning and B. E. Britigan, *Photochemistry and Photobiology*, 2006, **82**, 466-473.
98. N. C. Munro, A. Barker, A. Rutman, G. Taylor, D. Watson, W. J. McDonald-Gibson, R. Towart, W. A. Taylor, R. Wilson and P. J. Cole, *Journal of Applied Physiology*, 1989, **67**, 316-323.
99. T. G. O'Riordan, R. Otero, Y. Mao, I. Lauredo and W. M. Abraham, *American Journal of Respiratory and Critical Care Medicine*, 1997, **155**, 1522-1528.
100. R. Forteza, I. T. Lauredo, R. Burch and W. M. Abraham, *American Journal of Respiratory and Critical Care Medicine*, 1994, **149**, 687-693.
101. J. Gutteridge, *Clinical Chemistry*, 1995, **41**, 1819-1828.
102. B. Chance, H. Sies and A. Boveris, *Physiological Reviews*, 1979, **59**, 527-605.
103. C. A. Fulcher, *Pseudomonas aeruginosa* PAO1 Pathway: Pyocyanin Biosynthesis, http://pseudocyc.pseudomonas.com:1555/PSEUDO/NEW-IMAGE?type=PATHWAY&object=PWY-6666&detail-level=3, (accessed 25 August, 2020).
104. A. Cernat, A. Canciu, M. Tertis, F. Graur and C. Cristea, *Analytical and Bioanalytical Chemistry*, 2019, **411**, 3829-3838.
105. J. F. Parsons, B. T. Greenhagen, K. Shi, K. Calabrese, H. Robinson and J. E. Ladner, *Biochemistry*, 2007, **46**, 1821-1828.
106. G. M. Denning, M. A. Railsback, G. T. Rasmussen, C. D. Cox and B. E. Britigan, *American Journal of Physiology-Lung Cellular and Molecular Physiology*, 1998, **274**, L893-L900.
107. A. S. Hussain, J. Bozinovski, D. H. Maurice, B. E. McLaughlin, G. S. Marks, J. F. Brien and K. Nakatsu, *Canadian Journal of Physiology and Pharmacology*, 1997, **75**, 398-406.
108. D. V. Vukomanovic, D. E. Zoutman, J. A. Stone, G. S. Marks, J. F. Brien and K. Nakatsu, *Biochemical Journal*, 1997, **322**, 25-29.
109. J. B. Warren, R. Loi, N. B. Rendell and G. W. Taylor, *Biochemical Journal*, 1990, **266**, 921-923.
110. D. V. Mavrodi, R. F. Bonsall, S. M. Delaney, M. J. Soule, G. Phillips and L. S. Thomashow, *Journal of Bacteriology*, 2001, **183**, 6454.

111. C. N. Cruickshank and E. J. Lowbury, *British Journal of Experimental Pathology*, 1953, **34**, 583-587.
112. J. Nutman, M. Berger, P. A. Chase, D. G. Dearborn, K. M. Miller, R. L. Waller and R. U. Sorensen, *The Journal of Immunology*, 1987, **138**, 3481.
113. R. Schoental, *British Journal of Experimental Pathology*, 1941, **22**, 137-147.
114. C. D. Cox, *Infection and Immunity*, 1986, **52**, 263-270.
115. G. M. Denning, L. A. Wollenweber, M. A. Railsback, C. D. Cox, L. L. Stoll and B. E. Britigan, *Infection and Immunity*, 1998, **66**, 5777.
116. I. T. Lauredo, J. R. Sabater, A. Ahmed, Y. Botvinnikova and W. M. Abraham, *Journal of Applied Physiology*, 1998, **85**, 2298-2304.
117. B. E. Britigan, G. T. Rasmussen and C. D. Cox, *Infection and Immunity*, 1997, **65**, 1071.
118. H. M. Hassan and I. Fridovich, *Journal of Bacteriology*, 1980, **141**, 156.
119. R. A. Miller, G. T. Rasmussen, C. D. Cox and B. E. Britigan, *Infection and Immunity*, 1996, **64**, 182.
120. R. Franco-Duarte, L. Černáková, S. Kadam, K. S. Kaushik, B. Salehi, A. Bevilacqua, M. R. Corbo, H. Antolak, K. Dybka-Stępień, M. Leszczewicz, S. Relison Tintino, V. C. Alexandrino de Souza, J. Sharifi-Rad, H. D. M. Coutinho, N. Martins and C. F. Rodrigues, *Microorganisms*, 2019, **7**, 130.
121. T. A. Webster, H. J. Sismaet, J. L. Conte, I. P. Chan and E. D. Goluch, *Biosensors and Bioelectronics*, 2014, **60**, 265-270.
122. V. Velusamy, K. Arshak, O. Korostynska, K. Oliwa and C. Adley, *Biotechnology Advances*, 2010, **28**, 232-254.
123. R. D. Holland, J. G. Wilkes, F. Rafii, J. B. Sutherland, C. C. Persons, K. J. Voorhees and J. O. Lay, Jr., *Rapid Communications in Mass Spectrometry*, 1996, **10**, 1227-1232.
124. A. Cherkaoui, J. Hibbs, S. Emonet, M. Tangomo, M. Girard, P. Francois and J. Schrenzel, *Journal of Clinical Microbiology*, 2010, **48**, 1169-1175.
125. F. A. Alatraktchi, M. Dimaki, N. Støvring, H. K. Johansen, S. Molin and W. E. Svendsen, *Analytical Biochemistry*, 2020, **593**, 113586.
126. B. Ciui, M. Tertiş, A. Cernat, R. Săndulescu, J. Wang and C. Cristea, *Analytical Chemistry*, 2018, **90**, 7761-7768.
127. H. Do, S. R. Kwon, K. Fu, N. Morales-Soto, J. D. Shrout and P. W. Bohn, *Langmuir*, 2019, **35**, 7043-7049.
128. A. A. Elkhawaga, M. M. Khalifa, O. El-Badawy, M. A. Hassan and W. A. El-Said, *PLoS One*, 2019, **14**, e0216438.
129. M. M. Khalifa, A. A. Elkhawaga, M. A. Hassan, A. M. Zahran, A. M. Fathalla, W. A. El-Said and O. El-Badawy, *Scientific Reports*, 2019, **9**, 18320.
130. J. Elliott, J. Duay, O. Simoska, J. B. Shear and K. J. Stevenson, *Analytical Chemistry*, 2017, **89**, 1267-1274.
131. Y. Wang and D. K. Newman, *Environmental Science & Technology*, 2008, **42**, 2380-2386.
132. Y. Yang, Y. Y. Yu, Y. Z. Wang, C. L. Zhang, J. X. Wang, Z. Fang, H. Lv, J. J. Zhong and Y. C. Yong, *Biosensors and Bioelectronics*, 2017, **98**, 338-344.
133. Z. Taleat, A. Khoshroo and M. Mazloum-Ardakani, *Microchimica Acta*, 2014, **181**, 865-891.

134. S. Fletcher, in *Electrochemistry of Carbon Electrodes*, ed. R. C. Alkire, Bartlett, P. N., Lipkowski, J., Wiley-VCH Verlag GmbH & Co., Weinheim, Germany, 2015, pp. 425-444.
135. M. Li, D.-W. Li, G. Xiu and Y.-T. Long, *Current Opinion in Electrochemistry*, 2017, **3**, 137-143.
136. M. A. Alonso-Lomillo, O. Domínguez-Renedo and M. J. Arcos-Martínez, *Talanta*, 2010, **82**, 1629-1636.
137. E. Bernalte, C. M. Sánchez and E. P. Gil, *Analytica Chimica Acta*, 2011, **689**, 60-64.
138. A. Giacomino, O. Abollino, M. Malandrino and E. Mentasti, *Talanta*, 2008, **75**, 266-273.
139. A. J. Scott-Thomas, M. Syhre, P. K. Pattemore, M. Epton, R. Laing, J. Pearson and S. T. Chambers, *BMC Pulmonary Medicine*, 2010, **10**, 56.
140. I. Gandouzi, M. Tertis, A. Cernat, D. Saidane-Mosbahi, A. Ilea and C. Cristea, *Materials (Basel)*, 2019, **12**.
141. I. Gandouzi, M. Tertis, A. Cernat, A. Bakhrouf, M. Coros, S. Pruneanu and C. Cristea, *Bioelectrochemistry*, 2018, **120**, 94-103.
142. J. P. Metters, D. K. Kampouris and C. E. Banks, *Analyst*, 2014, **139**, 3999-4004.
143. E. Baldrich, F. X. Muñoz and C. García-Aljaro, *Analytical Chemistry*, 2011, **83**, 2097-2103.
144. O. Simoska, M. Sans, L. S. Eberlin, J. B. Shear and K. J. Stevenson, *Biosensors and Bioelectronics*, 2019, **142**, 111538.
145. O. Simoska, M. Sans, M. D. Fitzpatrick, C. M. Crittenden, L. S. Eberlin, J. B. Shear and K. J. Stevenson, *ACS Sensors*, 2019, **4**, 170-179.
146. J. Duay, J. Elliott, J. B. Shear and K. J. Stevenson, *Analytical Chemistry*, 2015, **87**, 10109-10116.
147. J. Elliott, O. Simoska, S. Karasik, J. B. Shear and K. J. Stevenson, *Analytical Chemistry*, 2017, **89**, 6285-6289.
148. S. Griveau and F. Bedioui, *Analytical and Bioanalytical Chemistry*, 2013, **405**, 3475-3488.
149. R.-I. Stefan, J. F. v. Staden and H. Y. Aboul-Enein, *Critical Reviews in Analytical Chemistry*, 1999, **29**, 133-153.
150. D. Quinton, A. Girard, L. T. Thi Kim, V. Raimbault, L. Griscom, F. Razan, S. Griveau and F. Bedioui, *Lab on a Chip*, 2011, **11**, 1342-1350.
151. F. A. M. Davide, C. Di Natale and A. D'Amico, *Sensors and Acuators B*, 1993, 327-332.
152. O. Niwa, *Electroanalysis*, 1993, **7**, 606-613.
153. J. C. Liao, M. Mastali, V. Gau, M. A. Suchard, A. K. Møller, D. A. Bruckner, J. T. Babbitt, Y. Li, J. Gornbein, E. M. Landaw, E. R. McCabe, B. M. Churchill and D. A. Haake, *Journal of Clinical Microbiology*, 2006, **44**, 561-570.
154. R. Sheybani and A. Shukla, *Biosensors and Bioelectronics*, 2017, **92**, 425-433.
155. J. Duay, J. M. Goran and K. J. Stevenson, *Analytical Chemistry*, 2014, **86**, 11528-11532.
156. R. G. Compton, G. G. Wildgoose, N. V. Rees, I. Streeter and R. Baron, *Chemical Physics Letters*, 2008, **459**, 1-17.

157. R. Chen, Y. Li, K. Huo and P. K. Chu, *RSC Advances*, 2013, **3**, 18698-18715.
158. M. Fleischmann and S. Pons, *Analytical Chemistry*, 1987, **59**, 1391A-1399A.
159. P. Kissinger and W. R. Heineman, *Laboratory Techniques in Electroanalytical Chemistry, Revised and Expanded*, CRC Press, 2018.
160. P. Zhang, X. Zhang, S. Zhang, X. Lu, Q. Li, Z. Su and G. Wei, *Journal of Materials Chemistry B*, 2013, **1**, 6525-6531.
161. C. W. Lee, H. Y. Chang, J. K. Wu and F. G. Tseng, *Biosensors and Bioelectronics*, 2019, **133**, 215-222.
162. J. I. A. Rashid, V. Kannan, M. H. Ahmad, A. A. Mon, S. Taufik, A. Miskon, K. K. Ong and N. A. Yusof, *Materials Science and Engineering: C*, 2021, **120**, 111625.
163. Y. V. Kaneti, J. Tang, R. R. Salunkhe, X. Jiang, A. Yu, K. C. W. Wu and Y. Yamauchi, *Advanced Materials*, 2017, **29**, 1604898.
164. X. Zhang, G. Xie, D. Gou, P. Luo, Y. Yao and H. Chen, *Biosensors And Bioelectronics*, 2019, **142**.
165. S. Goggins, B. J. Marsh, A. T. Lubben and C. G. Frost, *Chemical Science*, 2015, **6**, 4978-4985.
166. N. Krithiga, K. B. Viswanath, V. S. Vasantha and A. Jayachitra, *Biosensors and Bioelectronics*, 2016, **79**, 121-129.
167. R. Jarošová, S. E. McClure, M. Gajda, M. Jović, H. H. Girault, A. Lesch, M. Maiden, C. Waters and G. M. Swain, *Analytical Chemistry*, 2019, **91**, 8835-8844.
168. X. Liu, J. Xiong, Y. Lv and Y. Zuo, *Progress in Organic Coatings*, 2009, **64**, 497-503.
169. A. C. d. S. Pires, N. d. F. F. Soares, L. H. M. da Silva, M. d. C. H. da Silva, M. V. De Almeida, M. Le Hyaric, N. J. d. Andrade, R. F. Soares, A. B. Mageste and S. G. Reis, *Sensors and Actuators B: Chemical*, 2011, **153**, 17-23.
170. Y. Wang, W. Knoll and J. Dostalek, *Analytical Chemistry*, 2012, **84**, 8345-8350.
171. P. Leonard, S. Hearty, J. Brennan, L. Dunne, J. Quinn, T. Chakraborty and R. O'Kennedy, *Enzyme and Microbial Technology*, 2003, **32**, 3-13.
172. M. Varshney and Y. Li, *Biosensors and Bioelectronics*, 2009, **24**, 2951-2960.
173. Y. Li, R. Afrasiabi, F. Fathi, N. Wang, C. Xiang, R. Love, Z. She and H.-B. Kraatz, *Biosensors and Bioelectronics*, 2014, **58**, 193-199.
174. R. Hernández, C. Vallés, A. M. Benito, W. K. Maser, F. Xavier Rius and J. Riu, *Biosensors and Bioelectronics*, 2014, **54**, 553-557.
175. H. Tang, W. Zhang, P. Geng, Q. Wang, L. Jin, Z. Wu and M. Lou, *Analytica Chimica Acta*, 2006, **562**, 190-196.
176. K. Bekir, F. Bousimma, H. Barhoumi, K. Fedhila, A. Maaref, A. Bakhrouf, H. Ben Ouada, P. Namour, N. Jaffrezic-Renault and H. Ben Mansour, *Environmental Science and Pollution Research*, 2015, **22**, 18669-18675.
177. Y. Li, H. J. Schluesener and S. Xu, *Gold Bulletin*, 2010, **43**, 29-41.
178. M. A. Morales and J. M. Halpern, *Bioconjugate Chemistry*, 2018, **29**, 3231-3239.
179. M. Moreno, in *Encyclopedia of Analytical Science (Third Edition)*, eds. P. Worsfold, C. Poole, A. Townshend and M. Miró, Academic Press, Oxford, 2019, pp. 150-153.

180. J. Chambers, B. Arulanandam, L. Matta, A. Weis and J. Valdes, *Current Issues in Molecular Biology*, 2008, **10**, 1-12.
181. M. Giardi and E. Piletska, *Biotechnological Applications of Photosynthetic Proteins: Biochips, Biosensors and Biodevices*, 2006.
182. M. Mehrvar and M. Abdi, *Analytical Sciences*, 2004, **20**, 1113-1126.
183. J. E. Pearson, A. Gill and P. Vadgama, *Annals of Clinical Biochemistry*, 2000, **37**, 119-145.
184. P. Fanjul-Bolado, M. B. González-García and A. Costa-García, *Analytical and Bioanalytical Chemistry*, 2005, **382**, 297-302.
185. J. J. Gau, E. H. Lan, B. Dunn, C. M. Ho and J. C. Woo, *Biosensors and Bioelectronics*, 2001, **16**, 745-755.
186. B. Mecheri, L. Piras, L. Ciotti and G. Caminati, *IEEE Sensors Journal*, 2004, **4**, 171-179.
187. C. N. Campbell, D. Gal, N. Cristler, C. Banditrat and A. Heller, *Analytical Chemistry*, 2002, **74**, 158-162.
188. M. Dequaire and A. Heller, *Analytical Chemistry*, 2002, **74**, 4370-4377.
189. R. M. Umek, S. W. Lin, J. Vielmetter, R. H. Terbrueggen, B. Irvine, C. J. Yu, J. F. Kayyem, H. Yowanto, G. F. Blackburn, D. H. Farkas and Y. P. Chen, *The Journal of Molecular Diagnostics*, 2001, **3**, 74-84.
190. E. Williams, M. I. Pividori, A. Merkoçi, R. J. Forster and S. Alegret, *Biosensors and Bioelectronics*, 2003, **19**, 165-175.
191. C. Liu, G.-M. Zeng, L. Tang, Y. Zhang, Y.-P. Li, Y.-Y. Liu, Z. Li, M.-S. Wu and J. Luo, *Enzyme and Microbial Technology*, 2011, **49**, 266-271.
192. D. L. Bellin, H. Sakhtah, J. K. Rosenstein, P. M. Levine, J. Thimot, K. Emmett, L. E. P. Dietrich and K. L. Shepard, *Nature Communications*, 2014, **5**, 3256.
193. D. Koley, M. M. Ramsey, A. J. Bard and M. Whiteley, *Proceedings of the National Academy of Sciences*, 2011, **108**, 19996.
194. J. L. Connell, J. Kim, J. B. Shear, A. J. Bard and M. Whiteley, *Proceedings of the National Academy of Sciences*, 2014, **111**, 18255.
195. E. Marsili, J. B. Rollefson, D. B. Baron, R. M. Hozalski and D. R. Bond, *Applied and Environmental Microbiology*, 2008, **74**, 7329.
196. R. B. Congdon, A. S. Feldberg, N. Ben-Yakar, D. McGee, C. Ober, B. Sammakia and O. A. Sadik, *Analytical Biochemistry*, 2013, **433**, 192-201.
197. J. Gamby, A. Pailleret, C. B. Clodic, C.-M. Pradier and B. Tribollet, *Electrochimica Acta*, 2008, **54**, 66-73.
198. S. Kim, G. Yu, T. Kim, K. Shin and J. Yoon, *Electrochimica Acta*, 2012, **82**, 126-131.
199. A. Dheilly, I. Linossier, A. Darchen, D. Hadjiev, C. Corbel and V. Alonso, *Applied Microbiology and Biotechnology*, 2008, **79**, 157-164.
200. A. J. Robb, S. Vinogradov, A. S. Danell, E. Anderson, M. S. Blackledge, C. Melander and E. G. Hvastkovs, *Electrochimica Acta*, 2018, **268**, 276-282.
201. S. M. Vinogradov, J. E. Satterwhite-Warden, R. P. Hicks, E. Anderson and E. G. Hvastkovs, *Electrochimica Acta*, 2015, **186**, 245-252.
202. T. A. Webster, H. J. Sismaet, I. P. Chan and E. D. Goluch, *Analyst*, 2015, **140**, 7195-7201.
203. D. M. Ramsey and D. J. Wozniak, *Molecular Microbiology*, 2005, **56**, 309-322.

204. V. B. Wang, S.-L. Chua, B. Cao, T. Seviour, V. J. Nesatyy, E. Marsili, S. Kjelleberg, M. Givskov, T. Tolker-Nielsen, H. Song, J. S. C. Loo and L. Yang, *PLoS One*, 2013, **8**, e63129.
205. M. Roushani, M. Sarabaegi and F. Pourahmad, *Microchimica Acta*, 2019, **186**, 725.
206. M. Liang and X. Yan, *Accounts of Chemical Research*, 2019, **52**, 2190-2200.
207. R. Das, A. Dhiman, A. Kapil, V. Bansal and T. K. Sharma, *Analytical and Bioanalytical Chemistry*, 2019, **411**, 1229-1238.
208. M. Sarabaegi, M. Roushani and H. Hosseini, *Talanta*, 2021, **223**, 121700.
209. E. Miller and H. D. Sikes, *Nanobiomedicine*, 2015, **2**.
210. C. I. L. Justino, A. C. Freitas, R. Pereira, A. C. Duarte and T. A. P. R. Santos, *Trends in Analytical Chemistry*, 2015, **68**, 2-17.
211. K. J. Odenthal and J. J. Gooding, *Analyst*, 2007, **132**, 603-610.
212. I. Palchetti and M. Mascini, *Analyst*, 2008, **133**, 846-854.
213. P. A. Piunno and U. J. Krull, *Analytical and Bioanalytical Chemistry*, 2005, **381**, 1004-1011.
214. J. Wang, *Nucleic Acids Research*, 2000, **28**, 3011-3016.
215. A. Kravets, M. Shcherbakov, M. Kultsova and O. Shabalina, *Creativity in Intelligent Technologies and Data Science: First Conference, CIT&DS 2015, Volgograd, Russia, September 15-17, 2015. Proceedings*, Springer International Publishing, 2015.
216. M. M. Bellah, *Journal of Nanomedicine Research*, 2017, **6**.
217. S. J. Kulkarni, *International Journal of Scientific Research in Computer Science, Engineering and Information Technology*, 2016, **1**, 19-23.
218. G. Maduraiveeran, M. Sasidharan and V. Ganesan, *Biosensors and Bioelectronics*, 2018, **103**, 113-129.

CHAPTER TWO

THEORETICAL BACKGROUND

2.1. Additive Manufacturing

Additive manufacturing (AM) was utilised throughout this project for electrode prototyping and manufacture. AM generally involves the sequential deposition of materials to form complex 3D geometries. [1, 2] Designs are built from computer aided design (CAD) models and can be produced rapidly, with little human intervention. The medical industry is the third-largest AM market, next to automotive and consumer electronics, claiming 16 % of the industry's overall revenue as of 2017. [2] Medical products can be manufactured on demand, enabling remote fabrication of essential tools. [2, 3] Applications include surgical, pharmaceutical, dentistry and medical devices. [2, 4-9] In 2015, the AM market was worth approximately $5 billion, and was expected to almost triple in size by 2020. Its development could increase its value to circa $350 billion by 2035. [10, 11] AM is becoming more accessible as the industry continues to grow, with prices decreasing in line with the expiration of patents. [2]

The main advantages of AM are its efficiency and cost effectiveness. Designs can be produced quickly from a CAD file, facilitating faster prototype iterations, and eliminating the need for skilled machinists or programmers. This reduces any potential for misinterpretation of a design and also introduces the possibility of facile customisation. [1, 11] Parts can be built cheaply, which permits trial and error in the design process, and allows form, fit and function tests to be performed early. [1]

Compared to conventional manufacturing methods, AM displays material efficiency, in that its additive nature ensures few waste products are produced. Often, leftover materials can be reused. In contrast, subtractive manufacturing calls for sizeable volumes of material to be removed to achieve the desired geometry. The fact that designs can be fully built within AM devices eradicates the need for auxiliary

resources or factory setup. [1, 11] This leads to improved supply chain dynamics. [1] Spare parts can also be manufactured on demand. [12] Parts can be manufactured without tooling constraints; thus, complex geometries can be printed and functionality need not be sacrificed. [1]

Despite its many assets, AM still has limitations which affect how it performs compared to conventional manufacturing methods. Generally, liquid polymers, or resin/plaster powders are used. This leads to size limitations, since larger parts will suffer from low strength and will take too long to build. Surface quality can also be poor, depending on which technique is used. Further, the upfront cost of AM equipment can be sizeable, with the potential need for expensive consumables over time. Future developments in the field of AM will include more efficient technologies which will contribute to reducing build time. Laser optics and machine controls will advance, permitting better build accuracy and surface finish. Research will also result in a wider range of materials being available for printing. [1]

2.1.1 Technologies

The International Organization for Standardization ISO/ASTM52900-15 [13] identifies the seven categories of AM as:

- Binder jetting
- Directed energy deposition
- Powder bed fusion
- Sheet lamination
- Material jetting
- Material extrusion

- Vat polymerisation

These technologies may also be referred to as 3D printing. A brief summary of their principles shall be discussed, with vat polymerisation explored in greater depth, being pertinent to this project.

Binder Jetting

Binder jetting begins with the spreading of the selected powder medium over the build platform using a roller. A layer of binder is deposited on top, per the object design; this combines the powder to form a solid layer in the correct geometry. The build platform is then lowered, allowing for the next layer to be printed. [14, 15] Often, a curing process is then necessary to improve the strength of the part. [15, 16]

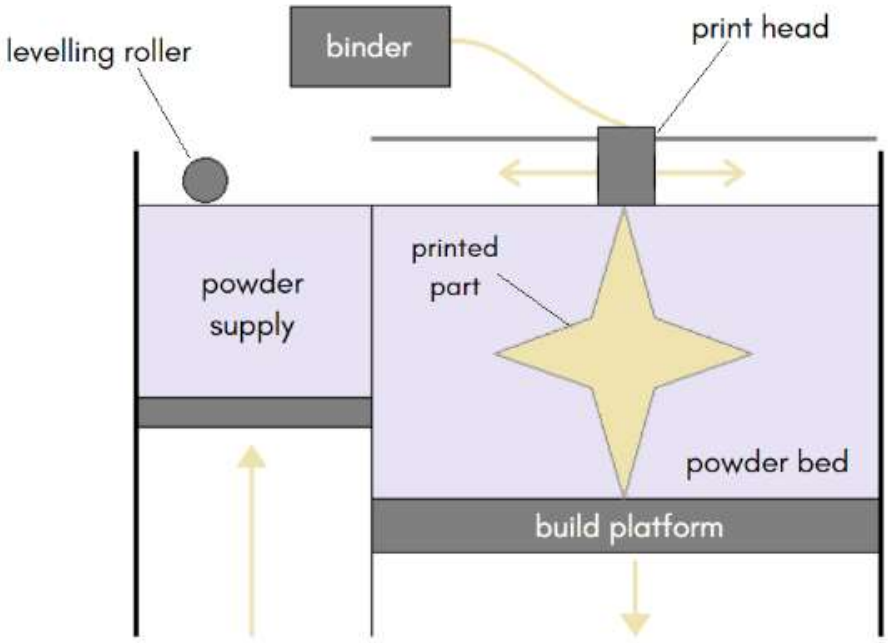

Figure 2.1: Binder Jetting schematic diagram. Adapted from Mohammed et al. [16]

This technique facilitates the use of many different materials and does not cause any warping or shrinkage. Since two separate materials are utilised in the binder and powder, different combinations can be explored. Furthermore, any leftover powder may be reused for future builds, thus reducing waste. However, post-processing is required, adding to manufacture time, and parts can suffer in terms of strength. [14]

Directed Energy Deposition

Directed energy deposition (DED) involves the use of a focused thermal energy source (for example, an electron beam) to melt and deposit materials (typically powder or wire) [17, 18] onto the build platform. [14, 17, 18] The nozzle is mounted onto a robotic arm, which has up to five mobile axes. [17, 18] Materials may be wire-based or powder-based and are typically metals, although the technique can also be used for ceramics and polymers. [14] DED is commonly utilised in the repair of industrial parts, for example turbine blades. [18] Most DED printers are large industrial machines, which require a closed, regulated environment. [17] Electron beam-based processes require a vacuum to ensure that there is no interaction with air molecules. If reactive metals are utilised, laser-based machines must utilise an inert chamber. Shielding gas may also be employed to prevent contamination of the metal material. [18]

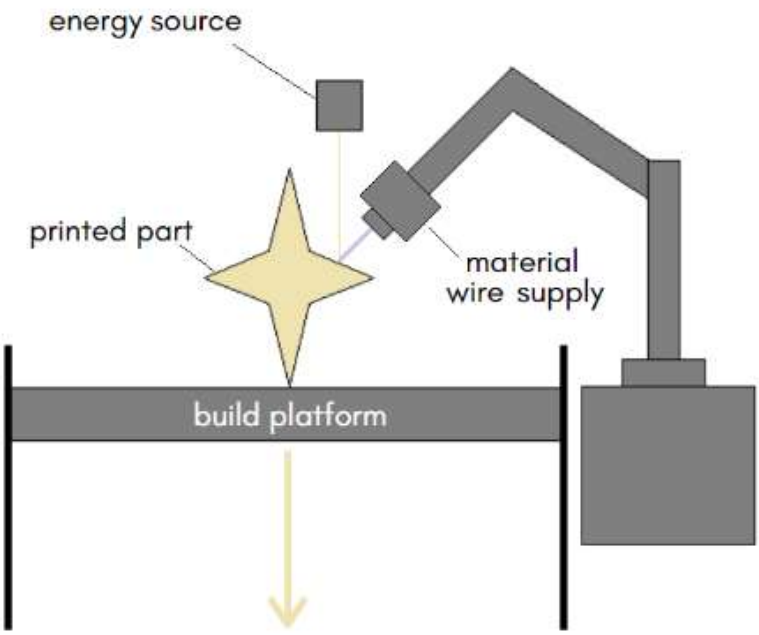

Figure 2.2: Directed Energy Deposition schematic diagram. Adapted from 3DExperience. [17]

DED boasts rapid building capabilities and the production of strong, dense parts. Sizes of builds are less limited than for other techniques, and it is possible to produce custom alloy parts. Despite this, it is an expensive AM solution, and lower resolution results in the need for secondary part processing, as surface quality may be poor. [14]

Powder Bed Fusion

Powder bed fusion (PBF) includes four energy source categories: thermally fused, electron beam fused, laser fused and fused with agent and energy. The energy source is used to fuse together the required powder (either plastic or metal) via melting or sintering. [2, 14, 19, 20] A roller is used to deposit a fine layer of powder – typically 0.1 mm thick - evenly across the build platform before fusing. [19] The platform is then lowered down, and the design is built up layer-by-layer.

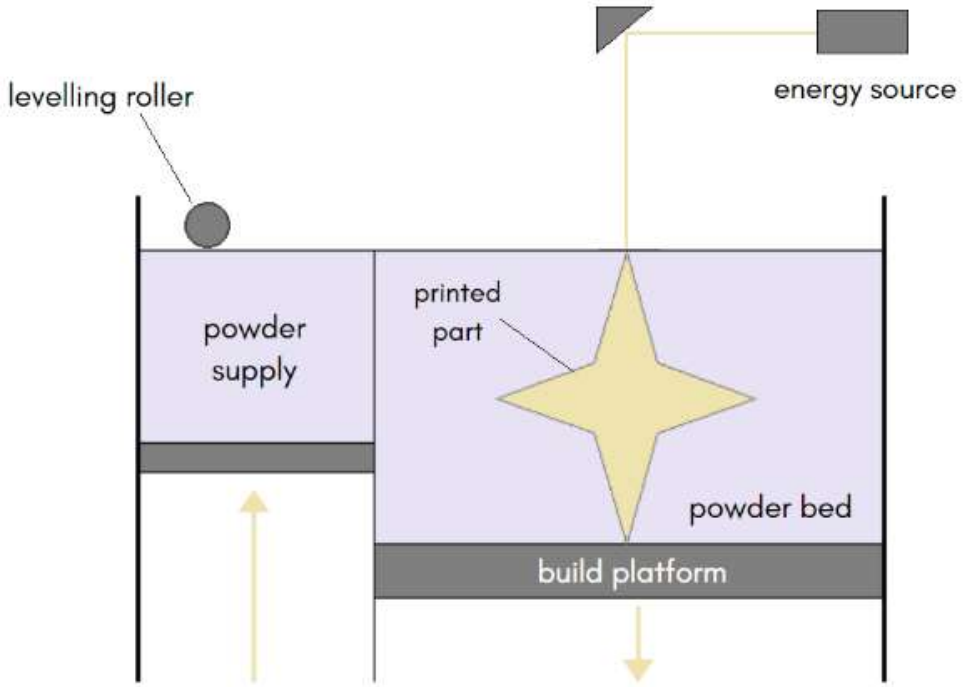

Figure 2.3: Powder Bed Fusion schematic diagram. Adapted from Loughborough University. [19]

This technique includes selective laser sintering (SLS), direct metal laser sintering (DMLS), selective laser melting (SLM) and electron beam melting (EBM). [21] SLS, DMLS, and SLM involve the use of a laser which is directed using mirrors, whilst EBM utilises an electron beam which is directed using electromagnetic coils. This renders the technique more costly since vacuum conditions are required. [2] The sintering process produces parts with rough surface characteristics and a porous internal structure. Melting provides further consolidation, generating parts with enhanced mechanical properties and high density. [2, 22]

PBF is a relatively low-cost method, which enables the use of a variety of materials. [14, 23] It is also possible to use more than one material within a build. However, it is a somewhat slow method, with lengthy print times and the need for post-processing.

Structural properties may be weak and surface quality may vary. There is also a risk of thermal distortion, particularly for polymers. [14]

Sheet Lamination

Sheet lamination involves the sequential stacking and lamination of thin material sheets. [11, 14] Materials can be paper or composite-based. [24] These sheets may be laminated via bonding, ultrasonic welding, or brazing. Each layer is placed atop the previous, and, depending on the technique, may or may not be bonded to it. There are seven different sheet lamination processes:

- Laminated Object Manufacturing (LOM)
- Plastic Sheet Lamination (PSL)
- Selective Deposition Lamination (SDL)
- Ultrasonic Additive Manufacturing (UAM)
- Composite Based Additive Manufacturing (CBAM)
- Selective Lamination Composite Object Manufacturing (SLCOM)
- Computer Aided Manufacturing of Laminated Engineering Materials (CAM-LEM)

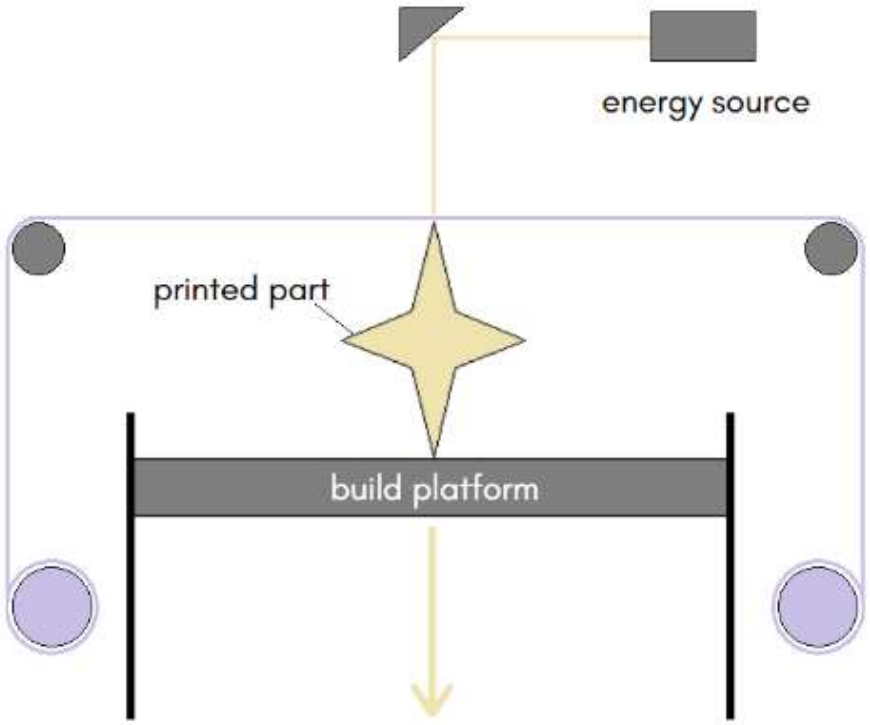

Figure 2.4: Sheet lamination schematic diagram. Adapted from Sireesha et al. [11]

Sheet lamination offers a relatively cheap, simple, and rapid AM solution, and enables the layering of multiple materials. It is best suited for rapid prototyping since it has the lowest resolution of all AM technologies. Post-processing is often required, which can be challenging and tedious. Furthermore, material options are limited and hollow parts may be difficult to produce. [14]

Material Extrusion

Material extrusion is the most accessible AM technology for the general consumer. It utilises a continuous filament which is heated and extruded through a nozzle onto the build platform. Materials may be thermoplastic or composite and are built up in layers. Fused deposition modelling (FDM) is a common extrusion technique, whereby filaments are extruded through a heated nozzle. [2, 23] Direct Ink Writing (DIW) utilises

pneumatic or mechanical means to extrude materials, and is commonly used for bioprinting. [2]

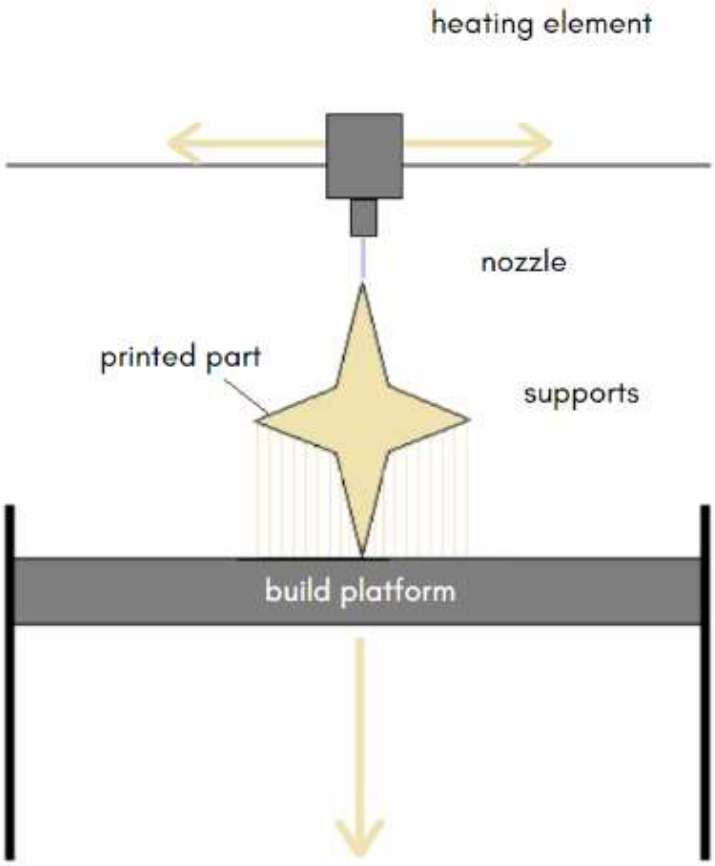

Figure 2.5: Material extrusion schematic diagram. Adapted from 3DExperience. [25]

There are many advantages to material extrusion, not least its ease of use and cost effectiveness. A wide variety of materials may be employed, and printing tolerances are desirable. However, builds are weak and have low resolution along the z-axis. [14, 23] As part area and resolution increases, so too does print time. Safety considerations are also required due to the use of toxic materials. [14]

Material Jetting

Material jetting is a similar process to inkjet printing, involving the line-wise deposition of materials, through hundreds of small nozzles, onto a build platform. [14, 26] Generally, wax-like materials are used, which then cool and solidify, such that another layer may be deposited on top. [14] This technique requires support structures, which can be easily removed post-print, without damaging the build. [27]

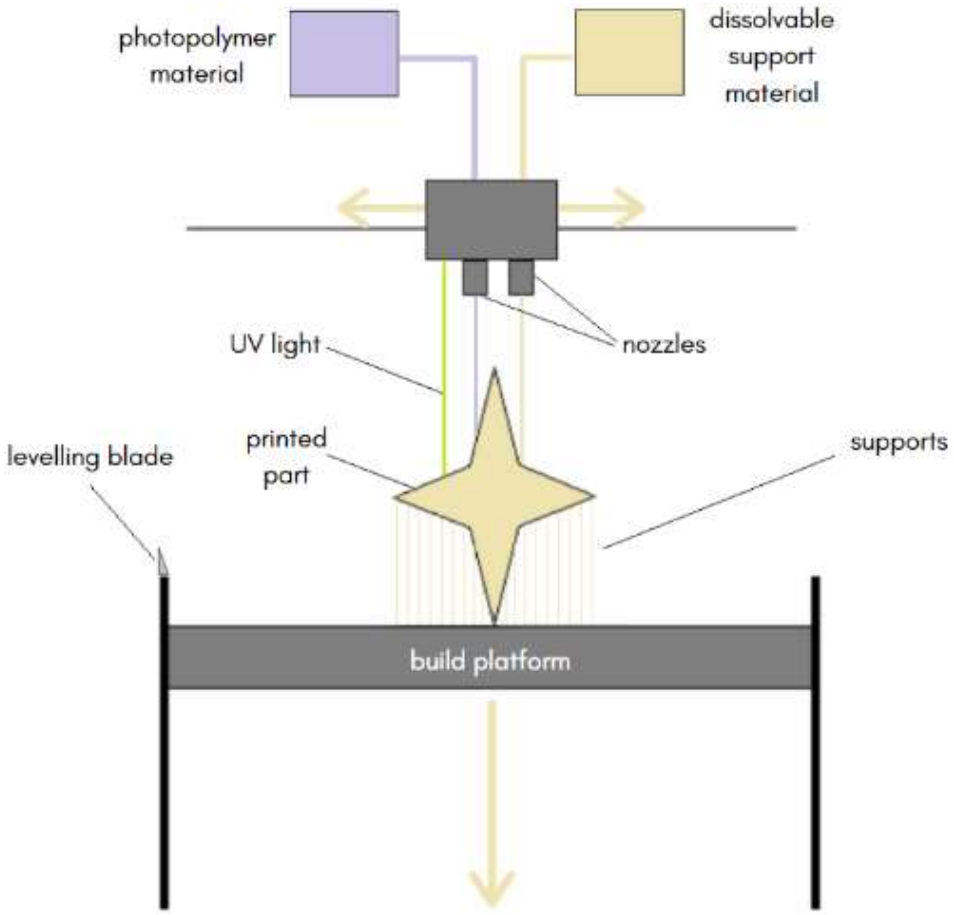

Figure 2.6: Material jetting schematic diagram. Adapted from 3DExperience. [26]

This technique offers superior detail, accuracy and surface quality. [14, 26] However, the process is slow and material selection is limited. Builds are also fragile due to the wax-like nature of the materials. [14]

Vat Polymerisation

Vat polymerisation is the process by which a vat of resin is photopolymerised layer-by-layer, using light of a certain wavelength. [2, 14] This technique is comparatively rapid versus other AM technologies and provides favourable accuracy and surface finish. It is an expensive technique, limited to photocurable resins which may continue to be affected by UV light post-print. Post-processing times can be lengthy. [14] Vat polymerisation techniques may utilise a 'top-down' approach, where the build platform is suspended upside-down above the vat, with the energy source underneath, or a 'bottom-up' approach, where the energy source is situated above the vat, and the build platform is progressively lowered into the resin. [28] The three main processes are stereolithography (SLA), digital light processing (DLP), and continuous digital light processing (CDLP). [14] SLA involves the use of a laser to cure each layer of photopolymerisable resin. [2, 23]

DLP is a rapid process, which sees a light projector underneath the resin vat curing each layer at a time. Subsequently, the printing platform is shifted, allowing fresh resin to be cured on top. [2, 29] CDLP has the same principal, but with the continuous motion of the build block in the z-direction, to further reduce print time. [2, 30]

The vat has a transparent membrane base through which either UV or white-light light is projected. [31] This membrane acts as a substrate against which each layer of resin can cure. This process is further illustrated in Figure 2.7. Depending on the complexity of the system, some machines include heated vats, allowing for a more controlled environment. A roller or wiper may also sweep across the vat between each layer, to keep the resin well mixed. [29]

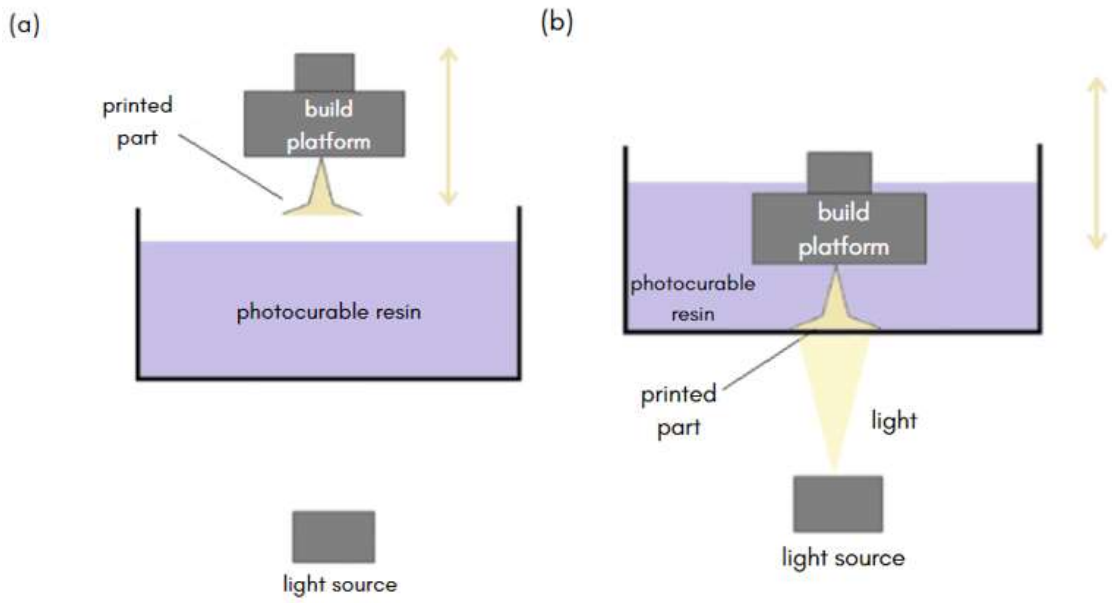

Figure 2.7: Schematic diagram of digital light processing. Adapted from Formlabs. [29]

DLP produces high-resolution builds, with features as small as 1 μm, [29, 32] in an efficient and cost effective manner. Further, the fact that there need only be enough resin to keep the vat membrane covered makes materials easier to swap, maintain and clean. However, the peel forces which occur as the print is lifted from the vat may cause damage and limit the use of flexible materials. Significant support structures may also be required. [29]

2.1.2. Photopolymerisation

The mechanism by which stereolithography (SLA) technologies cure resin layers is known as photopolymerisation. This process involves the linking together of monomer units to form chains, known as polymers. Free radical polymerisation is a key process regarding SLA, and its four stages – free radical formation, initiation, propagation, and termination – are described in Figure 2.8. [33]

A photoinitiator is added to the resin, which serves as a catalyst for the initiation of the reaction. The further the reaction is able to advance, the longer the polymer chain will be. This increases the molecular weight of the chain, which is an asset. Once the polymer chains have grown sufficiently to be in close proximity with one another, cross-linking is free to occur, which strengthens the material. [32] Termination may occur via recombination, where two chain ends combine with each other, forming a chain with double the molecular weight; [34] disproportionation, where a hydrogen atom is abstracted from one chain end to another; [35] or the occlusion of the free radical by a polymer. [32, 36]

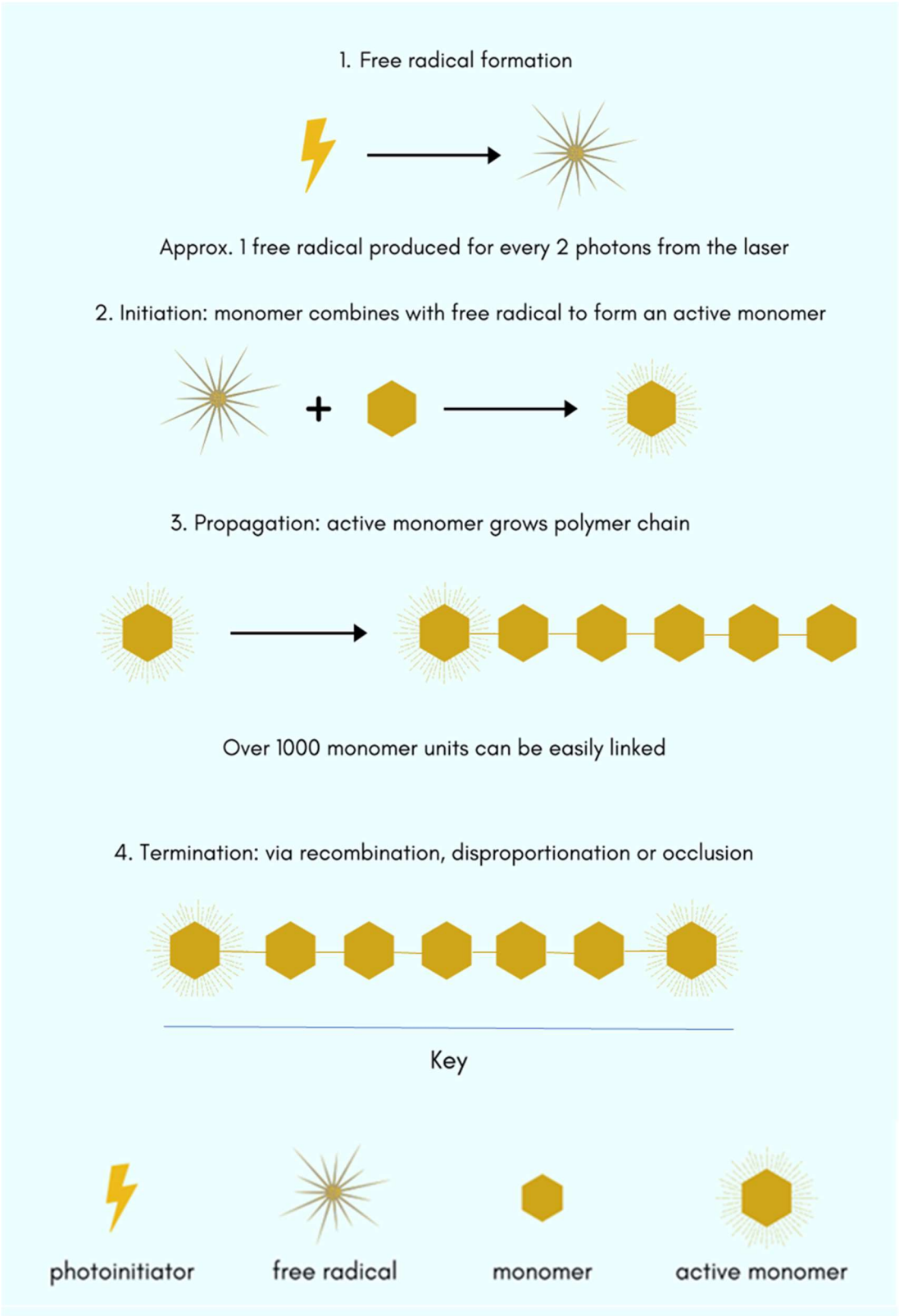

Figure 2.8: Schematic diagram of the free radical polymerisation process. Adapted from Rosen. [32]

2.1.3. Materials

PEGDA

Poly(ethylene glycol) diacrylate (PEGDA) is a biocompatible, [37] cross-linkable polymer which is formed by end capping polyethylene glycol (PEG) with acrylate groups. [38, 39] Cross-linked PEGDA boasts exceptional stiffness; [40, 41] PEGDA has been used as an additive in hydrogels to encourage cross-linking and slow biodegradation. [42] It can be readily photopolymerised; thus, it may be utilised in some 3D printing processes. [37, 38] Varying the composition of PEGDA materials, as well as adjusting photopolymerisation parameters, enables adjustment of the material's chemical and mechanical properties. [43]

Carbon-based materials

Carbon-based materials are a diverse material class, including micro- to nano-sized particles with varying complexities. They may be insulating or conductive, and their surface properties range from flat to porous. [44] Structures also vary in hardness and reactivity, and range in cost. Well established carbon materials include graphite, glassy carbon and carbon black; more recently, the category has evolved to include microfabricated carbon, including nanotubes, conductive diamond and carbon composites. [45]

In the field of bioelectrochemistry, carbon materials are one of the most favoured for the construction and modification of electrodes, [45, 46] since they display a high sorption ability, and their surfaces are electrochemically inert. Compared to metal electrodes, carbon-based electrodes enable stronger electrocatalytic reactions, due to carbon's surface oxides and predisposition to adsorb molecules from solution. [45]

Glassy Carbon

Glassy carbon (GC) is an isotropic carbon allotrope [47-49] which consists primarily of non-graphitising, [50, 51] sp^2-bonded carbons. [52, 53] It is formed by the controlled pyrolysis of organic polymers and displays glassy, ceramic and graphitic properties. [54] Its many benefits include gas and liquid impermeability; [48, 53, 54] excellent thermal and chemical stability; [55] and biocompatibility. [47, 53] GC is a popular choice for electrode manufacture, due to its physical properties and chemical inertness. [48, 56] It is employed widely in the field of electrochemistry [54] and benefits from a wide electrochemical stability window. [53]

GC Structure

GC has a turbostratic-like structure, [57] which exists somewhere between an amorphous carbon phase and a crystalline graphite phase [58] and produces an isotropic material. [54] It consists of randomly oriented ribbon molecules which link together graphite-like hexagonal layers. [51, 54, 57, 59] Both trigonal and tetrahedral carbon atoms exist in GC, with tetrahedral carbons forming the bulk of the linkages between graphitic layers. [51] Its low density (1.3 – 1.5 gcm^{-3}) [49, 57] is attributed to its porous microstructure [60] and the presence of tetrahedral cross-links between layers. [57]

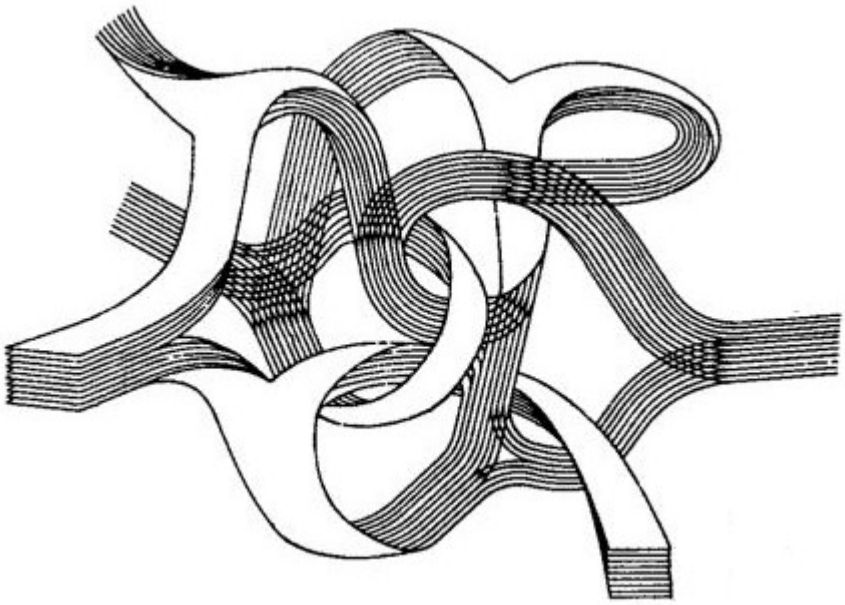

Figure 2.9: Schematic diagram of glassy carbon structure, as proposed by Jenkins et al. [59]

Carbon Nanotubes

CNTs are rapidly gaining interest in the field of analytical chemistry, since their structure lends itself so well to high conductivity and a large surface area for electrochemical assessment. [61-64] Their nanometre dimensions and highly symmetrical structure endow them with exceptional electronic properties. [65, 66] The nature of the chemical bonds between carbon atoms and the geometric arrangement of these bonds contribute to the mechanical properties of CNTs. Their structure exclusively contains σ bonding (formed by end-to-end orbital overlap), considered to be the strongest chemical bond in nature; thus, their mechanical properties are expected to be remarkable. [66] Generally, they are characterised via methods such as spectroscopy, microscopy, and diffraction. [67]

CNT Structure

CNTs can be defined as cylindrical fullerenes consisting of enrolled graphitic sheets, though it may be more accurate to state that their structure lies between that of fullerenes and graphite. [67, 68] Like graphite, their atoms are arranged in hexagonal structures. Their diameters are in the nanometre range, with lengths of micrometres; since they have a length to diameter ratio of over 1000, they can be considered as being virtually two-dimensional. Whilst some CNTs are open ended, others are closed with full fullerene caps. [67] The two main categories of CNTs are single-walled CNTs (SWCNTs) and multi-walled CNTs (MWCNTs).

Single-walled CNTs

The formation of SWCNTs can be considered as a single graphene layer being rolled into a seamless cylinder. They usually measure approximately ten atoms around the circumference and tubes are around one atom thick. [69] SWCNTs contain two distinct regions: the sidewall and end cap of the tube, which each exhibit different physical and chemical properties. Compared to MWCNTs, they have separate electric properties, and may behave as a metal or semiconductor based on their structure.

Multi-walled CNTs

MWCNTs are formed by multiple graphene layers being rolled in on themselves to form a cylinder. They can be considered as a group of concentric SWCNTs with varied diameters. [67] Their length and diameter is different to that of SWCNTs; the outer diameter of an MWCNT can reach up to 15 nm, where SWCNTs typically have a diameter in the 1 – 2 nm range. SWCNTs are often curved rather than straight. [69] Currently, MWCNTs are not as well-defined as SWCNTs due to their complex structure; however, they are known to be more thermally and chemically stable. [70]

Fabrication of CNT-based sensors

Much is still to be understood regarding the physical and chemical properties of CNTs. [71] Their use is wide; their physicochemical properties lend themselves well to fields such as microelectronics, [72, 73] medicinal therapy, [74] electrochemical biosensors [61, 75-78] and chemical sensors. [78-81] The potential of CNTs to be built as nanowire networks make them an ideal choice for sensing applications, especially when combined with recognition elements. Their high surface area permits a wide dynamic range and resistance to fouling. Biological analytes have been amperometrically detected by CNT films functionalised with enzymes. [71]

Another notable use of CNTs is in the fabrication of electronic tongues and noses. Multichannel arrays can be utilised for the simultaneous detection of multiple analytes, a similar process to olfaction and taste. [82] Sensor arrays based on CNTs have been used to detect volatile organic compounds [83, 84] and differentiate malignant cells from non-malignant cells. [85]

Carbon black

The use of carbon black (CB) in sensor and biosensor applications has gained traction in recent years, and it is now widely recognised for its chemical, mechanical, and physical properties. [44, 75, 86-91] Its low cost [44, 92] renders it widely accessible, and its high surface area [46, 87, 92] is a useful attribute. CB shows promise regarding its use in 3D printing technologies. Its dispersibility in solvents [93-98] coupled with its exceptional electrical conductivity [44, 92] could allow for the successful printing of conductive layers within a design.

The structure of CB lends itself well to electrochemical applications, and its use in electrochemistry is increasing. [44] It boasts fast electron transfer kinetics [44, 98] and has

excellent electrocatalytic properties. [96] Vicentini *et al.* successfully demonstrated that modified electrodes based on CB displayed enhanced electrochemical characteristics, including improved kinetic electron transfer and analytical sensitivity. [98, 99] Compared to other ubiquitous carbon materials, these characteristics proved to be comparable or in some cases better, particularly compared to CNTs. [45, 93, 98, 99]

CB Structure

CB is an amorphous, [97] quasi-graphitic material. [88] It is comprised of colloidal carbon particles [45] which have diameters in the nm range. [44 45, 92] These particles are produced via the incomplete combustion of carbon, [45, 97] and they fuse together to form aggregates. [97] CB's surface characteristics include an abundance of defect sites [99] and oxygenated species. [88]

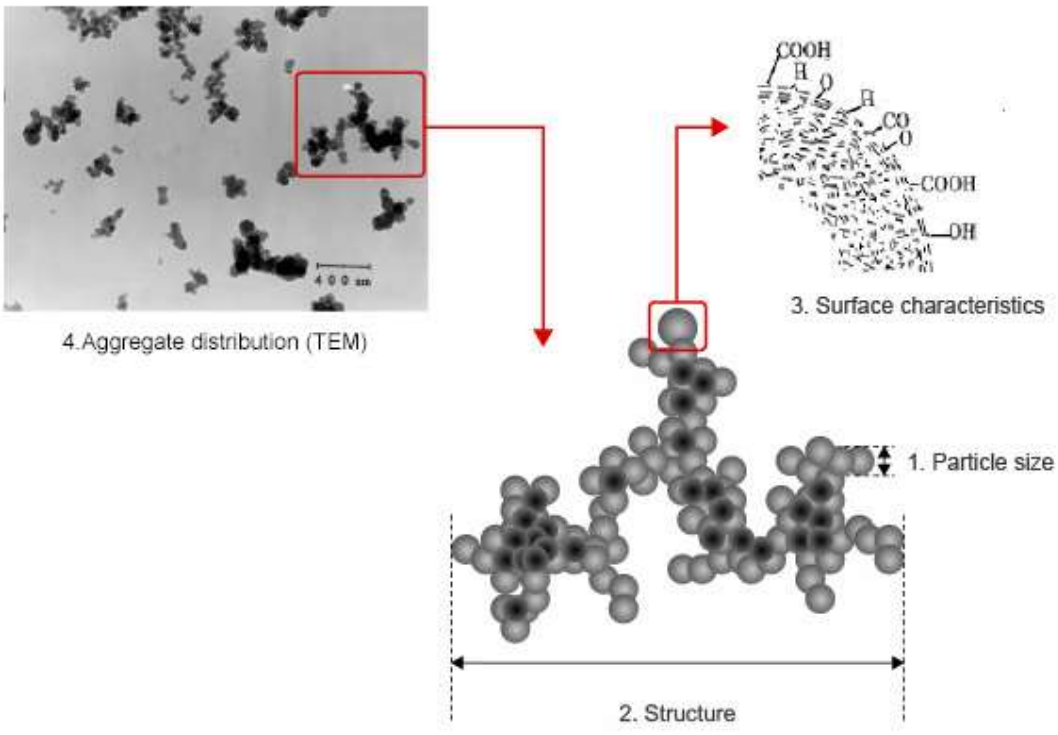

Figure 2.10: Carbon black structure and surface characteristics [100]

Fabrication of CB-based sensors

CB has been exploited across a wide range of sensor fabrication and modification. It has been used to create CB-based paste electrodes; [101-105] to modify GC electrodes; [44, 98, 106] to modify SPEs; [97, 102, 107-113] and in the 3D printing of an electrochemical sensing platform. [114] CB-modified electrodes have exhibited enhanced analytical sensitivity and an increased electron transfer rate. [98, 99] These benefits can be attributed to the ability of CB to modify conductivity and enzyme loading areas, resulting in heightened signals and high sensitivity. [92] Thus, CB is an attractive choice for biosensor design since it can be combined with enzymes to improve sensitivity. [93, 115-118] Utilising CB for the purposes of electroanalysis is a relatively new field of research, with a great deal of potential. [44] Various compounds have been detected by acetylene black modified sensors using voltammetric methods. [119-121]

2.2 Electrochemistry

2.2.1. Electron transfer reactions

Electron transfer describes the movement of an electron from a donor (a substance containing high energy electrons) to an acceptor (a substance containing low energy unfilled orbitals). The overall reaction comprises two half reactions: oxidation and reduction. Oxidation describes the loss of electrons and is achieved by the acceptor; reduction describes the gain of electrons and is achieved by the donor. [122]

A typical redox reaction can be expressed as shown in Equation 2.1:

$$Red1 + Ox2 \leftrightarrow Ox1 + Red2 \qquad (2.1)$$

where *Red1* is the reducing agent and *Ox1* is its oxidised form, following the transfer of electrons; and *Ox2* is the oxidising agent, whilst *Red2* is its reduced form. Thus,

Red1 is the reduced form of species 1, whilst *Ox2* is the oxidised form of species 2. This is a spontaneous reversible reaction, so it can be assumed that the donor orbitals have a higher energy than the acceptor orbitals. [122]

In dynamic experiments, the sample is often present in its completely oxidised or reduced form, whilst in static experiments, both forms are usually present. In reality, simple redox reactions may be perturbed by finite electron transfer rates, adsorption onto the electrode surface, or homogenous chemical kinetics. If one or more electroactive species exist in equilibrium, electrochemical methods may be used to perturb the equilibrium and solution chemistry may be studied. [123]

Electron transfer kinetics

The flow of current in an electrochemical cell is controlled by:

1. Electron transfer rate between the electrode and the solution species
2. The exchange of material at the electrode interface

Electron transfer kinetics are used to present a quantitative model of how electrode voltage influences electron transfer rates. The transfer of a single electron between two species (O) and (R) may be written:

$$O(s) + e^{-}(m) \leftrightarrow R(s) \qquad (2.2)$$

The current flowing in the reductive (i_c) and oxidative (i_a) steps can be predicted as follows:

$$i_c = -FAk_{red}[O]_O \quad (2.3)$$

$$i_a = FAk_{ox}[R]_O \quad (2.4)$$

Both currents are related to the area of the electrode (A), the electron transfer rate constant (k_{red}/k_{ox}) and Faraday's constant (F). The i_c relates to the reactant surface concentration ($[O]_o$) and is negative, whilst for i_a, the surface concentration is of species R. The currents have different signs to account for the current flowing in opposite directions. [124]

2.2.2. Fermi-level

Electrode reactions are driven by the application of a voltage, which in turn supplies electrical energy. The result is that the 'energy' of the individual electrons within a metal electrode may be altered. Atoms are closely packed within a metal, with strong overlap between them, which endows the metal with a continuum of energy levels. Available electrons fill the states from the bottom upward. [124]

The Fermi-level (E_F) describes the energy at which the 'top' layer of electrons sit. It is not a fixed value and may be altered by applying a voltage to the electrode. The pertinent orbital energies of a molecule (O) in solution are the highest occupied molecular orbital (HOMO) and the lowest unoccupied molecular orbital (LUMO). If the E_F of the metal has a lower value than the LUMO, it is thermodynamically unfavourable for an electron to transfer from the electrode to the molecule. If it has a higher value than the LUMO, then this process becomes favourable. Whether the process occurs depends on the kinetics of the electron transfer reaction. [124]

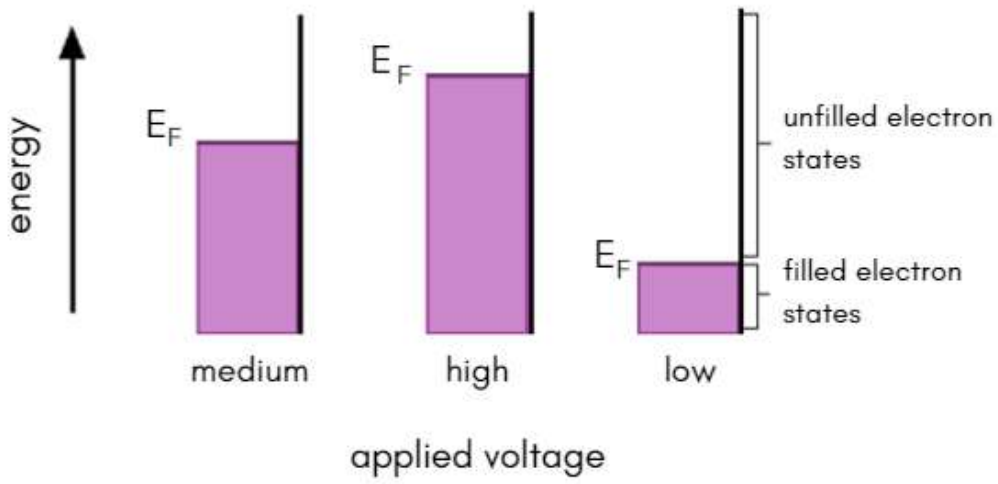

Figure 2.11: Applied voltages and their related Fermi-levels Adapted from Fisher, A.C. [124]

2.2.3. Electrolysis

Charge transfer between a species in solution and the electrode is termed electrolysis and involves passing a current through a substance (often a liquid) to incur a chemical reaction. This usually results in compound deposition onto the electrode surface. The electrolyte contains ions which are both positive and negative and can move freely towards the oppositely charged electrode. This results in a flow of electricity. [125]

The reaction involves three main steps:

1. The reactant moves towards the electrode surface
2. Electron transfer occurs between the electrode and the nearby reactant, via quantum mechanical tunnelling
3. Once formed, the product moves off into the solution and is replaced with fresh reactant [124]

Redox reactions at the surface of the electrodes allow electricity to continue to flow; the cathode gains electrons whilst the anode loses them. [125] There are many factors which may affect electron transfer reactions, including the voltage applied to the electrode, species reactivity, the nature of the electrode surface and the interfacial region structure. [124]

2.2.4. The Electrical Double Layer

The interface between the electrode and electrolyte causes disruption to the solution, as the interactions between the two will vary greatly to those in the solution. If electrodes are potentiostatically controlled, there will also be influence from the electrode's charge. The resultant interactions between the ions in the solution and the electrode surface are considerable and create a region known as the electrical double layer. Two main models exist to explain its effects: the Helmholtz model and the Stern model. [124]

Helmholtz Model

The Helmholtz model assumes that electron transfer reactions do not occur at the surface of the electrode and that the solution is purely electrolyte. Interactions between ions in the solution and at the electrode surface are assumed to be electrostatic since an abundance or deficiency of electrons at the electrode surface causes the electrode to hold a charge density. A neutral interface is achieved if the electrode charge is matched by redistribution of ions near the surface of the electrode.

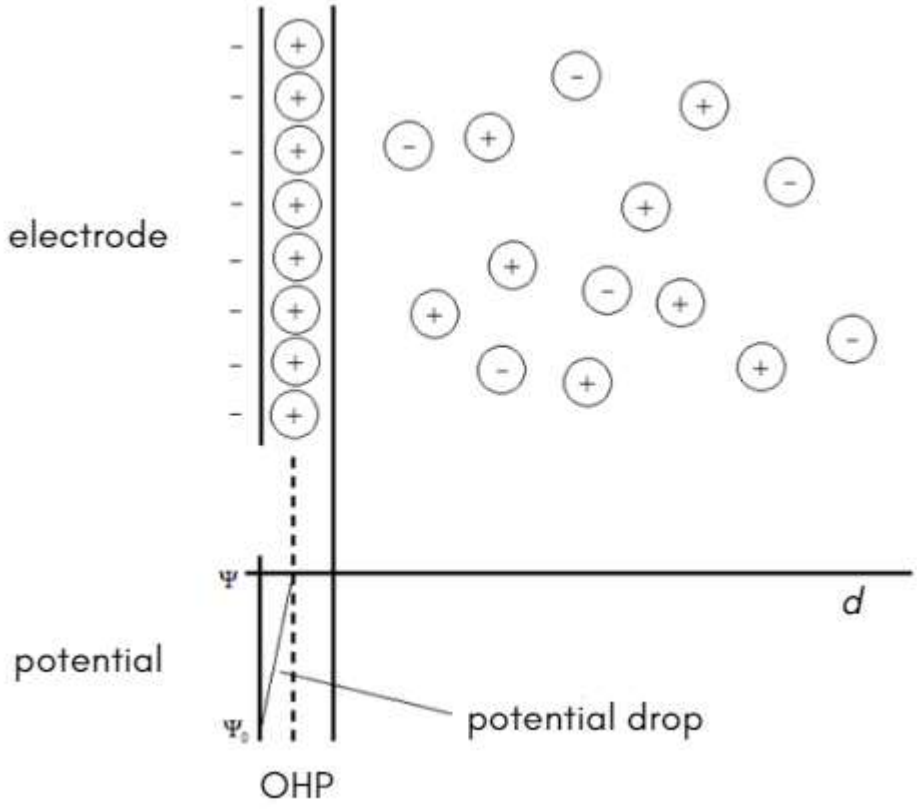

Figure 2.12: Helmholtz model of the electrical double layer. Adapted from Fisher, A.C. [124]

Ions attracted to the electrode surface are postulated to form a layer at the electrode surface which balances the electrode charge. The distance of approach is surmised to be restricted to the radius of the ion, plus a single surrounding sphere of solvation. Ultimately, two layers of charge are formed (known as the electrical double layer) along with a local potential drop, termed the outer Helmholtz plane (OHP). The result is that of the potential drop which occurs between the two plates of a capacitor; thus, capacitive elements are employed to model the response of an electrochemical system to electrolyte redistribution. [124]

Stern Model

The Helmholtz model gives a preliminary description of the behaviour of the electrical double layer but does not consider vital factors, such as solution diffusion or mixing, electrode surface adsorption and interactions between the electrode and solvent dipole moments. The Stern model accounts for some of these limitations. It is assumed that ions are able to move within the solution, which means that electrostatic interactions and Brownian motion are at odds with each other. There still exists a region local to the electron surface which contains an excess of one type of ion, but the potential drop now extends over a region known as the diffuse layer. Over time, these early models have been improved upon, with numerical modelling now utilised to explore redistribution effects as a result of varied electrode potential. [124]

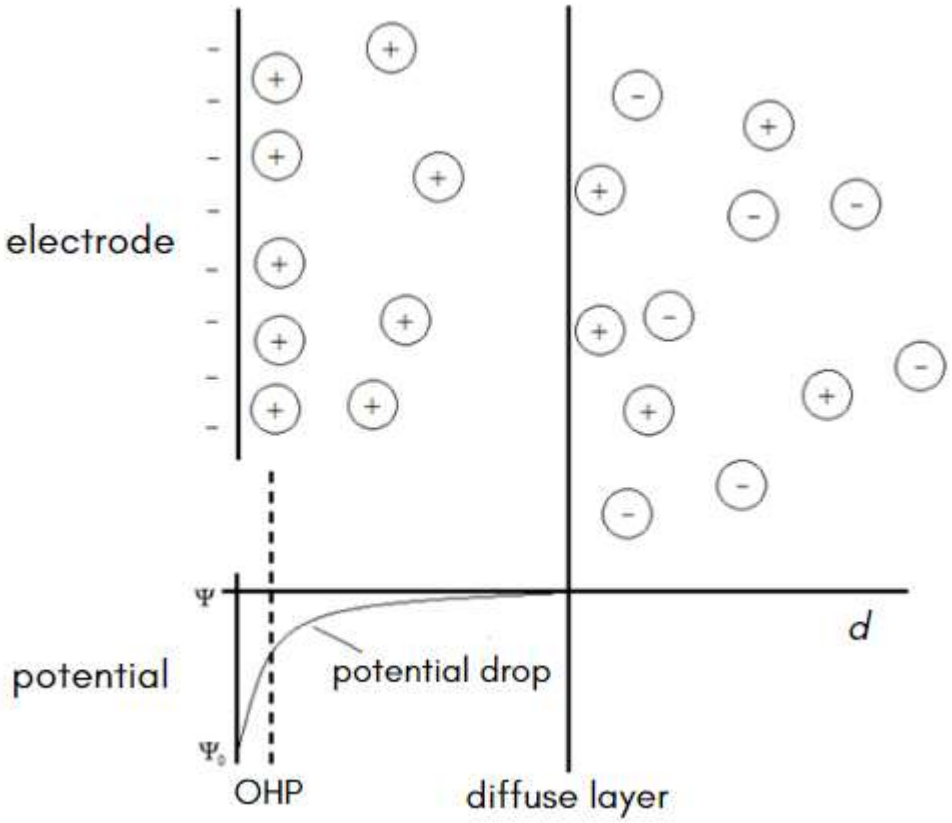

Figure 2.13: Stern model of the electrical double layer. Adapted from Fisher, A.C. [124]

2.2.5. Mass Transport

We can predict from the electron transfer model that as voltage increases, reaction rate and thus current will increase exponentially. Therefore, in theory, it should be possible to pass unlimited quantities of current. In reality, this is not the case, as Equation 2.3 demonstrates.

For a fixed electrode area, the reaction can be controlled by the rate constant (k_{red}) and the surface concentration of the reactant ($[O]_O$). A large rate constant causes reactant near the interface to be converted into products rapidly; therefore, current is controlled

by how much fresh reactant is able to reach the interface from the bulk solution. Mass transport describes the various ways in which material can move within a solution. There are three forms which can influence electrolysis: diffusion, convection, and migration.

Diffusion

Diffusion occurs in every solution and is the result of localised uneven reagent concentrations. Entropic forces are prevalent and act to smooth out uneven concentration distributions. When a barrier between two different reagents is removed, they are able to mix. On a microscopic scale, this is essentially random, however, on a large-scale model, statistics can be used to predict how far material will move over time. This is often termed the random walk model.

Diffusion is considerable within electrolysis experiments, as conversion can only occur at the electrode surface. This creates a concentration gradient, whereby a lower concentration of reactant exists near the electrode, compared to the bulk solution. The opposite is true for product concentration.

Fick proposed two laws to mathematically quantify the rate of movement of a material by diffusion:

$$J_O = -D_O\left(\frac{\partial C_o}{\partial x}\right) \quad (2.5)$$

Where J_O is termed diffusional flux. It is related to the concentration gradient and diffusion coefficient (D_O). A negative sign is required as the material is moving down a concentration gradient.

Fick's second law describes how material concentration varies as a function of time:

$$\frac{\partial C_o}{\partial t} = D_O\left(\frac{\partial^2 C_o}{\partial x^2}\right) \quad (2.6)$$

Diffusion is considered to be normal to the electrode surface in the x direction. Diffusion rate is influenced by the concentration gradient: the sharper the concentration increase, the greater the diffusion rate. Diffusion is commonly the most notable transport process for electrolysis reactions. Fick's second law can be used to predict species concentration digression as a function of time within an electrochemical cell. These expressions are often solved using computational models.

Convection

Convection occurs when force is applied to a solution. There are two forms: natural and forced convection. Natural convection is ubiquitous and occurs due to common thermal or density differences. It acts to indiscriminately mix the solution. Natural convection may have an impact on electrochemical experiments where the run time exceeds 20 seconds.

Forced convection is deliberately introduced convection. Its effects are several orders of magnitude higher than those of natural convection. Thus, it acts to expel any

random motion, contingent upon being introduced in a well-defined, quantitative manner. Forced convection may be applied to an experiment to increase the rate of mass transfer.

For laminar flow conditions, one dimensional convection is predicted by:

$$\frac{\partial C_o}{\partial t} = -v_x \left(\frac{\partial C_o}{\partial x}\right), \qquad (2.7)$$

where v_x is the solution velocity. [124]

Migration

Migration is an electrostatic effect which occurs due to voltage being applied across electrodes. A charged interface is created; nearby charged species will be electrostatically attracted to or repelled from it. The resultant migratory flux may be mathematically described in one dimension:

$$\frac{\partial C_o}{\partial t} = -uC_o \left(\frac{\partial \emptyset}{\partial x}\right) \qquad (2.8)$$

In practice, it is difficult to calculate migration effects accurately, as experimental solutions are affected by ion solvation and diffuse layer interactions.

In terms of creating a quantitative model of current at the electrode surface, it is impossible to account for the effects of 3-dimensional diffusion, convection, and migration. However, it is possible to surpass the need to by creating a well-controlled electrochemical experiment. [124]

2.2.6. Voltammetry

Instrumentation

The electrochemical cell contains a working electrode (WE), where the redox reaction takes place. Its potential is compared against that of a reference electrode (RE) which maintains a stable equilibrium potential. During a cyclic voltammetry (CV) scan, an excitation signal is applied across the WE and RE. [123, 126] Generally, a 2-electrode system may be used in cases of low current flow and high conductivity within the solvent-electrolyte system, since the applied voltage is the same as the real potential at the WE. [127]

However, a 3-electrode system is commonly utilised in cases where these conditions do not apply or for the interpretation of redox processes and/or sensor developments. The presence of a counter electrode (CE) ensures that the RE will not be subjected to large currents, which may alter its potential. The purpose of the CE is to supply enough current to sustain electrolysis at the WE. [123]

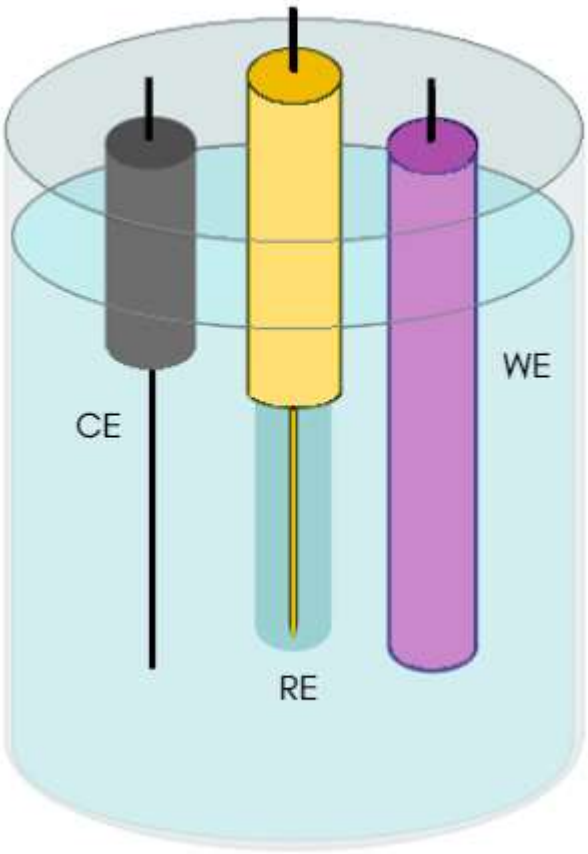

Figure 2.14: A typical three-electrode electrochemical cell. Adapted from Elgrishi et al. [128]

Both CV and differential pulse voltammetry (DPV) utilise a three-electrode arrangement, comprising a WE, CE and RE. [129] The WE is that at which the electrochemical event is occurring. When a potential is applied to the WE, the circuit through which the resulting current flows is closed by the CE. The RE provides a point of reference against which to compare potentials from the other electrodes. [128] An applied potential gives rise to a shift in current, indicative of a chemical reaction.

Cyclic voltammetry

Principles

CV facilitates the investigation of redox processes by quiescent molecular species, studying the resulting chemical reactions initiated by a potentiostat-applied potential.

A linear potential scan is applied across the WE and RE and sweeps from one potential to the other and back in a triangular waveform, as shown in Figure 2.15.

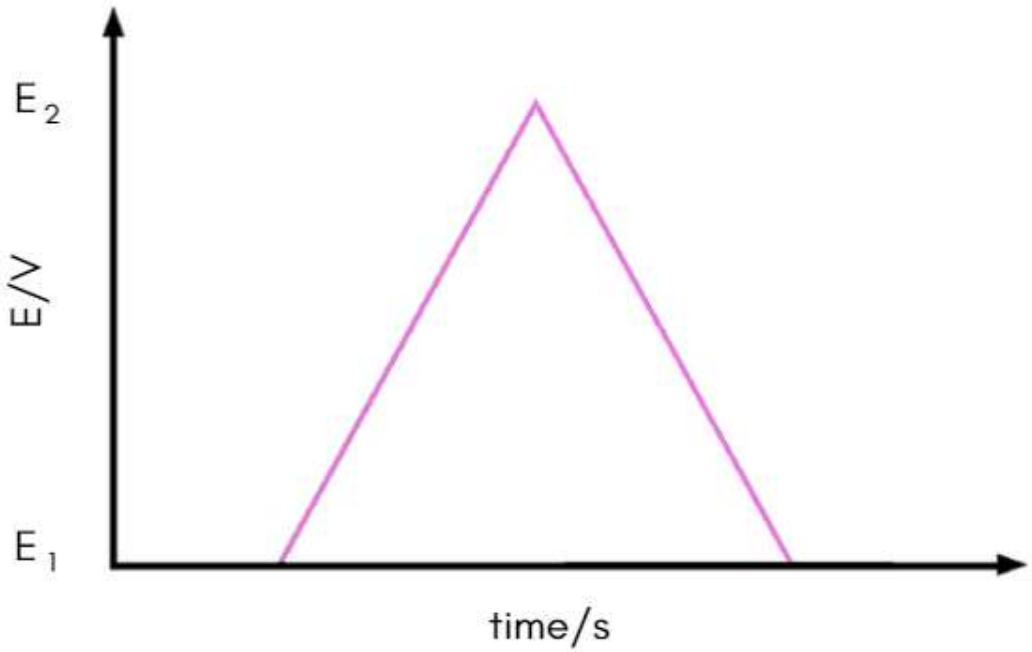

Figure 2.15: CV triangular input potential. Adapted from Fu et al. [130]

The forward scan causes a concentration of the product to be produced near the WE, before being oxidised during the reverse scan back to the original material. The resulting current is measured as the potential is ramped between each voltage. Therefore, a species may be generated during the forward scan and its fate probed with the reverse scan and any subsequent cycles. [123] Often multiple scans will be very similar, although any changes are valuable for providing insights into reaction mechanisms. [126]

Certain factors may affect the CV scan, leading to a deviation from expected results. A common concern is ohmic drop, which is characterised as a drop in potential

between the WE and RE. [131] This may arise due to resistance in the electrolyte or at interfaces, such as that caused by surface films. [132]

Ohmic drop (ΔE_{ohmic}) is defined as the product of the current (i) and the ohmic resistance (R_u):

$$\Delta E_{ohmi} = iR_u \qquad (2.9)$$

The resultant effects can impact electrolysis; however, they may be alleviated using a 3-electrode cell. This setup decreases ohmic loss through the solution, thus minimising voltage errors, by allowing the RE to be close to the WE. [133] Ohmic drop may also be minimised by introducing a supporting electrolyte and reducing the size of the WE (thus decreasing double layer capacitance). [131]

Diffusion is the sole means by which mass transport of electroactive species may occur. Thus, a supporting electrolyte of 0.1 M must be added to the solution to prevent migration currents from affecting the measurement. The rate of diffusion of ions across the ion bridge is variable, which causes separation of the RE from the solution. The net difference in the movement of cations and anions leads to a charge separation and, in turn, an electrochemical potential difference. The use of supporting electrolyte ions with similar diffusion coefficients can minimise this. [128, 133]

During cyclic voltammetry, the charged surface of the WE forms a capacitor with the ions which accumulate adjacent to it. The capacity of this system is defined according to Equation 2.10:

$$C = \frac{Q}{E} \qquad (2.10)$$

Where Q is the charge stored by the capacitor and E is the potential across it. The result is a current, known as capacitive current (i_c), which can cause inaccuracies within the electrochemical experiment. The current of interest is the Faraday current, which arises due to the electrochemical reaction, whereas i_c is a purely physical effect. This current acts to charge/discharge the capacitor and decays exponentially over time:

$$i = \frac{E^C}{R} e^{-\frac{t}{RC}} = i^0 e^{-\frac{t}{RC}} \qquad (2.11)$$

Where E^C is the charging potential, i^0 is initial current, R is circuit resistance and C is the capacity of the capacitor. The Faraday current decays with $t^{-1/2}$ for a free diffusing species in solution; thus, capacitive current decays at a much higher rate, as illustrated in Figure 2.16:

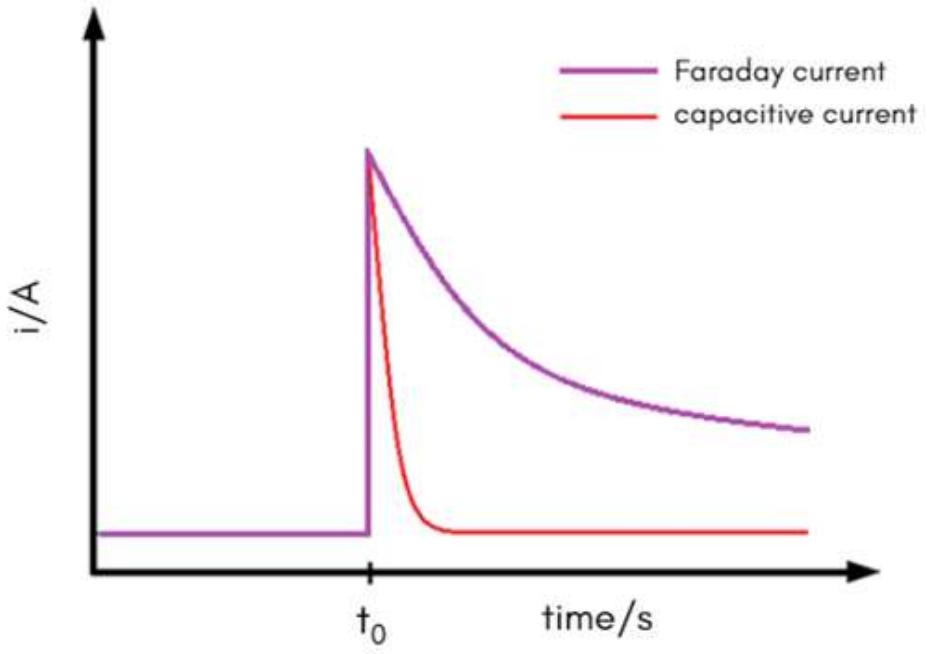

Figure 2.16: Capacitive vs. Faraday current over time. Adapted from PalmSens. [134]

Given that the electrode potential is continuously shifting during a CV scan, i_c is constantly present. In this case, the capacity can be calculated according to Equation 2.12:

$$C = \varepsilon_0 \varepsilon_r \frac{A}{d} \qquad (2.12)$$

This equation is based on a plate capacitor model, where ε_0 is the electric field constant, ε_r is the relative permeability of the inter-plate solution, d is the distance between the plates and A is their surface area. Of these variables, only A may be altered, as d and ε_r are solution dependent. Surface area A of the electrode may be reduced by polishing, thus reducing i_c.

However, the fact that digital potentiostats are incapable of providing a truly linear sweep also works in favour of reducing i_c. Since only discrete values can be applied, the potential is incrementally increased and the capacitive current is best described according to Equation 2.11. [134]

Applications

CV is used extensively within the area of electrochemistry to study the redox couple behaviour of electroactive species. This behaviour may be studied over a wide potential range within a relatively short time frame. [123] Applications of CV are far-reaching, largely due to its simplicity and cost effectiveness coupled with rapidity and sensitivity. CV lends itself to studying the electrochemical properties and behaviour of species of interest, as it can provide information on the relationship between structure, potential, and characteristic activities. [135] Further, CV may be used to study simple redox processes, characterise multi-electron transfer processes and provide insights into kinetics of electrode reactions, including coupled chemical reactions and

homo- and heterogenous electron transfer steps. [127] Of particular relevance to this body of work, CV has been used to characterise biosensors, since their performance relies on redox activity and capacitance. [136]

Interpretation of cyclic voltammograms

Reversible system

If a reaction can occur with enough speed for an equilibrium to be maintained at the electrode surface between the concentrations of the oxidised and reduced forms, the equilibrium potential is determined by the Nernst equation:

$$E = E^{0`} - \frac{RT}{nF} ln \left(\frac{[R]}{[O]}\right)_{x=0} \qquad (2.13)$$

Where E is the applied potential, $E^{0`}$ is the formal reduction potential of the redox couple against the electrode in volts, n is the number of electrons, *[R]* and *[O]* are the surface concentrations in mol cm^{-3} of the reduced and oxidised species respectively, F is Faraday's constant, R is the gas constant and T is the temperature in Kelvins. This equation is also used to calculate cell potential during the reaction, or when conditions are out with standard state.

For an electrochemically reversible couple, the formal peak potential equates to the average of peak potentials E_{pa} and $E_{pc:}$ [123, 127]

$$E^{0,} = \frac{E_{pa}+E_{pc}}{2} \qquad (2.14)$$

The separation between peak potentials can be used to determine the number of electrons (n) in the reaction: [123, 133]

$$\Delta E_p = E_{pa} - E_{pc} \cong \frac{0.059}{n} \qquad (2.15)$$

For an electrochemically reversible one-electron redox couple, this value is expected to be 59 mV. Increased peak separation suggests irreversibility and may be caused by ohmic drop. [128]

For a reversible system, the Randles-Sevcik equation (Equation 2.16) defines the peak current (at 25°C):

$$i_p = (2.69 \times 10^5) n^{3/2} A D^{1/2} C v^{1/2} \qquad (2.16)$$

Where n describes the number of electrons, A is the electrode area in cm^2, D is the diffusion coefficient, C is the bulk concentration in mol cm^{-3} and v is the scan rate in V s^{-1}. [123, 127, 129, 137, 138] This equation can also suggest if an analyte is diffusing freely in a solution, or to calculate diffusion coefficients. [128]

The ratio of i_{pa} to i_{pc} should be unity for a simple reversible couple:

$$\frac{i_{pa}}{i_{pc}} = 1 \qquad (2.17)$$

Experimentally, a reversible system would be implied when the ratio value is close to unity. The peak ratio is susceptible to effects from redox coupled chemical reactions and irreversibility. [123] These effects result in a deviation from unity, which may be indicative of slow electron transfer kinetics. [139]

Non-reversible system

In the case of non-reversible (irreversible or quasi-reversible) systems, Nernstian behaviour is not followed, so Equations 2.13 – 2.17 do not apply. If the exchange of electrons between the WE and the redox species is slow, the system is deemed

electrochemically irreversible. In the cyclic voltammogram, only one peak is observed in the forward scan as demonstrated in Figure 2.17. Compared to the potential scan rate or slow chemical reaction at the electrode surface, electron transfer processes are slow. In this case, the rate of the charge transfer processes is much slower than the rate of the mass transfer process. [123, 126, 140]

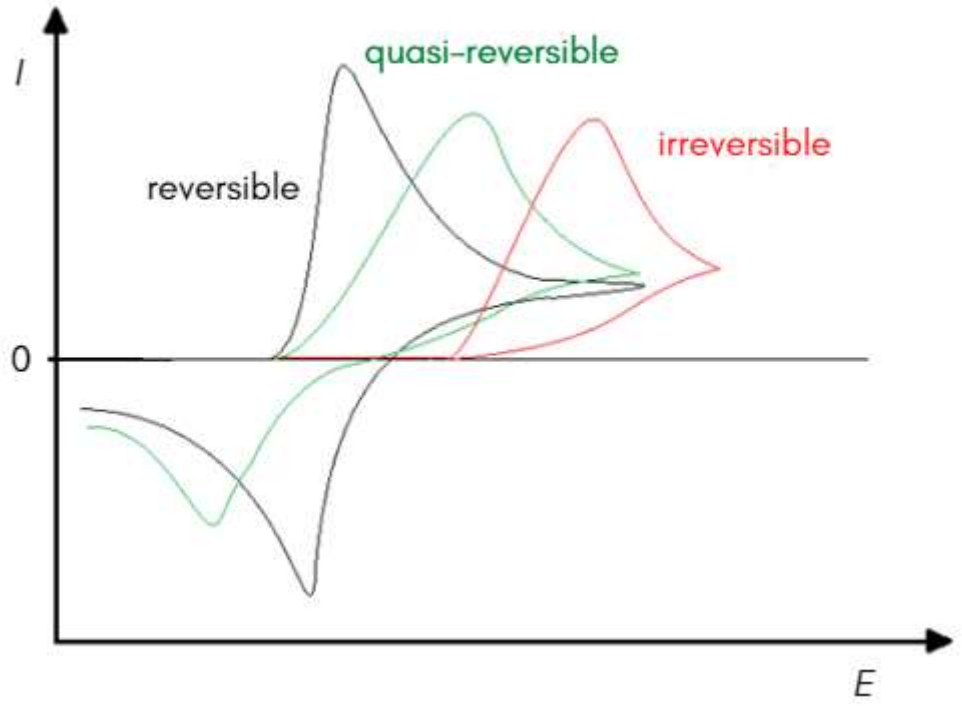

Figure 2.17: Cyclic voltammograms for reversible (black line), quasi-reversible (green line) and irreversible (red line) processes. Adapted from Wijeratne. [141]

Reactions may also be quasi-reversible; in that they may straddle the line between reversible and irreversible. In this case, the rates of mass transfer and charge transfer are competing and have similar values. The cyclic voltammogram is closer in appearance to that produced by a reversible system, as two peaks are observed. A larger peak separation indicates a slow redox reaction. [123, 126, 140]

Differential pulse voltammetry

Principles

The principles of DPV are similar to CV, although in this case the potential is applied by means of a series of pulses. DPV involves increasing the potential in only one direction, by means of a linear sweep.

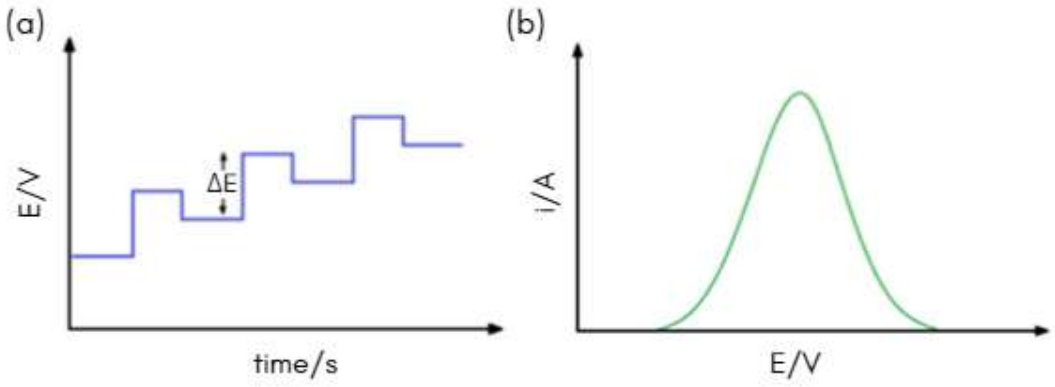

Figure 2.18: (a) staircase wave input potential (b) DPV voltammogram output. Adapted from Molina et al. [142]

The current is sampled before the pulse is applied and at the end of the pulse, enabling the elimination of capacitive current. Every pulse produces a discrete measuring point, $\Delta I_{n,dp}$:

$$\Delta I_{n,dp} = I_{n2} - I_{n1} \qquad (2.18)$$

Where n is the number of the respective pulse. The DPV output voltammogram represents each $\Delta I_{n,dp}$ data point as a function of V. [143]

Applications

DPV is the most widely applied voltammetric technique. [144, 145] This is largely due to its sensitivity. [143] DPV is more sensitive than CV for lower analyte concentrations,

eliciting a response for concentrations as low as 0.05 μM. [146] Its effectiveness as an analytical tool enables in-depth study of chemical reactions, including their mechanisms, kinetics and thermodynamics. DPV may also be used for quantitative analysis. [147]

2.3 Conclusion

The development of an electrochemical sensor for sensitive and facile *P. aeruginosa* detection would provide a significant breakthrough regarding the treatment of nosocomial infections. Carbon-based materials are particularly appropriate for this application, due to the presence of surface oxides, and ability to adsorb molecules from solution. Though a relatively new area of research, the utilisation of additive manufacturing techniques could prove to be advantageous in terms of manufacturing time and cost. Electrochemical techniques boast rapidity and sensitivity and are widely utilised for the detection of redox active analytes. The ultimate goal of this and future work is to print a three-electrode system whose design works to reduce possible limitations such as capacitive current. Disposable electrochemical sensors could be printed in high volumes and combined with techniques such as voltammetry to detect *P. aeruginosa* infections at an early stage. The aim of this project is to work towards the design and manufacture of a carbon-based, 3D printed electrochemical sensor for the detection of *P. aeruginosa.*

2.4 References

1. K. S. Prakash, T. Nancharaih and V. V. S. Rao, *Materials Today: Proceedings*, 2018, **5**, 3873-3882.
2. C. Y. Liaw and M. Guvendiren, *Biofabrication*, 2017, **9**, 024102.
3. T. Rayna and L. Striukova, *Technological Forecasting and Social Change*, 2016, **102**, 214-224.
4. C. L. Ventola, *Pharmacy and Therapeutics*, 2014, **39**, 704.
5. S. V. Murphy and A. Atala, *Nature Biotechnology*, 2014, **32**, 773-785.
6. J. Schweiger, F. Beuer, M. Stimmelmayr, D. Edelhoff, P. Magne and J. F. Güth, *British Dental Journal*, 2016, **221**, 555-560.
7. R. K. Chen, Y.-a. Jin, J. Wensman and A. Shih, *Additive Manufacturing*, 2016, **12**, 77-89.
8. S. Telfer, J. Pallari, J. Munguia, K. Dalgarno, M. McGeough and J. Woodburn, *BMC Musculoskeletal Disorders*, 2012, **13**, 84.
9. S. Kondor, C. G. Grant, P. Liacouras, M. A. J. J. R. Schmid, L. T. C. Michael Parsons, B. Macy, B. Sabart and C. Macedonia, *Journal of Medical Devices*, 2013, **7**.
10. J. J. Conti, *U.S. Energy Information Administration (EIA)*, 2012.
11. M. Sireesha, J. Lee, A. S. Kiran, J. b. Veluru, B. Kee and S. Ramakrishna, *RSC Advances*, 2018, **8**, 22460-22468.
12. M. Waller and S. Fawcett, *Journal of Business Logistics*, 2014, **35**.
13. International Organization for Standardization (ISO), *ISO /TC 261 Additive manufacturing*, 2015.
14. S. Mein, Understanding the Seven Types of Additive Manufacturing, https://www.firetrace.com/fire-protection-blog/additive-manufacturing, (accessed 22nd July, 2021).
15. 3DExperience, Binder jetting - BJ, https://make.3dexperience.3ds.com/processes/binder-jetting, (accessed 26th July, 2021).
16. A. Mohammed, A. Elshaer, P. Sareh, M. El-Sayed and H. Hassanin, *International Journal of Pharmaceutics*, 2020, **580**, 119245.
17. 3DExperience, Directed energy deposition - DED, LENS, EBAM, https://make.3dexperience.3ds.com/processes/directed-energy-deposition, (accessed 26th July, 2021).
18. V. Carlota, The Complete Guide to Directed Energy Deposition (DED) in 3D Printing, https://www.3dnatives.com/en/directed-energy-deposition-ded-3d-printing-guide-100920194/, (accessed 26th July, 2021).
19. Loughborough University, About Additive Manufacturing - Powder Bed Fusion, https://www.lboro.ac.uk/research/amrg/about/the7categoriesofadditivemanufacturing/powderbedfusion/, (accessed 26th July, 2021).
20. 3DExperience, Powder bed fusion - DMLS, SLS, SLM, MJF, EBM, https://make.3dexperience.3ds.com/processes/powder-bed-fusion, (accessed 26th July, 2021).

21. S. F. S. Shirazi, S. Gharehkhani, M. Mehrali, H. Yarmand, H. S. C. Metselaar, N. Adib Kadri and N. A. A. Osman, *Science and Technology of Advanced Materials*, 2015, **16**, 033502.
22. J. P. Kruth, P. Mercelis, J. Van Vaerenbergh, L. Froyen and M. Rombouts, *Rapid Prototyping Journal*, 2005, **11**, 26-36.
23. K. V. Wong and A. Hernandez, *ISRN Mechanical Engineering*, 2012, **2012**, 208760.
24. 3DExperience, Sheet lamination - LOM, SL, https://make.3dexperience.3ds.com/processes/sheet-lamination, (accessed 26th July, 2021).
25. 3DExperience, Material Extrusion - FDM, https://make.3dexperience.3ds.com/processes/material-extrusion, (accessed 26th July, 2021).
26. 3DExperience, Material jetting - MJ, NPJ, DOD, https://make.3dexperience.3ds.com/processes/material-jetting, (accessed 26th July, 2021).
27. AMFG Autonomous Manufacturing, A Comprehensive Guide to Material Jetting 3D Printing, https://amfg.ai/2018/06/29/material-jetting-3d-printing-guide/, (accessed 3rd August, 2021).
28. 3DExperience, Photopolymerization - VAT, SLA, DLP, CDLP, https://make.3dexperience.3ds.com/processes/photopolymerization, (accessed 29th July, 2021).
29. Formlabs, The Ultimate Guide to Stereolithography (SLA) 3D Printing, https://static.treatstock.com/static/fxd/wikiMaterials/resin/files/resin_3d_printing_guide.pdf).
30. J. R. Tumbleston, D. Shirvanyants, N. Ermoshkin, R. Janusziewicz, A. R. Johnson, D. Kelly, K. Chen, R. Pinschmidt, J. P. Rolland, A. Ermoshkin, E. T. Samulski and J. M. DeSimone, *Science*, 2015, **347**, 1349.
31. Q. Mu, L. Wang, C. K. Dunn, X. Kuang, F. Duan, Z. Zhang, H. J. Qi and T. Wang, *Additive Manufacturing*, 2017, **18**, 74-83.
32. D. W. Rosen, in *BioNanoFluidic MEMS*, ed. P. J. Hesketh, Springer US, Boston, MA, 2008, pp. 175-196.
33. P. F. Jacobs, *Rapid prototyping & manufacturing: fundamentals of stereolithography*, Society of Manufacturing Engineers, 1992.
34. Case Western Reserve University, Polymer Synthesis, https://web.archive.org/web/20100207162220/http://plc.cwru.edu/tutorial/enhanced/FILES/polymers/synth/synth.htm, (accessed 2nd August, 2021).
35. M. P. Stevens, *Polymer Chemistry: An Introduction* . , Oxford University Pres, New York, 1999.
36. C. H. Bamford, A. D. Jenkins and A. H. Wilson, *Proceedings of the Royal Society of London. Series A. Mathematical and Physical Sciences*, 1955, **228**, 220-237.
37. R. Mau, J. Nazir, S. John and H. Seitz, *Current Directions in Biomedical Engineering*, 2019, **5**, 249-252.
38. X. Tu, L. Wang, J. Wei, B. Wang, Y. Tang, J. Shi, Z. Zhang and Y. Chen, *Microelectronic Engineering*, 2016, **158**, 30-34.
39. X. Deng, B. Huang, R. Hu, L. Chen, Y. Tang, C. Lu, Z. Chen, W. Zhang and X. Zhang, *Journal of Materials Chemistry B*, 2021, **9**, 1315-1324.

40. M. P. Cuchiara, A. C. B. Allen, T. M. Chen, J. S. Miller and J. L. West, *Biomaterials*, 2010, **31**, 5491-5497.
41. V. Chan, J. H. Jeong, P. Bajaj, M. Collens, T. Saif, H. Kong and R. Bashir, *Lab on a Chip*, 2012, **12**, 2.
42. Y. Wang, M. Ma, J. Wang, W. Zhang, W. Lu, Y. Gao, B. Zhang and Y. Guo, *Materials (Basel)*, 2018, **11**.
43. Q. T. Nguyen, Y. Hwang, A. C. Chen, S. Varghese and R. L. Sah, *Biomaterials*, 2012, **33**, 6682-6690.
44. T. A. Silva and O. Fatibello-Filho, *Analytical Methods*, 2017, **9**, 4680-4687.
45. E. V. Suprun, F. Arduini, D. Moscone, G. Palleschi, V. V. Shumyantseva and A. I. Archakov, *Electroanalysis*, 2012, **24**, 1923-1931.
46. T. Kim, C. Ham, C. K. Rhee, S.-H. Yoon, M. Tsuji and I. Mochida, *Carbon*, 2009, **47**, 226-233.
47. J. Bauer, A. Schroer, R. Schwaiger and O. Kraft, *Nature Materials*, 2016, **15**, 438-443.
48. H. E. Zittel and F. J. Miller, *Analytical Chemistry*, 1965, **37**, 200-203.
49. O. J. A. Schueller, S. T. Brittain, C. Marzolin and G. M. Whitesides, *Chemistry of Materials*, 1997, **9**, 1399-1406.
50. S. Sharma, *Materials*, 2018, **11**.
51. T. Noda and M. Inagaki, *Bulletin of the Chemical Society of Japan*, 1964, **37**, 1534-1538.
52. P. J. F. Harris †, *Philosophical Magazine*, 2004, **84**, 3159-3167.
53. Y. Lim, J.-I. Heo, M. Madou and H. Shin, *Nanoscale Research Letters*, 2013, **8**, 492.
54. M. Hassler, in *Coatings for Biomedical Applications*, ed. M. Driver, Woodhead Publishing, 2012, pp. 75-105.
55. W. Chunlei, J. Guangyao, L. H. Taherabadi and M. J. Madou, *Journal of Microelectromechanical Systems*, 2005, **14**, 348-358.
56. A. Dekanski, J. Stevanović, R. Stevanović, B. Ž. Nikolić and V. M. Jovanović, *Carbon*, 2001, **39**, 1195-1205.
57. F. C. Cowlard and J. C. Lewis, *Journal of Materials Science*, 1967, **2**, 507-512.
58. P. Ruz, S. Banerjee, M. Pandey, V. Sudarsan, P. U. Sastry and R. J. Kshirsagar, *Solid State Sciences*, 2016, **62**, 105-111.
59. G. M. Jenkins and K. Kawamura, *Nature*, 1971, **231**, 175-176.
60. K. Kinoshita, *Carbon: electrochemical and physicochemical properties*, Wiley, 1988.
61. J. Wang, *Electroanalysis*, 2005, **17**, 7-14.
62. Ugo, P., L. M. Moretto and F. Vezza, *ChemPhysChem*, 2002, **3**, 917-925.
63. Q. Zhao, Z. Gan and Q. Zhuang, *Electroanalysis*, 2002, **14**, 1609-1613.
64. G. K. Knopf and A. S. Bassi, *Smart Biosensor Techology*, Boca Raton: CRC Press/Taylor & Francis, 2007.
65. M. S. Dresselhaus, G. Dresselhaus and A. Jorio, *Annual Review of Materials Research*, 2004, **34**, 247-278.
66. R. Ghasempour and H. Narei, in *Carbon Nanotube-Reinforced Polymers*, ed. R. Rafiee, Elsevier, 2018, pp. 1-24.
67. A. Aqel, K. M. M. A. El-Nour, R. A. A. Ammar and A. Al-Warthan, *Arabian Journal of Chemistry*, 2012, **5**, 1-23.

68. T. Yamabe, K. Fukui and K. Tanaka, *The Science and Technology of Carbon Nanotubes*, Elsevier Science, 1st edn., 1999.
69. N. Saifuddin, A. Z. Raziah and A. R. Junizah, *Journal of Chemistry*, 2013, **2013**, 676815.
70. J. Choi and Y. Zhang, Single, Double, MultiWall Carbon Nanotube Properties & Applications, https://www.sigmaaldrich.com/technical-documents/articles/materials-science/single-double-multi-walled-carbon-nanotubes.html).
71. V. Schroeder, S. Savagatrup, M. He, S. Lin and T. M. Swager, *Chemical Reviews*, 2019, **119**, 599-663.
72. Q. Cao and J. A. Rogers, *Advanced Materials*, 2009, **21**, 29-53.
73. S. Park, M. Vosguerichian and Z. Bao, *Nanoscale*, 2013, **5**, 1727-1752.
74. G. Hong, S. Diao, A. L. Antaris and H. Dai, *Chemical Reviews*, 2015, **115**, 10816-10906.
75. J. J. Gooding, *Electrochimica Acta*, 2005, **50**, 3049-3060.
76. W. Qiu, H. Xu, S. Takalkar, A. S. Gurung, B. Liu, Y. Zheng, Z. Guo, M. Baloda, K. Baryeh and G. Liu, *Biosensors and Bioelectronics*, 2015, **64**, 367-372.
77. A. U. Alam and M. J. Deen, *Analytical Chemistry*, 2020, **92**, 5532-5539.
78. D. Xu, B. Hou, L. Qian, X. Zhang and G. Liu, *Molecules (Basel, Switzerland)*, 2019, **24**, 3411.
79. M. Meyyappan, *Small*, 2016, **12**, 2118-2129.
80. D. R. Kauffman and A. Star, *Angewandte Chemie International Edition*, 2008, **47**, 6550-6570.
81. V. Saino Hanna, N. Remya, G. N. Baiju, T. Hanajiri, T. Maekawa and Y. Y. a. D. S. Kumar, *Current Nanoscience*, 2010, **6**, 331-346.
82. W. J. Peveler, M. Yazdani and V. M. Rotello, *ACS Sensors*, 2016, **1**, 1282-1285.
83. J. M. Schnorr, D. van der Zwaag, J. J. Walish, Y. Weizmann and T. M. Swager, *Advanced Functional Materials*, 2013, **23**, 5285-5291.
84. S. F. Liu, L. C. H. Moh and T. M. Swager, *Chemistry of Materials*, 2015, **27**, 3560-3563.
85. G. O. Silva, Z. P. Michael, L. Bian, G. V. Shurin, M. Mulato, M. R. Shurin and A. Star, *ACS Sensors*, 2017, **2**, 1128-1132.
86. B. C. Janegitz, T. A. Silva, A. Wong, L. Ribovski, F. C. Vicentini, M. d. P. Taboada Sotomayor and O. Fatibello-Filho, *Biosensors and Bioelectronics*, 2017, **89**, 224-233.
87. T. A. Silva, H. Zanin, P. W. May, E. J. Corat and O. Fatibello-Filho, *ACS Applied Materials & Interfaces*, 2014, **6**, 21086-21092.
88. T. A. Silva, F. C. Moraes, B. C. Janegitz and O. Fatibello-Filho, *Journal of Nanomaterials*, 2017, **2017**, 4571614.
89. I. Švancara, K. Vytřas, K. Kalcher, A. Walcarius and J. Wang, *Electroanalysis*, 2009, **21**, 7-28.
90. M. Pumera, A. Ambrosi, A. Bonanni, E. L. K. Chng and H. L. Poh, *TrAC Trends in Analytical Chemistry*, 2010, **29**, 954-965.
91. R. A. Medeiros, B. C. Lourenção, R. C. Rocha-Filho and O. Fatibello-Filho, *Analytical Chemistry*, 2010, **82**, 8658-8663.

92. F. Arduini, S. Cinti, V. Mazzaracchio, V. Scognamiglio, A. Amine and D. Moscone, *Biosensors and Bioelectronics*, 2020, **156**, 112033.
93. F. Arduini, F. D. Giorgio, A. Amine, F. Cataldo, D. Moscone and G. Palleschi, *Analytical Letters*, 2010, **43**, 1688-1702.
94. F. Arduini, A. Amine, C. Majorani, F. Di Giorgio, D. De Felicis, F. Cataldo, D. Moscone and G. Palleschi, *Electrochemistry Communications*, 2010, **12**, 346-350.
95. F. Arduini, C. Zanardi, S. Cinti, F. Terzi, D. Moscone, G. Palleschi and R. Seeber, *Sensors and Actuators B: Chemical*, 2015, **212**, 536-543.
96. S. Cinti, F. Arduini, M. Carbone, L. Sansone, I. Cacciotti, D. Moscone and G. Palleschi, *Electroanalysis*, 2015, **27**, 2230-2238.
97. V. Mazzaracchio, M. R. Tomei, I. Cacciotti, A. Chiodoni, C. Novara, M. Castellino, G. Scordo, A. Amine, D. Moscone and F. Arduini, *Electrochimica Acta*, 2019, **317**, 673-683.
98. F. C. Vicentini, A. E. Ravanini, L. C. S. Figueiredo-Filho, J. Iniesta, C. E. Banks and O. Fatibello-Filho, *Electrochimica Acta*, 2015, **157**, 125-133.
99. F. C. Vicentini, P. A. Raymundo-Pereira, B. C. Janegitz, S. A. S. Machado and O. Fatibello-Filho, *Sensors and Actuators B: Chemical*, 2016, **227**, 610-618.
100. Asahi Carbon Co. Ltd., Carbon Black Properties, https://www.asahicarbon.co.jp/global_site/cb/outline.html, (accessed 7th June, 2021).
101. S. B. Hočevar and B. Ogorevc, *Talanta*, 2007, **74**, 405-411.
102. S. I. R. Malha, J. Mandli, A. Ourari and A. Amine, *Electroanalysis*, 2013, **25**, n/a-n/a.
103. E. A. Zakharova, E. E. Elesova, G. N. Noskova, M. Lu and R. G. Compton, *Electroanalysis*, 2012, **24**, 2061-2069.
104. D. Lowinsohn, P. Gan, K. Tschulik, J. S. Foord and R. G. Compton, *Electroanalysis*, 2013, **25**, 2435-2444.
105. S. I. R. Malha, A. A. Lahcen, F. Arduini, A. Ourari and A. Amine, *Electroanalysis*, 2016, **28**, 1044-1051.
106. M. R. Pacheco, S. C. Barbosa, R. F. N. Quadrado, A. R. Fajardo and D. Dias, *Analytical and Bioanalytical Chemistry*, 2019, **411**, 3269-3280.
107. D. Talarico, F. Arduini, A. Amine, I. Cacciotti, D. Moscone and G. Palleschi, *Analytical and Bioanalytical Chemistry*, 2016, **408**, 7299-7309.
108. F. Arduini, F. Di Nardo, A. Amine, L. Micheli, G. Palleschi and D. Moscone, *Electroanalysis*, 2012, **24**, 743-751.
109. N. Colozza, K. Kehe, G. Dionisi, T. Popp, A. Tsoutsoulopoulos, D. Steinritz, D. Moscone and F. Arduini, *Biosensors and Bioelectronics*, 2019, **129**, 15-23.
110. S. Cinti, V. Mazzaracchio, I. Cacciotti, D. Moscone and F. Arduini, *Sensors*, 2017, **17**.
111. S. Cinti, N. Colozza, I. Cacciotti, D. Moscone, M. Polomoshnov, E. Sowade, R. R. Baumann and F. Arduini, *Sensors and Actuators B: Chemical*, 2018, **265**, 155-160.
112. S. Cinti, D. Moscone and F. Arduini, *Nature Protocols*, 2019, **14**, 2437-2451.
113. S. I. R. Malha, J. Mandli, A. Ourari and A. Amine, *Electroanalysis*, 2013, **25**.
114. E. M. Richter, D. P. Rocha, R. M. Cardoso, E. M. Keefe, C. W. Foster, R. A. A. Munoz and C. E. Banks, *Analytical Chemistry*, 2019, **91**, 12844-12851.

115. D. G. Mita, A. Attanasio, F. Arduini, N. Diano, V. Grano, U. Bencivenga, S. Rossi, A. Amine and D. Moscone, *Biosensors and Bioelectronics*, 2007, **23**, 60-65.
116. M. Portaccio, D. Di Tuoro, F. Arduini, D. Moscone, M. Cammarota, D. G. Mita and M. Lepore, *Electrochimica Acta*, 2013, **109**, 340-347.
117. S. Nadifiyine, M. Haddam, J. Mandli, S. Chadel, C. C. Blanchard, J. L. Marty and A. Amine, *Analytical Letters*, 2013, **46**, 2705-2726.
118. G. J. Mattos, J. T. Moraes, E. C. M. Barbosa, P. H. C. Camargo, R. F. H. Dekker, A. M. Barbosa-Dekker and E. R. Sartori, *Bioelectrochemistry*, 2019, **129**, 116-123.
119. X. Dang, C. Hu, Y. Wei, W. Chen and S. Hu, *Electroanalysis*, 2004, **16**, 1949-1955.
120. H. Zhang, *Journal of Membrane Science*, 2005, **251**, 43-49.
121. H. Zhang, *Bioelectrochemistry*, 2006, **68**, 197-201.
122. D. Wertz, *A Molecular Science General Chemistry I: Chapter 11: Electron Transfer Reactions and Electrochemistry*, Advanced Instructional Systems Inc. and NC State College of Sciences Foundation, 3rd edn., 2014.
123. P. T. Kissinger and W. R. Heineman, *Journal of Chemical Education*, 1983, **60**, 702-706.
124. A. C. Fisher, Electrochemistry Fundamentals, https://www.ceb.cam.ac.uk/research/groups/rg-eme/research/undergraduate-teaching-notes, (accessed 28 July, 2020).
125. R. L. Wolke, in *The Gale Encyclopedia of Science*, eds. K. L. Lerner and B. W. Lerner, Gale, Farmington Hills, MI, 5th ed. edn., 2014, vol. 3, pp. 1517-1520.
126. G. A. Mabbott, *Journal of Chemical Education*, 1983, **60**, 697-702.
127. J. Heinze, *Angewandte Chemie International Edition in English*, 1984, **23**, 831-847.
128. N. Elgrishi, K. J. Rountree, B. D. McCarthy, E. S. Rountree, T. T. Eisenhart and J. L. Dempsey, *Journal of Chemical Education*, 2018, **95**, 197-206.
129. S. P. Kounaves, *Handbook of Instrumental Techniques for Analytical Chemistry*, 1997.
130. H. Fu, H. Chow, M. Lew, S. Menon, C. Scratchley and M. A. Parameswaran, *Cornell University*, 2015.
131. Metrohm, Ohmic Drop, https://www.metrohm.com/content/metrohm/en_gb/applications/application-notes/autolab-applikationen-anautolab/an-ec-003.html).
132. BioLogic, *EC-Lab – Application Note #27*, 2010.
133. A. J. Bard and L. R. Faulkner, *Electrochemical Methods: Fundamentals and Applications*, Wiley & Sons, Inc., 2nd edn., 2001.
134. PalmSens, Capacitive Current, https://www.palmsenscorrosion.com/knowledgebase/, (accessed July 2020).
135. P. Chooto, *Voltammetry*, IntechOpen, 2019.
136. A. Bott, *Current Separations*, 2001, **19**.
137. A. J. Veloso, X. R. Cheng and K. Kerman, *Biosensors for Medical Applications*, Woodhead Publishing Limited, Cambridge, 1st edn., 2012.
138. M. Arredondo, M. Stoytcheva, V. Zlatev and V. Gochev, *Mini-Reviews in Medicinal Chemistry*, 2012, 1301-1313.

139. BASinc, Cyclic Voltammetry - Data Analysis, https://www.basinc.com/manuals/EC_epsilon/Techniques/CycVolt/cv_analysis).
140. J. J. Van Benschoten, J. Y. Lewis, W. R. Heineman, D. A. Roston and J. Kissinger, *Journal of Chemical Education*, 1983, **60**, 772-776.
141. K. Wijeratne, Linkö ping University, Sweden, 2018.
142. A. Molina, E. Laborda, E. I. Rogers, F. Martinez-Ortiz, C. Serna, J. G. Limon-Petersen, N. V. Rees and R. G. Compton, *Journal of Electroanalytical Chemistry*, 2009, **634**, 73-81.
143. F. Scholz, *ChemTexts*, 2015.
144. Z. Stojek, in *Electroanalytical Methods. Guide to experiments and applications.*, Springer, Berlin, 2010, ch. II.2 Pulse Voltammetry.
145. A. Molina and J. Gonzalez, in *Monographs in electrochemistry*, Springer, Berlin, 2015.
146. Z. Stojek, in *Electroanalytical Methods*, 2005, ch. II.2 Pulse Voltammetry.
147. Gamry, Differential Pulse Voltammetry Purpose, https://www.gamry.com/Framework%20Help/HTML5%20-%20Tripane%20-%20Audience%20A/Content/PV/Experimental_Techniques/Differential%20Pulse%20Voltammetry/, (accessed 8th April, 2020).

CHAPTER THREE

EXPERIMENTAL METHODS

3.1 Materials and reagents

Ferrocene [$Fe(C_5H_5)_2$] (98%, Sigma Aldrich) solutions were prepared using lithium perchlorate 0.1 M $LiClO_4$ (Sigma Aldrich) and acetonitrile (ACN) (VWR International). PyoC (Sigma Aldrich) solutions were prepared using 0.1 M phosphate-buffered saline (PBS) (Thermo-Scientific). All aqueous solutions were prepared using milli-Q water (18 mΩ cm).

All electrodes and test samples were manufactured using a commercially available 3D printer (Asiga Pico plus 27). CAD models were created with Autodesk Inventor and sliced using Asiga Composer. The resolution is stated to be 27 μm in the X-Y plane, with a minimum build layer thickness of 1 μm.

3D printing resins contain both a base monomer material and a photoinitiator. Absorbers may also be added to control light penetration into the material. In this case, the monomer utilised was poly(ethylene glycol) diacrylate (PEGDA, MW 250) (Merck) and phenylbis(2,4,6-trimethylbenzoyl) phosphine oxide (Irgacure 819) (Merck) was the photoinitiator. Sudan 1 (S1) (Merck) was used as an absorber in concentrations of 0.4% and 0.35% (w/w) for structural layers, and 0.1% (w/w) for conductive layers. Irgacure was added in concentrations of 1% w/w. Preparations were mixed using an RCT basic mixer (Pfizer) for 30 minutes before use and stored away from light sources to protect the resin.

Conductive resins were prepared using MWCNTs (Nanocyl) with an average diameter of 9.5 nm and average length of 1.5 mm and carbon black Super-P (CB) (Fisher Scientific). MWCNTs were added in concentrations of 0.5% and 1% (w/w). MWCNT

resins were mixed by Benjamin Tiller. Prints were cleaned, during manufacture and post-processing, with isopropyl alcohol (Sigma Aldrich).

Calibration square resins constituted 0.5 % (w/w) CB in PEGDA. S1 and Irgacure 819 were added in concentrations of 0.1 % and 0.3 % respectively. For surface modification resins, CB was added in concentrations of 0.5 % and 1 % (w/w), then diluted to make further solutions of 0.2 %, 0.4 %, 0.6 % and 0.8 % CB. Solutions were mixed using a Thinky ARE-250 conditioning planetary mixer on program 2 (Mixing: 5 mins/1900 rpm, defoaming: 4 mins/1500 rpm).

Wires were attached to electrode chips using Araldite Instant 90 second adhesive (RS Components) and Ag paint (Agar Scientific). All materials were used as received.

Ferrocene [$Fe(C_5H_5)_2$] (98 %, Sigma Aldrich) solutions were prepared using lithium perchlorate 0.1 M $LiClO_4$ (Sigma Aldrich) and acetonitrile (ACN) (VWR International). Gentamicin (GN) sulfate (Thermo-Scientific) solutions were prepared using 0.1 M phosphate-buffered saline (PBS) (Thermo-Scientific). All aqueous solutions were prepared using deionised water.

3.2 Sample Preparation

10 mM [$Fe(C_5H_5)_2$] stock solutions in 0.1 M $LiClO_4$ in ACN were used for the assessment of electrochemical activity. PyoC solutions ranging from 20 to 500 µM were prepared in 0.1 M PBS. For biological samples, human pooled serum (Merck) was spiked with 25 µM and 50 µM PyoC. Electrochemical interrogation for Chapter 5 was performed using 5 mM [$Fe(C_5H_5)_2$]. 100 µg/mL gentamicin (GN) solution was prepared in 0.1 M PBS.

5 mM [$Fe(C_5H_5)_2$] in 0.1 M $LiClO_4$ in ACN was utilised in the initial electrochemical assessment of both the GC and CB-modified GC electrodes in Chapter 6. GN solutions ranging from 10 µg/mL to 200 µg/mL were prepared in 0.1 M PBS. For biological samples, human pooled serum (Merck) was spiked with 50 µg/mL and 100 µg/mL GN.

3.3 CNT Electrode Preparation

MWCNT electrodes were 3D printed using an ASIGA Pico2 HD 27 UV 3D printer (ASIGA). Their design consisted of an initial layer of 0.4 % weight/weight Sudan 1 (S1) (Sigma Aldrich) PEGDA (Sigma Aldrich). The WE and CE components were printed using a solution of 0.1 % S1 1 % (w/w) MWCNT-PEGDA. Tiller *et al.* [1] have elsewhere described the preparation of this solution. A further insulating layer of 0.4 % (w/w) S1 PEGDA was then printed over the MWCNT electrodes, leaving the working and counter electrodes exposed for contact with the solution. Silver paint (Agar Scientific) formed a conductive connection between electrodes and wires. Electrode areas were determined using ImageJ software.

3.4 CB-modified GC Electrode Preparation

Ten GC electrodes were polished for four minutes each in 1 µm, 0.3 µm and 0.05 µm MicroPolish Alumina (Buehler) respectively. Electrodes were modified with 4 µL of CB solution, ranging from 0.2 % to 1 % (2 electrodes per concentration).

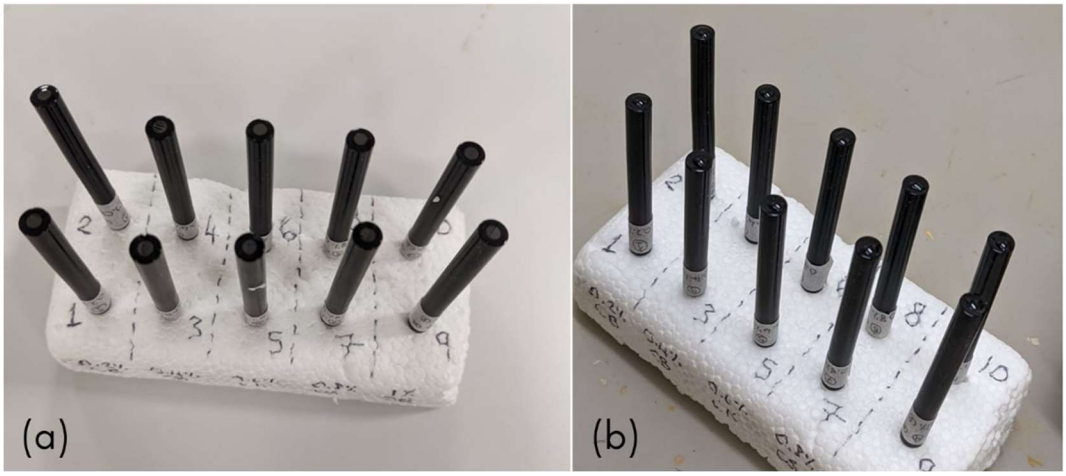

Figure 3.1: (a) Unmodified GC electrode array and (b) GC electrodes modified with varying CB concentrations.

CB-modified GC electrodes were cured under an IUV250 Hand Lamp (Intertronics) for 50 minutes. Electrodes modified with 0.2 % CB were cured for a further 20 minutes. The intensity of the UV light was measured to be 7.31 mW/cm^2, using an Analytik Jena 97-0015-02(UVX) Digital Ultraviolet Intensity Radiometer. Samples sat at a height of approximately 17.3 cm in the z-direction.

3.5 Instrumentation

Electrochemical interrogation was performed using a PalmSens EmStat Blue potentiostat (PalmSens Version EM Stat 3, PalmSens, Houten, Netherlands) using a standard three electrode electrochemical set-up. Commercial macroelectrodes included an Ag/AgCl reference electrode (RE), a 3 mm diameter GC WE and a platinum (Pt) CE. All electrodes were purchased from CH Instruments (UK). CV was monitored over the potential range $0 \leq E \leq 0.7$ V vs Ag/AgCl at a scan rate of 100 mVs^{-1}. DPV parameters were optimised according to which values for step potential, pulse potential and pulse duration gave the highest reduction peak. The resultant

parameters specified pulse amplitude 100 mV, 50 ms pulse width and 0.05 Vs^{-1} scan rate. A schematic of the 3D printed electrode setup is shown in Figure 3.2.

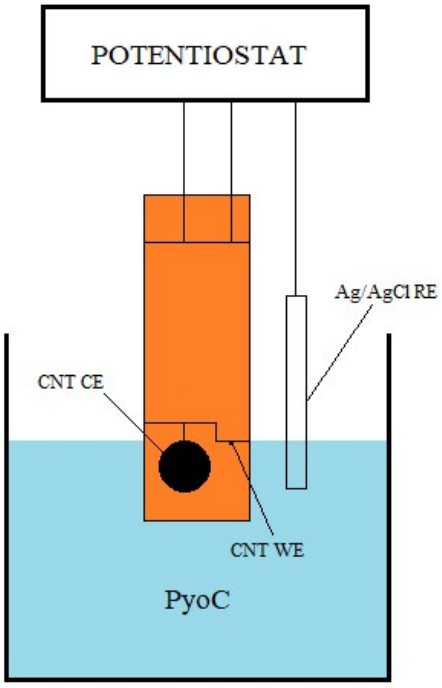

Figure 3.2: Schematic of experimental setup featuring
3D printed MWCNT WE and CE and Ag/AgCl RE in PyoC solution.

3.6 3D Printing

The absorption of the printing material and the intensity of the light source must be taken into account when considering an appropriate exposure time. [2] Consider a photopolymerisable resin, such as that illustrated in Figure 3.3, whose surface is defined as $z = 0$. The material has absorption coefficient α, which is measured in μm^{-1}, and an optical irradiance at its surface of I_0, in W/cm^2.

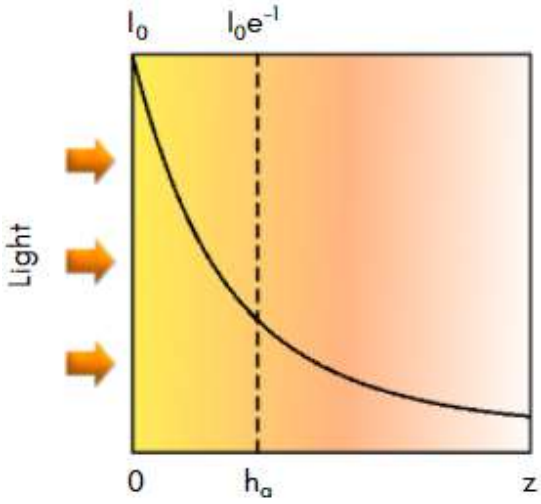

Figure 3.3: Beer's law schematic diagram. Adapted from Gong et al. [2]

The characteristic penetration depth of the material is defined as:

$$h_a = 1/\alpha \qquad (3.1)$$

Beer's law gives the irradiance at depth z:

$$I(z) = I_0 e^{-\alpha z} \qquad (3.2)$$

The corresponding dose at depth z is defined as:

$$D(z,t) = tI(z) \qquad (3.3)$$

where t is the exposure time in seconds. [2]

The critical dose (D_c) is defined as that at which polymerisation has progressed adequately, such that the material can be considered a solid. Print thickness (D_t) can be expressed in terms of dose energy:

$$D_t = \frac{1}{\alpha}(lnD_0 - lnD_c) \qquad (3.4)$$

Values for D_C and α can be estimated for printing composites by measuring the cured height (z_p) of a single layer of the resin at increasing exposure times and fitting the results to Equation 3.4. [1]

To allow for a combination of structural and conductive layers, prints were paused at the appropriate stage to allow resins to be switched. Before the new resin vat was placed, the partial print was cleaned using isopropyl alcohol. The surface of the print was then allowed to dry for 10 to 20 minutes. If the surface was not completely dry, the subsequent layers would not properly adhere to the former. The initial MWCNT electrode sensor had an exposure time of 8 seconds, and the recessed design had an exposure time of 7 seconds. It was important that both structural and conductive resins were able to cure within the given exposure time, as parameters cannot be altered during printing. Since carbon materials are highly pigmented, relatively long exposure times were employed so that the UV light was able to penetrate. The concentration of S1 in the structural resin was then matched to allow for complete curing within the required exposure time. S1 concentration for the initial design was 0.4 % (w/w); for the recessed design, which utilised a lower MWCNT concentration, the S1 concentration was 0.35 % (w/w). All designs had a slice thickness of 10 μm. Once the build was finished, it was removed from the build platform and rinsed using isopropyl alcohol. Any residual resin from the burn-in layer was carefully removed with tweezers. Prints were then allowed to air dry thoroughly before use.

3.7 Materials Study

Calibration squares

Initial investigation of CB as a conductive additive for photopolymerisable resins involved printing calibration squares at increasing exposure times and comparing their thickness, to explore whether the material conformed to Beer's Law. Squares measured 2×2 cm and were printed in a single layer. Print parameters specified a layer thickness of 0.01 mm. The build platform was removed from the printer, allowing squares to be photopolymerised onto the build tray membrane. Two squares each were cured using exponentially increasing exposure times (4 seconds, 8 seconds, 16 seconds, and 32 seconds). Following curing, squares were removed from the membrane and rinsed in isopropyl alcohol. Their thickness was measured using a micrometer screw gauge (Moore & Wright).

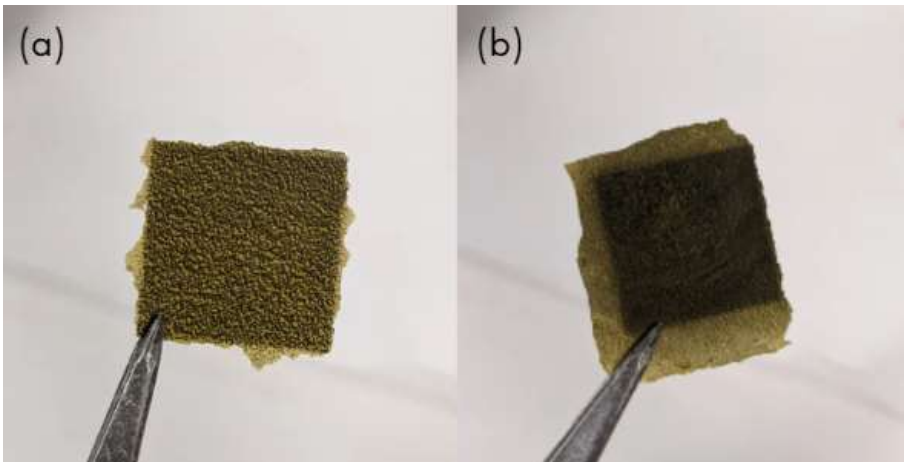

Figure 3.4: Calibration squares printed over (a) 8 seconds (b) 32 seconds

CB-modified GC electrodes

To inform the final electrode design, a study was created to determine which concentration of CB would be optimal, i.e., which had the best trade-off between electrochemical function and cost. Ten CB-modified GC electrodes (see Section 5.3.2) were electrochemically assessed in $Fe(C_5H_5)_2$ and GN and their responses compared.

3.8 References

1. B. Tiller, A. Reid, B. Zhu, J. Guerreiro, R. Domingo-Roca, J. Curt Jackson and J. F. C. Windmill, *Materials & Design*, 2019, **165**, 107593.
2. H. Gong, M. Beauchamp, S. Perry, A. T. Woolley and G. P. Nordin, *RSC Advances*, 2015, **5**, 106621-106632.

CHAPTER FOUR

CHARACTERISING THE RESPONSE OF NOVEL 3D PRINTED CNT ELECTRODES TO THE VIRULENCE FACTOR PYOCYANIN

4.1 Overview

Electrochemical based sensors have become increasingly popular within biomedical applications. Their low cost, high portability, and flexibility in regard to manufacturing makes them ideal candidates for point of care sensors. The virulence factor pyocyanin is a useful diagnostic biomarker for the detection of the *Pseudomonas aeruginosa* (*P. aeruginosa*) bacterium, and its phenolic functionality makes it an ideal candidate for electrochemical detection. Multi-walled carbon nanotubes (MWCNT) offer superb conductivity and boast high electroactive surface area, as well as being low cost. Thus, they are considered a desirable material for the manufacture of electrochemical sensors. In-house 3D printed MWCNT sensing platforms for the detection of clinically relevant concentrations of pyocyanin were investigated. Comparison was drawn against a traditional glassy carbon electrode, with MWCNT electrodes achieving detection limits down to 1 μM, as well as interelectrode reproducibility of 19 % and a linear response across the entire therapeutic range. These results demonstrate the feasibility of manufacturing MWCNT sensors for point-of-care devices, with analytical performance largely comparable to more costly conventional electrode systems.

4.2 Introduction

Early detection of infection within clinical settings is an imperative step towards reducing infection-related complications and mortality.[1] The virulence factor pyocyanin (PyoC) is produced by the gram-negative bacterium *Pseudomonas aeruginosa* (*P. aeruginosa*); its presence is common in patients with compromised immune systems. Given its resistance to many common antibiotics, infections involving this bacterium cause major morbidity and mortality. Rapid detection *in-situ* is therefore vital for early treatment and prevention of further contamination. [2]

Bacterial culture remains the gold standard for clinical detection of *P. aeruginosa*. It involves observing the bacterium's characteristics under certain conditions, such as gram-negative or gram-positive status, or monitoring the activities of molecules such as PyoC. [3] Various selective media are used for this purpose; Lowbury *et al.* [4] developed a medium containing cetrimide, which proved to be highly selective and became a common selective media for *P. aeruginosa*. This medium was later improved upon by Brown *et al.* [4, 5] Szita *et al.* [6] developed a culture medium based on *P. aeruginosa's* unique ability to produce ammonia during the breaking down of acetamide. Though widely used in hospital settings, these cultures are liable to become cross-contaminated, lack sensitivity and are time-consuming. [3] Automated systems, such as Vitek 2 (BioMérieux, France), [7] Phoenix 100 (BD Biosciences, USA) [8] and MicroScan WalkAway (Dade Behrig, Inc., USA) [9] can return results more rapidly. However, these systems tend to have a lower rate of accuracy regarding *P. aeruginosa* identification. [3]

Electrochemical techniques such as cyclic voltammetry (CV) and differential pulse voltammetry (DPV) allow for efficient detection of micro-organisms via detection of toxins such as PyoC. [10-13] For point-of-care electrochemical detection, use of commercial electrodes can add significantly to manufacturing costs. Cheaper alternatives are being investigated to overcome this financial issue whilst maintaining the standard of electrochemical activity required for electrochemical analysis.

Novel 3D printing techniques enable cheap, rapid prototyping of electrodes. Designs are printed from a 3D CAD design, layer-by-layer. Printing can be paused at any time, rendering printing materials interchangeable. Thus, conductive layers can be printed within insulated polymer layers, creating functional electrodes. Multi-walled carbon nanotubes (MWCNTs) were utilised for electrode construction due to their superior conductivity. They boast a high surface area and an ability to form interconnecting networks, allowing electrons to be efficiently transported through them. [14] MWCNTs were successfully incorporated into poly(ethylene glycol) diacrylate (PEGDA) for use in 3D printing, resulting in a MWCNT

electrode which incorporates a working (WE) and counter (CE) electrode. Its economical design is favourable for use in point-of-care settings, with an overall aim to detect infections at high sensitivity.

Here, we describe the comparison between the effectiveness of the MWCNT electrodes compared to conventional glassy carbon (GC) electrodes for PyoC detection, an important initial step towards assessing their suitability for infection detection.

4.3. Results and Discussion

4.3.1. Electrochemical Characterisation

The electrochemical behaviour of the MWCNT electrodes was investigated using a standard redox compound, $[Fe(C_5H_5)_2]$, and compared to a standard GC electrode, as shown in Figure 4.1.

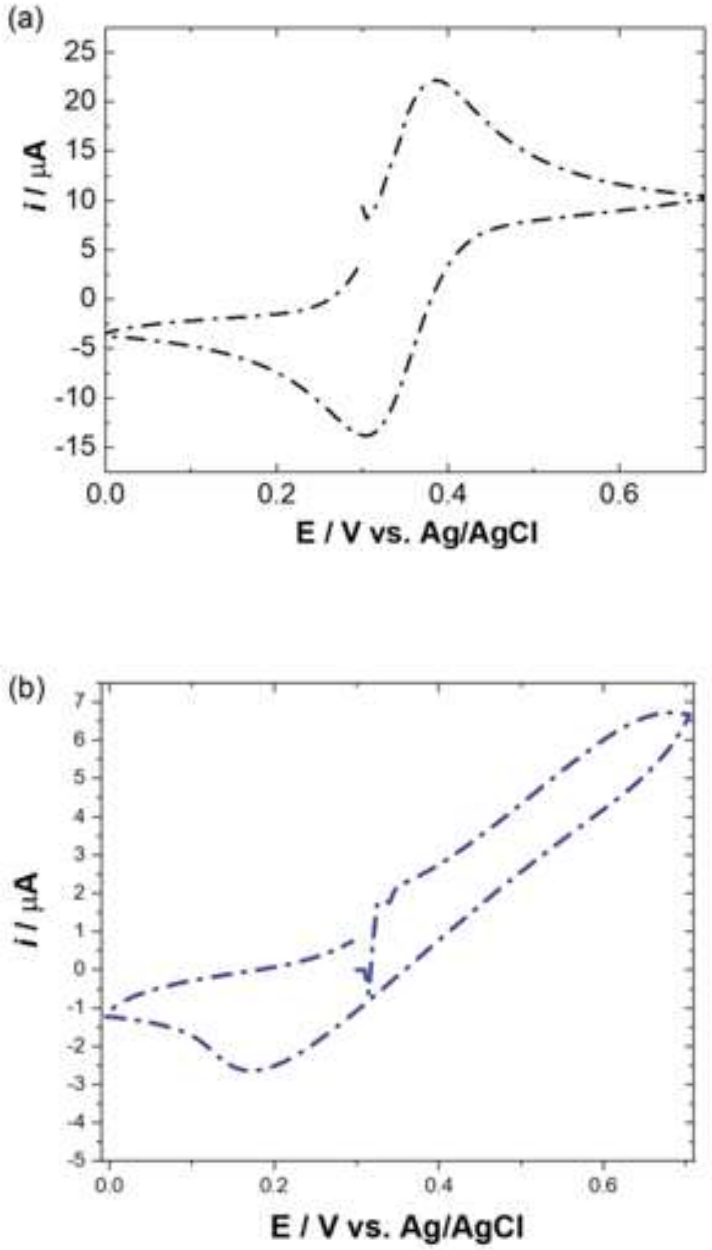

Figure 4.1: Typical cyclic voltammogram of 10 mM $[Fe(C_5H_5)_2]$ in 0.1 M $LiClO_4$ in ACN for(a) a GC and (b) 3D printed MWCNT electrode over the potential range 0 ≤ E vs Ag/AgCl ≤0.7 V at scan rate of 0.1 V s^{-1}.

The GC electrode displayed typical redox behaviour for the Fe redox couple, showing a redox peak at ~0.38 V vs Ag/AgCl. [16] The peak separation is 80 mV, close to the

ideal value of 59 mV for a reversible one-electron reaction. [17] The overall shape of this curve can be explained with reference to the Nernst equation (Equation 4.1), which describes the equilibrium between ferrocenium (Fc^+) and $Fe(C_5H_5)_2$:

$$E = E^{0,} + 2.3026\frac{RT}{F} log_{10}\frac{[Fc^+]}{[Fe(C_5H_5)_2]}, \qquad (4.1)$$

where E = cell potential, E^0 = standard species potential, R = universal gas constant, T = temperature, F = Faraday's constant. [18]

In contrast, the typical MWCNT electrode response exhibits very different behaviour. [19] Here, a notable decrease in the magnitude of the current response was observed, likely linked to the smaller surface area of the MWCNT WE. Though the size of the MWCNT WE can vary to a degree between prints, image analysis shows an area of approximately 10 μm^2 compared with the GC area of ~ 7 mm^2. Although there is no visible oxidation peak, a reduction peak can be observed at ~0.17 V vs. Ag/AgCl. This indicates that electron transfer to and from the electrode surface is hindered; hence oxidation is more energetically demanding, i.e., a higher voltage is required. The increase in peak-to-peak separation also implies that electron kinetics are being hampered, indicating that a quasi-reversible mechanism is being witnessed.

A similarly poor CV was obtained by Wei *et al.,* [19] for a screen-printed carbon electrode (SPCE) in ferricyanide ($Fe(CN)_0^{3-/4-}$). They observed an irreversible response with a large peak separation of 480 mV, indicating a slow electron transfer process. This poorer electrochemical behaviour may be linked to the mineral binders or insulating polymers contained within printing inks for improved substrate adhesion. Electrochemically active carbon particles may therefore be sheltered, resulting in an

increased resistance toward electron transfer. This in turn slows kinetics of the heterogeneous reaction required for the redox processes and may lead to quasi-reversible or irreversible redox processes at the electrode surface. SPCEs exhibited a response comparable to a polished GC electrode following one hour of pre-treatment in sodium hydroxide (NaOH). It was postulated that organic binders at the electrode surface were removed during this step, effectively increasing the electroactive area (A_{ea}). Indeed, the A_{ea} of the SPCE rose to seventeen-fold its apparent geometric area following pre-treatment, indicating a sharp increase in the number of active carbon particles exposed at the electron surface. [19] The use of polymers in the 3D printing process may affect MWCNT conductivity, and presence of organic binders could limit the A_{ea} of the electrodes.

Mahshid *et al.* [20] compared the performance of titanium dioxide (TiO_2) electrodes to those modified with platinum (Pt) and palladium (Pd). It was stated that Pd nanoparticles improved conductivity and electron transfer, due to their uniform deposition on the electrode surface. In this case, the opposite may be true for the MWCNT electrodes, as the MWCNTs form erratic and non-uniform networks. Compared to the CV response of the Pd-modified electrode, the Pd-Pt-modified electrode showed the oxidation peak shift to more negative potential, thus decreasing peak separation. This is explained as being due to the electrodes' high conductivity and catalytic activity. The design and uniformity of the GC electrode may therefore lend itself to higher conductivity than the MWCNT electrodes, resulting in a decreased and more defined peak separation in the case of the GC electrode. [20]

Despite the poor CV response of the MWCNT electrodes in $Fe(C_5H_5)_2$, it was deemed pertinent to explore their response to PyoC using DPV. Their design is extremely cheap and has potential for large-scale automation. Additionally, their disposable nature is beneficial within a clinical environment since it limits the possibility of cross-contamination. Therefore, if they can detect PyoC at similar concentrations to the current gold standard, their effectiveness must be considered.

4.3.2. PyoC Detection

PyoC is the redox-active virulence factor produced by *P. aeruginosa,* which also acts as a quorum-sensing molecule for the pathogen. [2, 21-25] Prior works have shown that PyoC undergoes both reversible phenazine redox reactions circa -0.18 V and -0.25 V vs SCE as well as a non-reversible phenolic oxidation at ~0.85 V following the reaction shown in Scheme 4.1. [26]

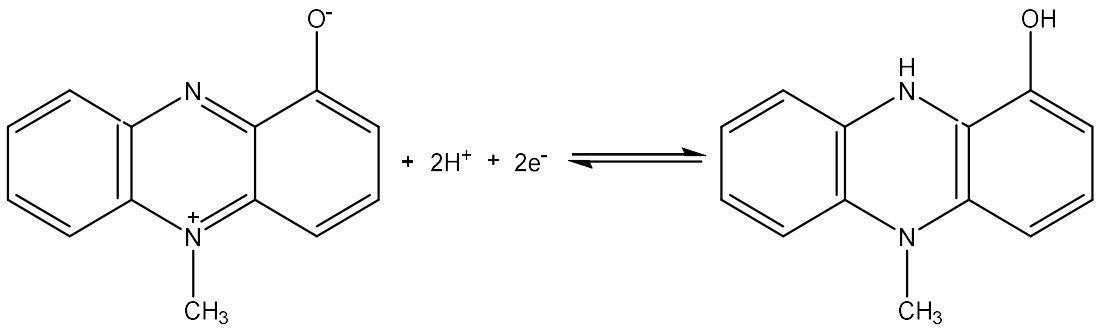

Scheme 4.4: Scheme of pyocyanin (PyoC) redox reaction. Adapted from Sharp et al. [26]

Given the fact that the phenolic oxidation of PyoC can result in polymerisation which in turn leads to an increase in peak height and current with increasing scan rates, the potential range investigated within this study was focused around the phenazine

transformation observed at ~ -0.21 V and -0.09 V for the GC and MWCNT electrodes respectively, as shown in Figure 4.2.

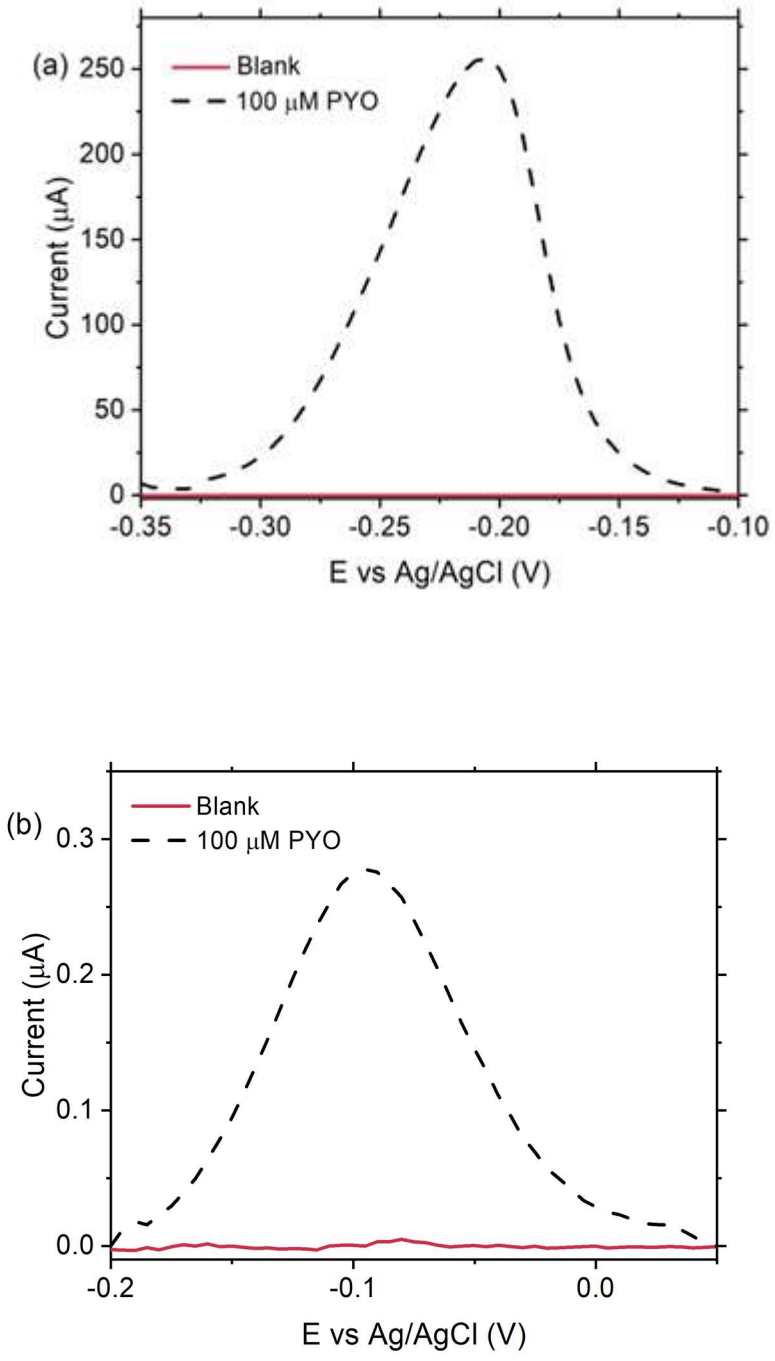

Figure 4.2: DPV responses for controls in 0.1 M PBS (red) and response from 100 μM PyoC in 0.1 M PBS (black) for (a) GC electrode and (b) MWCNT electrode recorded at scan rate of 0.1 Vs^{-1}.

The reduction potential observed at the MWCNT electrode is ~100 mV more positive than that observed at the GC electrode. This shift toward a more positive potential may be indicative of the reaction proceeding more easily at this potential for MWCNT electrodes, however this potential is in agreement with previous studies utilising carbon fibres. [26] The reduced positive potential required to induce reduction of PyoC at the MWCNT will reduce the demand on any equipment required in future clinical applications, which is an advantage regarding translation from laboratory to clinical settings. Both electrodes exhibit clear and identifiable responses in the presence of PyoC, which are clearly distinguishable from the baseline, indicating that the MWCNT electrodes are equally capable of detecting the virulence factor.

4.3.3. Analytical performance

Figure 4.3 displays the DPV response of both the GC and MWCNT electrodes to increasing concentrations of PyoC, over the concentration range $0 \leq [\text{PyoC}] \leq 100$ μM, in addition to the dependence of the peak intensity upon PyoC concentration. This concentration range is in agreement with clinical ranges and several prior studies [26-28] - it includes concentrations present within clinical samples and the determined micromolar range for PyoC concentrations from *in vitro* cellular environments. [29-31] Lung inflammation is documented to occur at PyoC concentrations of 10-100 μM, [26, 27, 32-34] whilst cellular PyoC occurs at higher concentrations, as documented by Simoska *et al.* [29] who reported a large linear dynamic range (LDR) of 1-250 μM. [29]

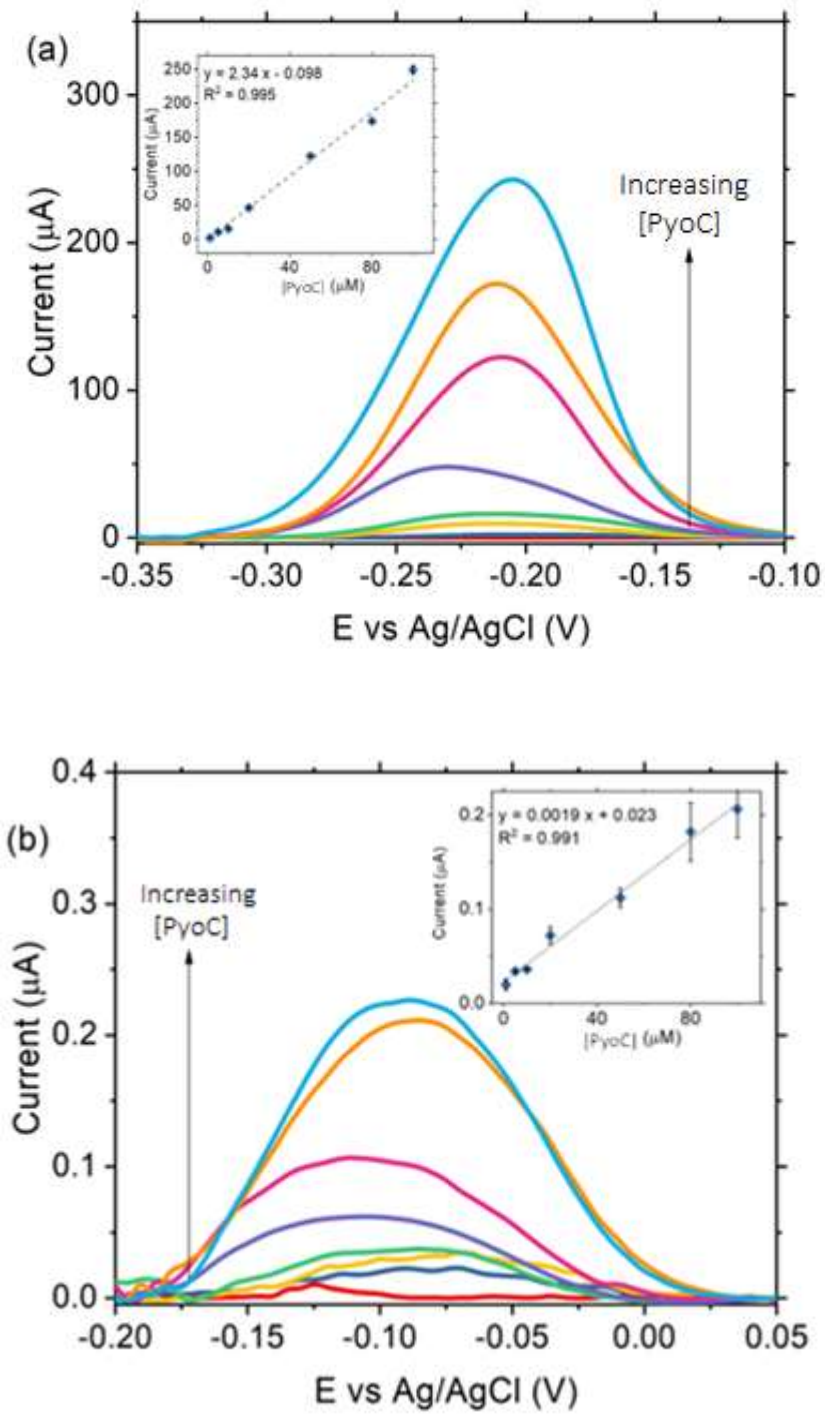

Figure 4.3: Typical DPV responses for (a) GC electrode and (b) MWCNT electrode obtained for 0 to 100 µM PyoC in 0.1 M PBS at a scan rate of 0.1 V s^{-1}. Insets show the corresponding linear relationship of this response with [PyoC]. Error bars represent triplicate responses.

Maximum peak intensity was recorded at a potential of approximately -0.09 V for the MWCNT electrode, compared to -0.21 V for the GC electrode. This is the expected potential vs. a 1 M KCl Ag/AgCl reference for samples containing PyoC. [35] Several other studies have also reported peaks at this potential, using transparent carbon ultramicroelectrode arrays, [29] unmodified carbon electrodes [27] and catechol-chitosan modified Ag electrodes. [36] PyoC detection in biological human samples may result in slight potential shifts, due to reactive, complexing, or chelating compounds in addition to matrix complexity. [27, 37, 38]

For both electrode materials, the maximum current was observed to vary linearly over the concentration range with a coefficient of 0.991 and 0.995 for the MWCNT and GC electrodes respectively (Figure 4.3). Detection limits for each electrode material were calculated as 3 times the standard deviation of the intercept over the slope of the calibration line. [39] This revealed a LOD of 0.5 μM for the GC electrode and 2.5 μM for the MWCNT electrode. Figure 4.4 displays the DPV response of the GC and MWCNT electrodes to 5 μM and 1 μM PyoC against a blank response, indicating that the MWCNT electrode can achieve detection down to 1 μM still distinguishable from the blank.

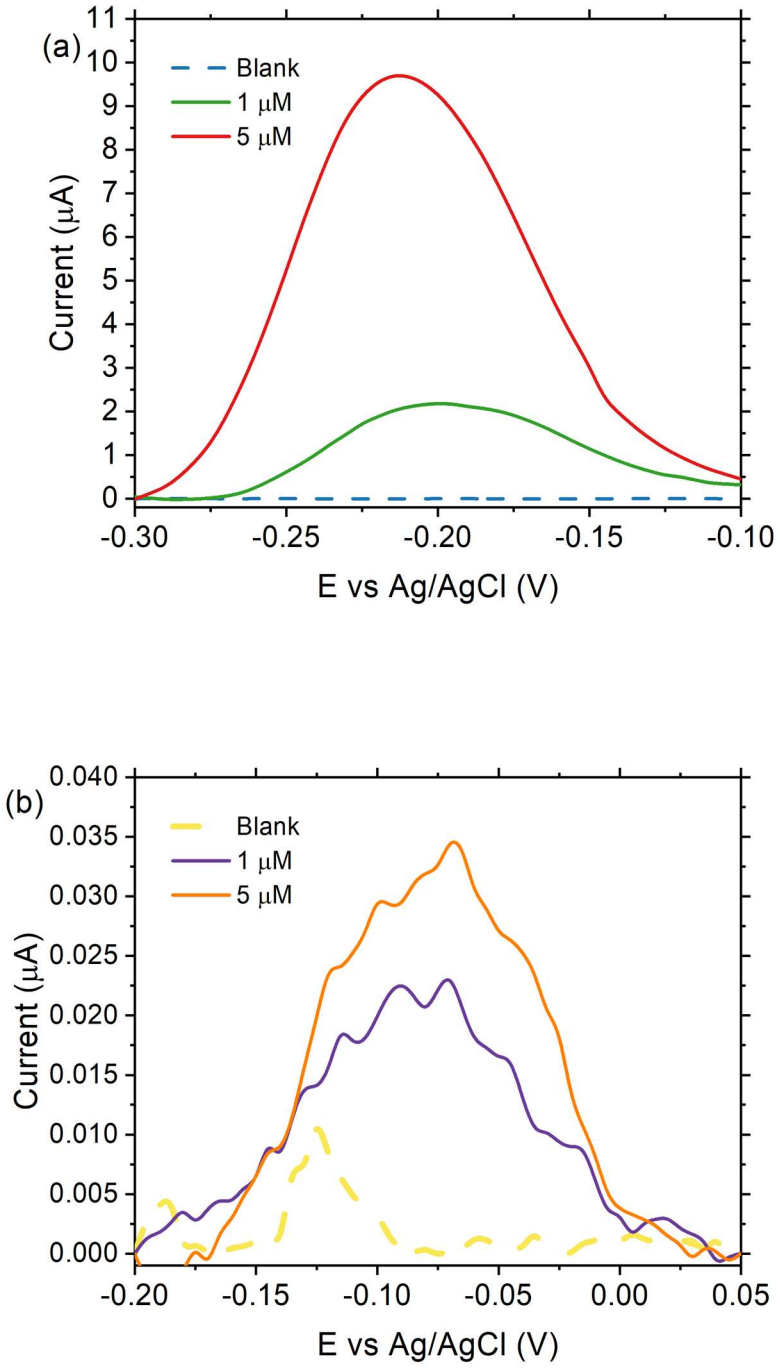

Figure 4.4: DPV responses for (a) GC electrodes for 0.1 M PBS (blue). 1 μM (green) and 5 μM (red) PyoC and (b) MWCNT electrode for 0.1 M PBS (yellow), 1 μM (purple) and 5 μM (orange) PyoC at a scan rate of 0.1 V s^{-1}.

Studies using better established electrode materials have on occasion achieved LOD which are orders of magnitude smaller than what was observed. Sharp *et al.* [26] recorded detection limits as low as 0.03 μM whilst Kim *et al.* [36] achieved a LOD of 0.05 μM. However, the use of MWCNTs is fairly novel, and their effectiveness in 3D printing applications is not yet fully understood. Further investigation is required to optimise the process. Electrode sensitivity depends upon high conductivity, which can only occur if MWCNTs can form fully interconnecting networks within the PEGDA solution. Homogenous MWCNT dispersion may be achieved by a number of methods such as solution casting or in situ polymerisation, as well as ultrasonication. [40-43] Surfactant use can also promote this effect. [41, 43] However, it was beyond the scope of this study to explore such methods – the primary focus was considered to be ease of manufacture and potential scaleup. Another factor limiting electrode sensitivity is the inability to polish the MWCNT PEGDA surface, which may result in the deposition of material which could block the electroactive area. Despite this, the detection limits achieved can be considered sufficient for detecting PyoC from infected patient samples. Concentrations from the sputa of infected patients have been reported in the range of 1-130 μM, with a median value of 8.1 μM, [30, 31, 44] whilst concentrations in ear secretions from patients with *P. aeruginosa*-induced ear infections have been reported in the millimolar range. [27, 31, 45] Given the 1 μM detection limit displayed by the MWCNT electrode, it was confirmed that the sensing system could be applicable to real clinical applications.

The reproducibility of the manufactured electrodes was interrogated, with a confirmed relative deviation of 18.5 % across six electrodes.

Table 4.1:Relative standard deviation across six different MWCNT electrodes in 100 µM PyoC.

	CNT 1	CNT 2	CNT 3	CNT 4	CNT 5	CNT 6
i_p (µA)	**0.129**	**0.113**	**0.152**	**0.193**	**0.167**	**0.158**
$\bar{\imath}_p$ (µA)		**0.152**				
SD		**0.028**				
RSD (%)		**18.5**				

Table 4.2: Relative standard deviation across six different GC electrodes in 100 µM PyoC.

	GC 1	GC 2	GC 3	GC 4	GC 5	GC 6
i_p (µA)	**345**	**337**	**357**	**334**	**315**	**329**
$\bar{\imath}_p$ (µA)	**336**					
SD	**14**					
RSD (%)	**4**					

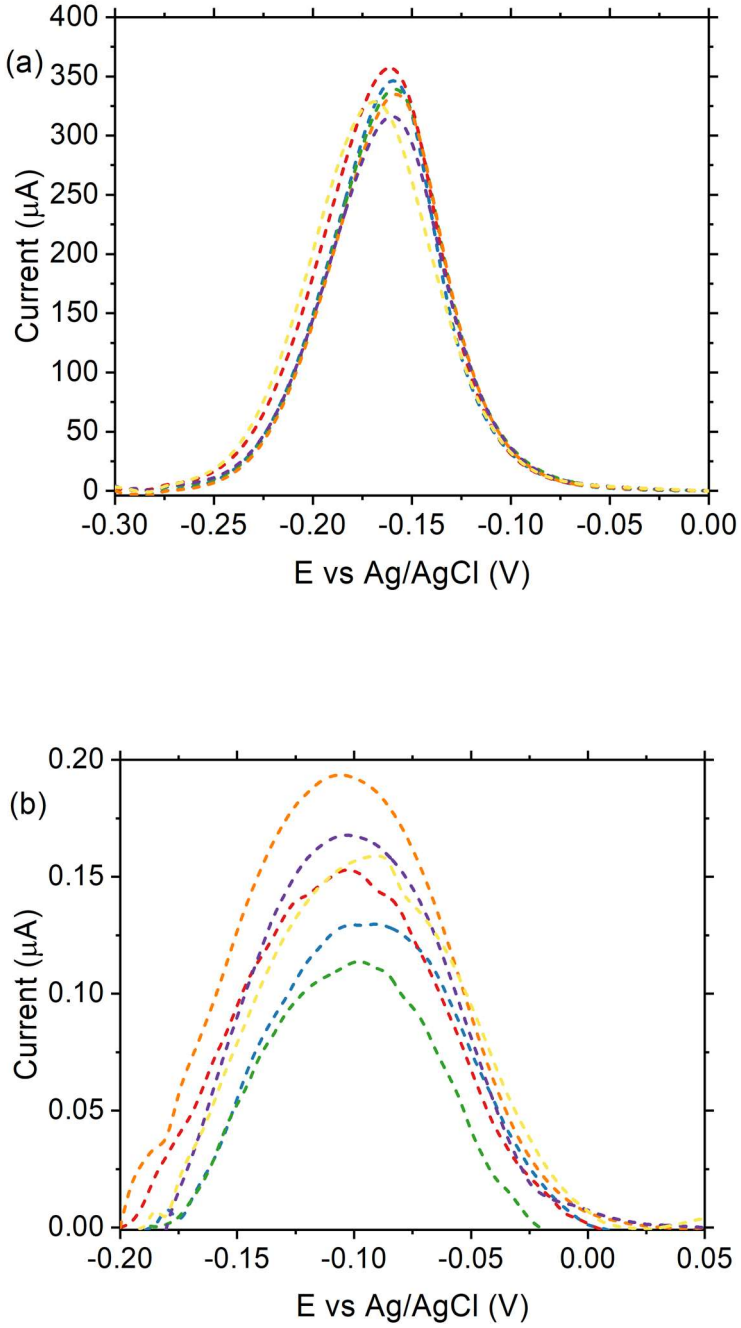

Figure 4.5: (a) six different GC electrodes and (b) six independent MWCNT electrodes at 100 μM PyoC in 0.1 M PBS at a scan rate of 0.1 V s^{-1}.

Compared to a commercial GC electrode, interelectrode repeatability was poor, as evidenced by the ~ 5-fold increase in the relative standard deviation (RSD) of the

MWCNT compared with the GC. Again, this is likely due to a combination of failure of the MWCNTs to form interconnecting networks within the insulating PEGDA environment and the use of relatively rudimentary wire connections. The resistivity values for the MWCNT 3D electrodes, shown in Table 4.3, also support this theory. Imaging of these electrodes would provide more detailed information on the interconnecting profiles of the MWCNTs within the PEGDA environment.

Table 4.3: Resistivity values for six CNT electrodes.

	CNT 1	**CNT 2**	**CNT 3**	**CNT 4**	**CNT 5**	**CNT 6**
i_p (µA)	0.129	0.113	0.152	0.193	0.167	0.158
$\bar{\imath}_p$ (µA)		0.152				
SD		0.028				
RSD (%)		18.5				
ρ (x 10^{-5} Ω cm)*	1.95	1.50	2.18	2.75	2.48	2.31

*Resistivity for a thin sheet was calculated based on the equation $\rho=(\pi t/\ln 2)(V/I)$ [46]

Long-term repeatability results proved to be more acceptable, with an RSD of 3.27 % (See Table 4.4), although given that the electrodes were designed to be disposable, this is less of a priority.

Table 4.4: Relative standard deviation across six MWCNT electrodes tested in triplicate over 6 days in 100 µM PyoC.

	Day 1	Day 2	Day 3	Day 4	Day 5	Day 6
i_{p1} (µA)	**0.22**	**0.20**	**0.22**	**0.18**	**0.19**	**0.19**
i_{p2} (µA)	**0.26**	**0.23**	**0.24**	**0.25**	**0.27**	**0.25**
i_{p3} (µA)	**0.28**	**0.25**	**0.25**	**0.27**	**0.27**	**0.27**
$\bar{\imath}_p$ (µA)	**0.25**	**0.23**	**0.24**	**0.24**	**0.24**	**0.24**
SD	**0.02**	**0.02**	**0.04**	**0.04**	**0.04**	**0.03**
					RSD (%)	**3.27**

Although interelectrode reproducibility was relatively high, further optimisation of the manufacturing process would ultimately improve this. Large scale manufacture could act towards reducing any inconsistency introduced through the current, small batch production of the sensing platform.

4.3.4. Biological Samples

Having established the feasibility of the inhouse manufactured electrodes for the detection of PyoC within ideal matrices, it was deemed prudent to assess their feasibility to operate within complex biological matrices. Detection of PyoC in spiked serum samples was carried out by Kelly Brown. PyoC was spiked into human pooled serum and analysed directly, with no sample purification performed. Initially, blank serum was analysed. This is an important step, as it is well documented that the large number of co-species contained within such biological matrices can impede electrochemical analysis. However, as demonstrated in Figure 4.6, blank serum produces an almost negligible signal within this negative potential region. Also advantageous is the fact that known interferents commonly found within clinical settings, such as caffeine, naturally occurring amino acids, and therapeutic drugs such as paracetamol do not undergo their typical redox processes within this region.

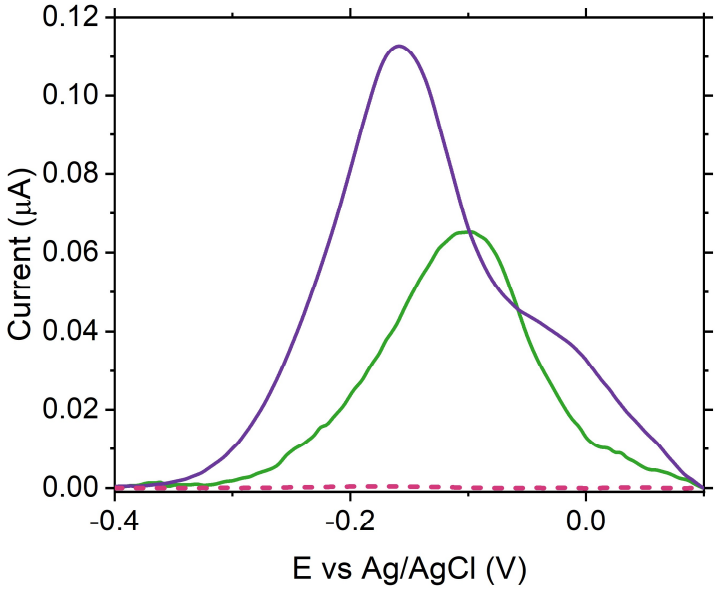

Figure 4.6: Average responses of 50 µM (purple) PyoC and 25 µM (green) PyoC within human pooled serum upon MWCNT electrodes at a scan rate of 0.1 V s^{-1}. The blank response is shown in red.

Figure 4.6 displays a slight positive shift in potential as [PyoC] is reduced from 50 µM to 20 µM. This may be due to issues with the CE, which was manufactured using the same materials and techniques as the WE, and thus may encounter similar problems such as current limitations. It is also possible that higher concentrations resulted in a breakdown of PyoC, which could be the cause of the additional shoulder observed on the purple waveform. Interactions with electroactive components of serum could also contribute to this.

To estimate the potential accuracy of the MWCNT sensor for the quantification of PyoC, % recoveries were estimated using the calibration curve constructed within Figure 4.3. This resulted in an average recovery across three measurements of 95 % for the 50 µM sample and 92 % for 25 µM. These demonstrate acceptable recoveries, within the typical analytical standard of 90 – 110 %, providing further proof that

successful translation of MWCNT sensing platforms to clinical settings may be possible in future.

4.4. Conclusion

3D printing is favourable as a fabrication technique due to its consistency, low cost, and potential for mass production. The 3D printed MWCNT sensing system, comprising WE and CE, is economical to produce compared to conventional electrodes. It is estimated that, given the low volume of materials required for electrode manufacture, as well as the absence of waste products regarding SLA techniques, these electrodes would cost ten pence or less each to manufacture. This can be compared to a typical GC electrode from Merck, which costs £187. However, it should be noted that this estimate does not account for the costs of running the lab, or for paying lab personnel. The disposable nature of the sensors is also favourable, considering their intended use within the clinical environment, where the possibility of cross-contamination must be minimised. The need for polishing to reactivate the electroactive area is also eliminated. Given that polishing is extremely time consuming, and ultimately adds to sensor cost in terms of consumables, this is advantageous, especially regarding the possible use of the sensing platform within a clinical environment. This study demonstrates a viable proof of concept regarding the use of MWCNT sensing systems for the reliable detection of the virulence factor PyoC. Detection was achieved down to clinically relevant levels, with a detection limit of 1 μM observed for the MWCNT sensors. Although this is double the detection limit of the traditional GC electrodes, the surface area of the manufactured electrodes was significantly reduced, and at this scale of production, the MWCNTs were not always able to form interconnecting networks within the PEGDA. Though the current process

does not demonstrate the optimum sensor design, it can achieve acceptable recoveries for PyoC within human pooled serum without the need for extraction or sample purification. The ability to detect down to clinically relevant concentrations indicates that further optimisation of the manufacturing process will produce a more sensitive and reproducible sensor at a significantly lower cost than is the current standard.

4.5 References

1. S. C. Davies, T. Fowler, J. Watson, D. M. Livermore and D. Walker, *Lancet*, 2013, **381**, 1606-1609.
2. F. A. a. Alatraktchi, H. K. Johansen, S. Molin and W. E. Svendsen, *Nanomedicine*, 2016, **11**, 2185-2195.
3. Y. Tang, Z. Ali, J. Zou, G. Jin, J. Zhu, J. Yang and J. Dai, *RSC Advances*, 2017, **7**, 51789-51800.
4. E. J. L. Lowbury and A. G. Collins, *Journal of Clinical Pathology*, 1955, **8**, 47.
5. V. I. Brown and E. J. L. Lowbury, *Journal of Clinical Pathology*, 1965, **18**, 752.
6. G. Szita and G. Bir ó, *Acta veterinaria Hungarica*, 1990, **38**, 7.
7. P. Joyanes, M. a. del Carmen Conejo, L. Martínez-Martínez and E. J. Perea, *Journal of Clinical Microbiology*, 2001, **39**, 3247.
8. G. Funke and P. Funke-Kissling, *Journal of Clinical Microbiology*, 2004, **42**, 1466.
9. L. Saiman, J. L. Burns, D. Larone, Y. Chen, E. Garber and S. Whittier, *Journal of Clinical Microbiology*, 2003, **41**, 492.
10. A. Buzid, F. Shang, F. J. Reen, E. Ó. Muimhneacháin, S. L. Clarke, L. Zhou, J. H. T. Luong, F. O'Gara, G. P. McGlacken and J. D. Glennon, *Scientific reports*, 2016, **6**, 30001-30001.
11. L. Dennany, P. C. Innis, G. G. Wallace and R. J. Forster, *The Journal of Physical Chemistry B*, 2008, **112**, 12907-12912.
12. L. Dennany, G. G. Wallace and R. J. Forster, *Langmuir*, 2009, **25**, 14053-14060.
13. L. Dennany, P. C. Innis, F. Masdarolomoor and G. G. Wallace, *The Journal of Physical Chemistry B*, 2010, **114**, 2337-2341.
14. Z. Spitalsky, D. Tasis, K. Papagelis and C. Galiotis, *Progress in Polymer Science*, 2010, **35**, 357-401.
15. B. Tiller, A. Reid, B. Zhu, J. Guerreiro, R. Domingo-Roca, J. Curt Jackson and J. F. C. Windmill, *Materials & Design*, 2019, **165**, 107593.
16. V. Aiello, N. Joo, J. Buckley, G. Nonglaton, F. Duclairoir, L. Dubois, J. C. Marchon, M. Gély, N. Chevalier and B. De Salvo, *Surface Science*, 2013, **612**, 57-62.
17. N. Elgrishi, K. J. Rountree, B. D. McCarthy, E. S. Rountree, T. T. Eisenhart and J. L. Dempsey, *Journal of Chemical Education*, 2018, **95**, 197-206.
18. O. Hammerich, Speiser, B., *Organic Electrochemistry: Revised and Expanded*, CRC Press, 2015.
19. H. Wei, J.-J. Sun, Y. Xie, C.-G. Lin, Y.-M. Wang, W.-H. Yin and G.-N. Chen, *Analytica Chimica Acta*, 2007, **588**, 297-303.
20. S. S. Mahshid, S. Mahshid, A. Dolati, M. Ghorbani, L. Yang, S. Luo and Q. Cai, *International Journal of Theoretical and Applied Nanotechnology (IJTAN)*, 2012, **1**.
21. A. Bianchi, S. Negrini and D. Shore, *Molecular Cell*, 2004, **16**, 139-146.
22. L. E. Dietrich, A. Price-Whelan, A. Petersen, M. Whiteley and D. K. Newman, *Molecular Microbiology*, 2006, **61**, 1308-1321.
23. K. Kanthakumar, G. Taylor, K. W. Tsang, D. R. Cundell, A. Rutman, S. Smith, P. K. Jeffery, P. J. Cole and R. Wilson, *Infection and Immunity*, 1993, **61**, 2848.
24. L. R. Usher, R. A. Lawson, I. Geary, C. J. Taylor, C. D. Bingle, G. W. Taylor and M. K. Whyte, *The Journal of Immunology*, 2002, **168**, 1861-1868.
25. D. Denning, *The Lancet*, 2003, **362**, 1142-1151.
26. D. Sharp, P. Gladstone, R. B. Smith, S. Forsythe and J. Davis, *Bioelectrochemistry*, 2010, **77**, 114-119.
27. T. A. Webster, H. J. Sismaet, J. L. Conte, I. P. Chan and E. D. Goluch, *Biosensors and Bioelectronics*, 2014, **60**, 265-270.
28. A. Cernat, A. Canciu, M. Tertis, F. Graur and C. Cristea, *Analytical and Bioanalytical Chemistry*, 2019, **411**, 3829-3838.

29. O. Simoska, M. Sans, M. D. Fitzpatrick, C. M. Crittenden, L. S. Eberlin, J. B. Shear and K. J. Stevenson, *ACS Sensors*, 2019, **4**, 170-179.
30. J. Elliott, O. Simoska, S. Karasik, J. B. Shear and K. J. Stevenson, *Analytical Chemistry*, 2017, **89**, 6285-6289.
31. R. Wilson, D. A. Sykes, D. Watson, A. Rutman, G. W. Taylor and P. J. Cole, *Infection and Immunity*, 1988, **56**, 2515-2517.
32. M. Muller, *Free Radical Biology and Medicine*, 2002, **33**, 1527-1533.
33. M. Muller, *Free Radical Biology and Medicine*, 2006, **41**, 1670-1677.
34. Y. Q. O'Malley, K. J. Reszka, D. R. Spitz, G. M. Denning and B. E. Britigan, *American Journal of Physiology-Lung Cellular and Molecular Physiology*, 2004, **287**, L94-L103.
35. Y. Wang and D. K. Newman, *Environmental Science & Technology*, 2008, **42**, 2380-2386.
36. E. Kim, T. Gordonov, W. E. Bentley and G. F. Payne, *Analytical Chemistry*, 2013, **85**, 2102-2108.
37. R. Cheluvappa, *Acta Biochimica Polonica*, 2008, **55**.
38. Y. H. Wen, H. M. Zhang, P. Qian, H. T. Zhou, P. Zhao, B. L. Yi and Y. S. Yang, *Journal of The Electrochemical Society*, 2006, **153**.
39. A. Nordon, A. Mills, R. T. Burn, F. M. Cusick and D. Littlejohn, *Analytica Chimica Acta*, 2005, **548**, 148-158.
40. Q. Wang, J. Dai, W. Li, Z. Wei and J. Jiang, *Composites Science and Technology*, 2008, **68**, 1644-1648.
41. X.-L. Xie, Y.-W. Mai and X.-P. Zhou, *Materials Science and Engineering: R: Reports*, 2005, **49**, 89-112.
42. J. Dai, Q. Wang, W. Li, Z. Wei and G. Xu, *Materials Letters*, 2007, **61**, 27-29.
43. C. A. Cooper, D. Ravich, D. Lips, J. Mayer and H. D. Wagner, *Composites Science and Technology*, 2002, **62**, 1105-1112.
44. T. A. Webster, H. J. Sismaet, I. P. Chan and E. D. Goluch, *Analyst*, 2015, **140**, 7195-7201.
45. A. Reimer, B. Edvaller and B. Johansson, *Acta Oto-Laryngologica Supplementum*, 2000, **543**, 86-88.
46. Bridge Technology, Four-Point Probe Manual, http://four-point-probes.com/four-point-probe-manual/).

CHAPTER FIVE

DEVELOPMENT OF A 3D PRINTED SENSING PLATFORM FOR ELECTROCHEMICAL ANALYSIS

5.1. Overview

This chapter details the additive manufacture of an electrochemical electrodes for the detection of the electroactive compound PyoC. Each stage of the design process will be discussed, with a focus on which elements were deemed most important for the development of an effective electrochemical sensor. Electrode platforms were successfully 3D printed using a combination of conductive and structural printing resins. This method of manufacture is rapid, cheap and has the potential to be scaled up. Having already assessed the effectiveness of MWCNT electrodes in Chapter 4, the feasibility of utilising carbon black (CB) as a conductive additive to PEGDA was explored by modifying GC electrodes with CB/PEGDA resins and assessing their response to $Fe(C_5H_5)_2$ and gentamicin (GN).

5.2 Introduction

The importance of developing a sensing device for the sensitive, facile detection of PyoC has been discussed at length in Chapter 1. Utilising additive manufacturing for mass production of electrochemical sensors would provide a rapid and low-cost solution, thus potentially filling a gap in the market. The myriad benefits of additive manufacturing are covered in Chapter 2. Here, the first steps towards the development of an electrochemical sensor via additive manufacturing are explored. To our knowledge, this is the first example of utilising DLP to manufacture an electrochemical sensor.

5.3 Results and Discussion

5.3.1. 3D Printing

Initial design

The initial design comprised two MWCNT elements, namely the WE (Ø = 0.2 mm) and CE (Ø = 5 mm). An initial 0.4 % S1 PEGDA platform was printed, onto which the electrodes and their conductive tracks were printed using 1 % MWCNT solution. These tracks were then insulated with a further layer of 0.4 % S1 PEGDA, with the exception of a small section at the end of the chip. This allowed for two wires to be glued on top of the insulating layer. Their ends were stripped and connected to the MWCNT tracks using Ag paint.

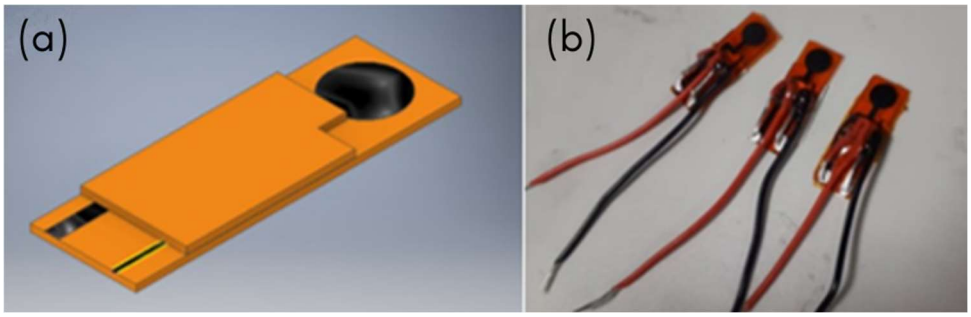

Figure 5.1: (a) 3D CAD and (b) fabricated model of MWCNT electrode chip

Chapter 4 discusses in detail the function of these electrode chips, and their effectiveness regarding PyoC detection. Notable advantages of this design include simplicity of manufacture, scalability, and disposability. However, a commercial RE was required to complete the electrochemical cell, so the sensing platform was not completely self-contained. Successfully submerging both the electrode chip and the

RE in solution could be difficult and time-consuming. Another important consideration was that conductive layers did not print consistently. Figure 5.2 demonstrates the discrepancies between the MWCNT density of two electrode chips.

Figure 5.2: Discrepancies between MWCNT dispersion in two electrode chips. On the left-hand side, a lack of opacity can be observed, indicative of poor MWCNT network formation.

A combination of tenuous MWCNT alignment and basic wire connections gave rise to inconsistent sensor performance. In terms of long-term performance, the Ag paint lost conductivity over time, which prohibited electrode function. Evidently, finding a more suitable material for electrode fabrication is vital for design optimisation.

Recessed design

A revised sensor structure was studied in part and included a small recess into which it was intended that a very small volume of solution could be deposited. Conductivity tests performed by Tiller *et al.* [2] concluded that there was little benefit to increasing

the MWCNT-PEGDA composite beyond 0.5 % w/w, so this was the concentration utilised in this design. These electrode chips were successfully printed but did not function well due to issues with the Ag paint used to connect the wires. Though the recess was not utilised, as electrodes were simply submerged in solution as before, this aspect of the design was taken forward as a way of reducing required sample size.

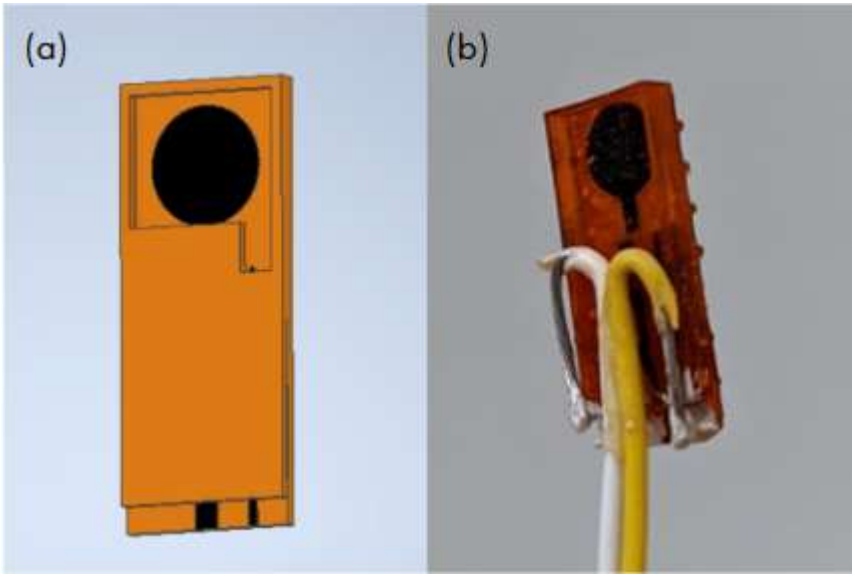

Figure 5.3: (a) 3D CAD design and (b) fabricated model of a MWCNT electrode chip with a recess for sample deposition. The initial design was modified to include small walls around the electrodes, enabling the containment of small volumes of liquid.

Staircase design

A further iteration, termed the 'staircase design', was also considered, which would have enabled electrodes to be printed using different conductive solutions. This would involve printing each electrode onto the insulating layer of the previous electrode. A pseudoreference could also be included by adding a conductive track, onto which Ag paint could be added. Printing electrodes in separate layers would allow resins to be

switched, so different combinations could be explored. A CAD mock-up of this design is included in Figure 5.4.

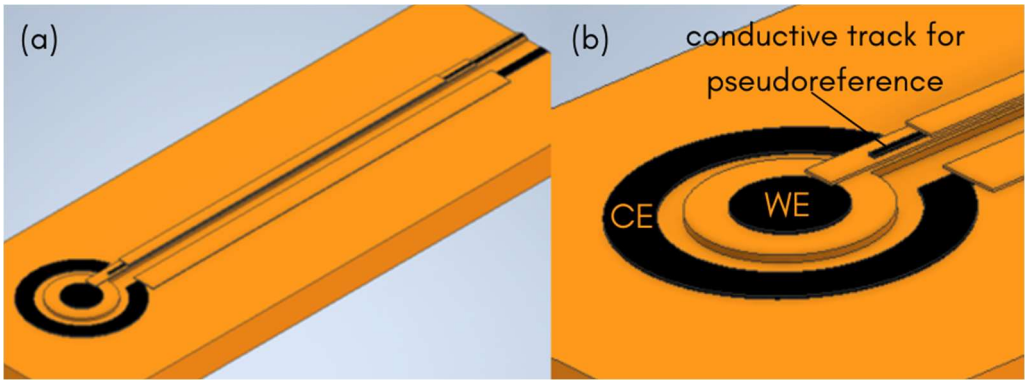

Figure 5.4: CAD mock-up of (a) staircase electrode assembly (b) electrode configuration

Compared to previous designs, electrode configuration is improved in this case, since the CE is now circumferential to the WE, rather than being placed next to it. This ensures a more uniform electric field, thus facilitating even electron transfer across the electrode. This set up forms the basis of many commercially available screen-printed electrodes (SPEs) and has been utilised across many studies which have produced successful electrochemical sensors. [3-11]

However, printing this electrode platform would have proved complicated, since insulating and conductive layers would have overlapped in places, despite careful design. It was also noted that wire attachment would be especially difficult, since the WE and RE conductive tracks sit above each other. It was not possible to investigate this design further due to time constraints, and the notion to print the electrodes separately using different resins may have proved impossible. Further exploration into how to utilise a range of materials may be a valuable prospect for future work.

As evidenced by the results presented in Chapter 4, electrodes printed using MWCNTs display poor reliability and interelectrode repeatability. Achieving homogenous MWCNT dispersion and alignment of MWCNTs may act to improve this, but this was deemed to be beyond the scope of this study. CB was selected as an alternative conductive material, being easily incorporated into resins for printing, as well as displaying excellent electrocatalytic properties. The advantages of CB are described in detail in Chapter 2.

Final design

The final version of the design included an updated electrode configuration and ensured facile manufacture, since all electrodes would be printed with the same resin and on the same layer. As demonstrated in Figure 5.5, electrodes are arranged similarly to commercial SPEs, with both the CE and RE surrounding the WE.

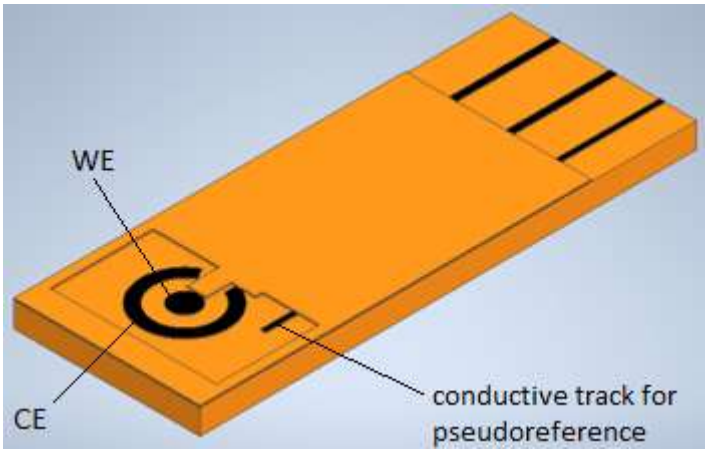

Figure 5.5: CAD drawing of the final electrode design

The WE is designed to be small (Ø = 0.2 mm) in order to reduce capacitive current. A circumferential CE ensures that $A_{CE} > A_{WE}$, which is essential for preventing current limitations. The inclusion of a conductive track allows for a pseudoreference to be added; in future, this electrode could also be partly circumferential, though this would

require screen-printing techniques to be employed post-manufacture. Tracks are well separated to allow for simpler wire attachment, and the inclusion of the pseudoreference renders the sensing platform fully functional, eliminating the need for costly commercial REs. Aside from wire attachment, the only post-processing step would be to add a small volume of Ag paint onto the conductive track. As previously discussed, the addition of a small recess would also enable low volumes of solution to be studied outwith a glass cell.

Design limitations

There are many factors to consider in terms of developing the design to be part of a point-of-care diagnostic system. First, repeatable manufacturing must be considered. Currently, there are limitations regarding homogeneity of printing resins, as discussed in Chapter 4, as well as issues with producing reliable wire connections. However, the simplicity of the electrode design renders it scalable, and it should be considered that large scale manufacturing would overcome many of the issues faced during small-scale, in-house fabrication.

Although the potentiostat currently utilised in conjunction with the printed electrodes is capable of operating via wireless Bluetooth connection, a desktop computer is still required for analysis of results. For the sensors to be rendered truly point-of-care, results must be analysed on site. Butterworth *et al.* have developed an integrated potentiostat and sensor platform, SimpleStat, which can indicate a positive or negative result for very simple measurements via a light-emitting diode (LED). This platform has been used to successfully detect the OXA-1 gene. [12] Although still in development, rapid, cost-effective sensing technology such as SimpleStat will prove to be pertinent

in terms of developing the sensing platform into a hand-held, point-of-care diagnostic system.

Another consideration is that of sample size and deposition. Currently, electrodes are submerged in a glass cell, requiring large analyte volumes. Though the possible addition of a small recess has been discussed, the introduction of microfluidics could be the key to further reducing sample volume, as well as lessening the risk of sample cross-contamination. This would also introduce the possibility of electrode miniaturisation. [13] Decreasing the WE area poses many benefits, including increasing mass transfer. [14-16] Miniaturisation also poses the benefit of closely assembled electrodes – assemblies with less than 100 nm spacing can increase sensitivity several-fold, since molecular transport time between electrodes is reduced. This limits capacitive current and is beneficial for reversible redox reactions, since the WE is close to the CE. [17-19] As such, these techniques could prove to be highly beneficial in the development of the electrodes. However, further research is required in this area to overcome issues with stability and reliability. [13]

5.3.2. Materials Study

Calibration squares

Figure 5.6 illustrates how increasing exposure time affected the thickness of a 0.5 % CB/PEGDA resin. Despite the graph having an overall upward trend, sample thickness was virtually the same between the 8 second and 16 second exposure times, with a small decrease of 1 μm. This is an unusual result; however, the overall variance in sample thickness is relatively low. These results can be compared to those obtained by Tiller *et al.* [2] for various resins and resin composites. S1/PEGDA resins showed the sharpest rise with increasing exposure times, with the slope of the graph reducing as

S1 concentrations increased. The resin composite which behaved most like the CB/PEGDA resin was S1/PEGDA containing 66 % barium titanate ($BaTiO_3$) nanopowder. In this case, the increase in sample thickness was much less between exposure times. It can be concluded that the opaquer a resin is, the less influence exposure time has on its thickness. Given that CB has such valuable optical properties, it may more readily absorb UV light than other conductive additives or absorbers.

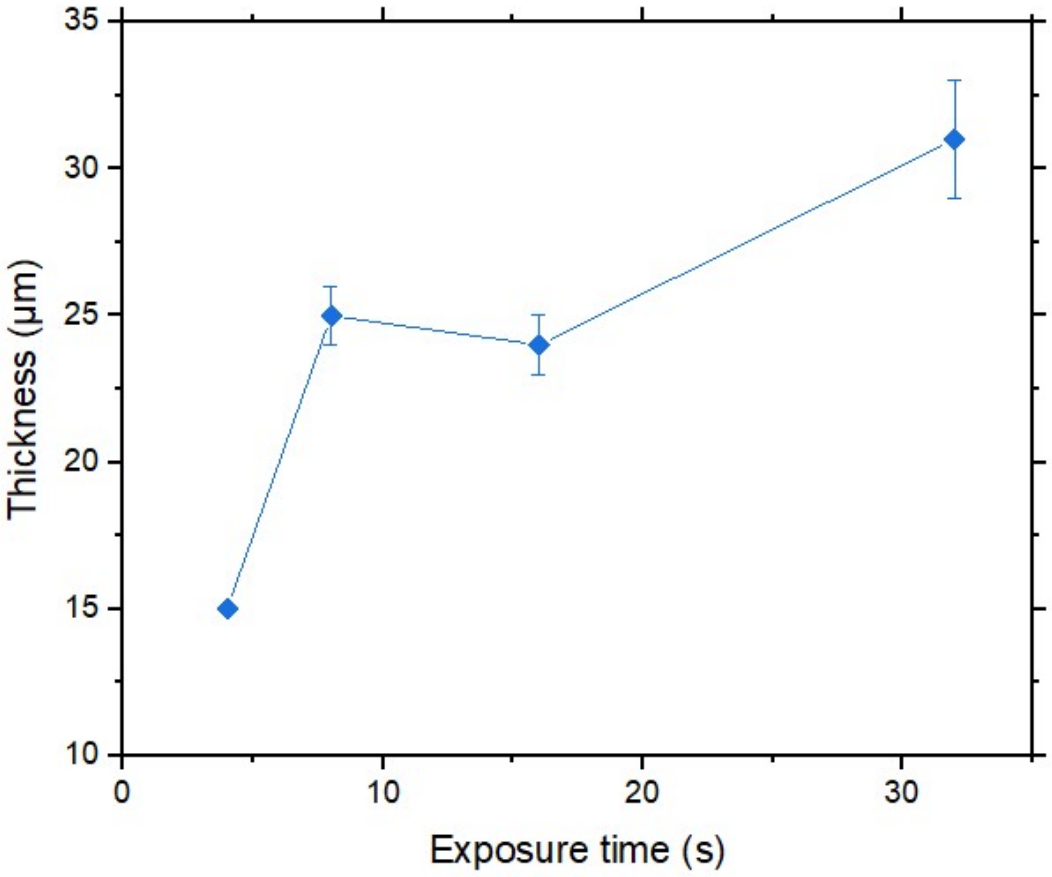

Figure 5.6: Measured membrane thickness for 0.5 % CB/PEGDA resin with increasing exposure time. Includes error bars for n = 2.

Thus, printing more complicated structures using CB resin may require altering other parameters such as UV intensity to control print thickness, rather than relying on

exposure time. The structural resins printed in conjunction would then need to be matched, such that they could be successfully cured within the required parameters.

CB-modified GC electrodes

Initial characterisation of the CB-modified GC electrodes involved exploring the magnitude of their response to $Fe(C_5H_5)_2$. This gives an indication as to how the CB resin will function in a 3D printed electrochemical sensor. Figure 5.7 (a) displays the CV response of five GC electrodes, modified with 0.2 – 1 % CB resin. Testing CB percentages above 1 % was considered unnecessary; the high pigmentation of CB would render the print material too opaque for successful photopolymerisation past this point. The oxidation peaks for each %CB are presented in Figure 5.7 (b).

As predicted, electrodes modified with low %CB (0.2 %, 0.4 % and 0.6 %) displayed extremely low redox peaks. It is likely that the small volumes of CB added to the PEGDA solution were not enough to render it sufficiently conductive. PEGDA is an insulating polymer; understanding how to add the correct conductive additive in the correct ratio is a vital step forward regarding 3D printed electrochemical sensors. This will constitute a key area of future research. A sharp increase in i_p is observed at 0.8 % CB, with similar oxidation peaks for 0.8 % and 1 % CB resins. Considering that CB percentages over 1 % would be unfavourable regarding the printing process, it was concluded that either 0.8 % or 1 % CB would be suitable for further investigation.

Electrode performance was further investigated through the use of DPV for gentamicin (GN) detection. GN is an antibiotic which is commonly used for the treatment of *P. aeruginosa* infections. [20-23] Its nature and electrochemical detection are described in more detail in Chapter 5. DPV responses to GN did not vary greatly, as evidenced in Figure 5.8.

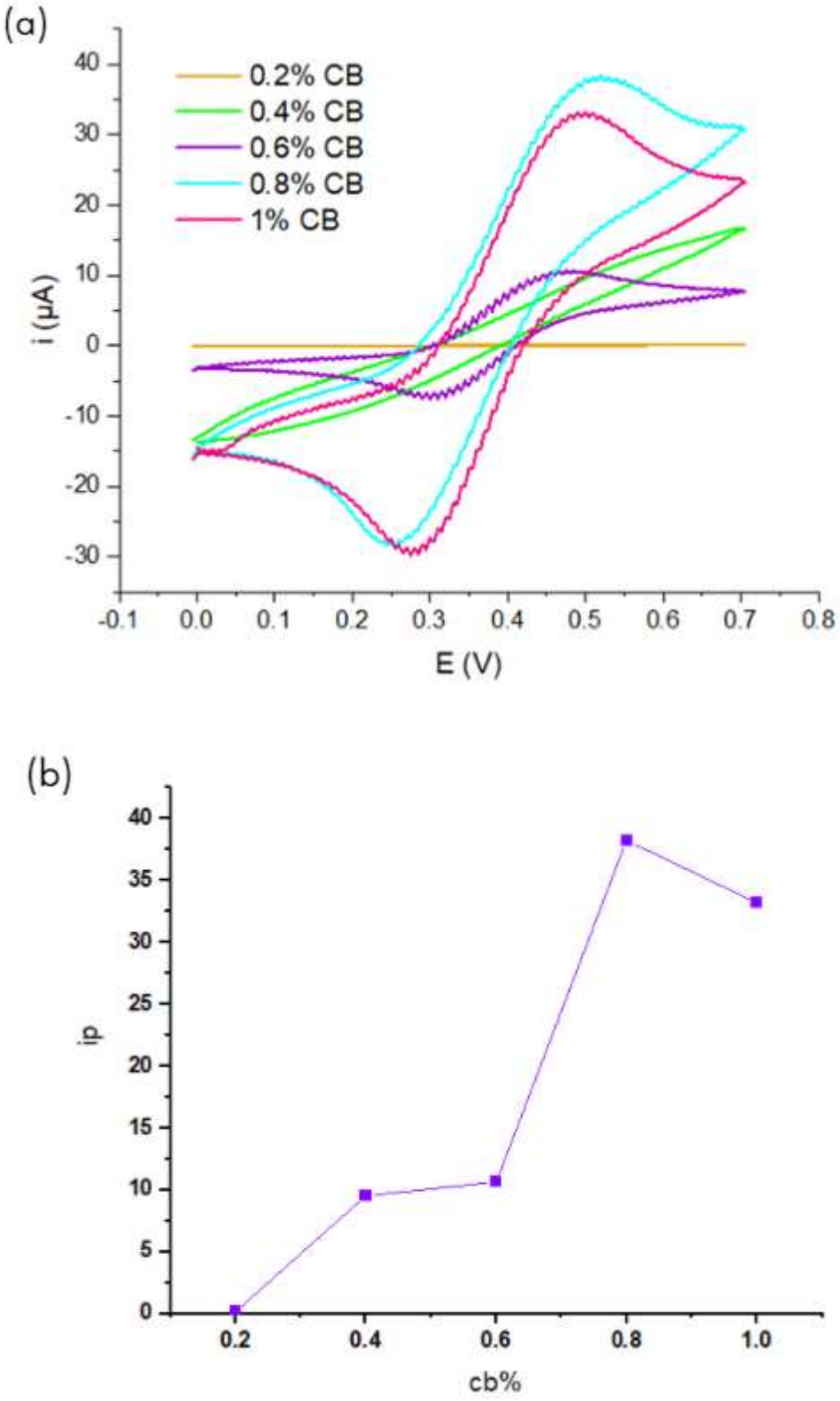

Figure 5.7: (a) Cyclic voltammograms of 5 mM $[Fe(C_5H_5)_2]$ in 0.1 M $LiClO_4$ in ACN for CB-modified GC electrodes over the potential range $0 \leq E$ vs Ag/AgCl ≤ 0.7 V at scan rate of 0.1 V s^{-1}. (b) Oxidation peaks vs. %CB.

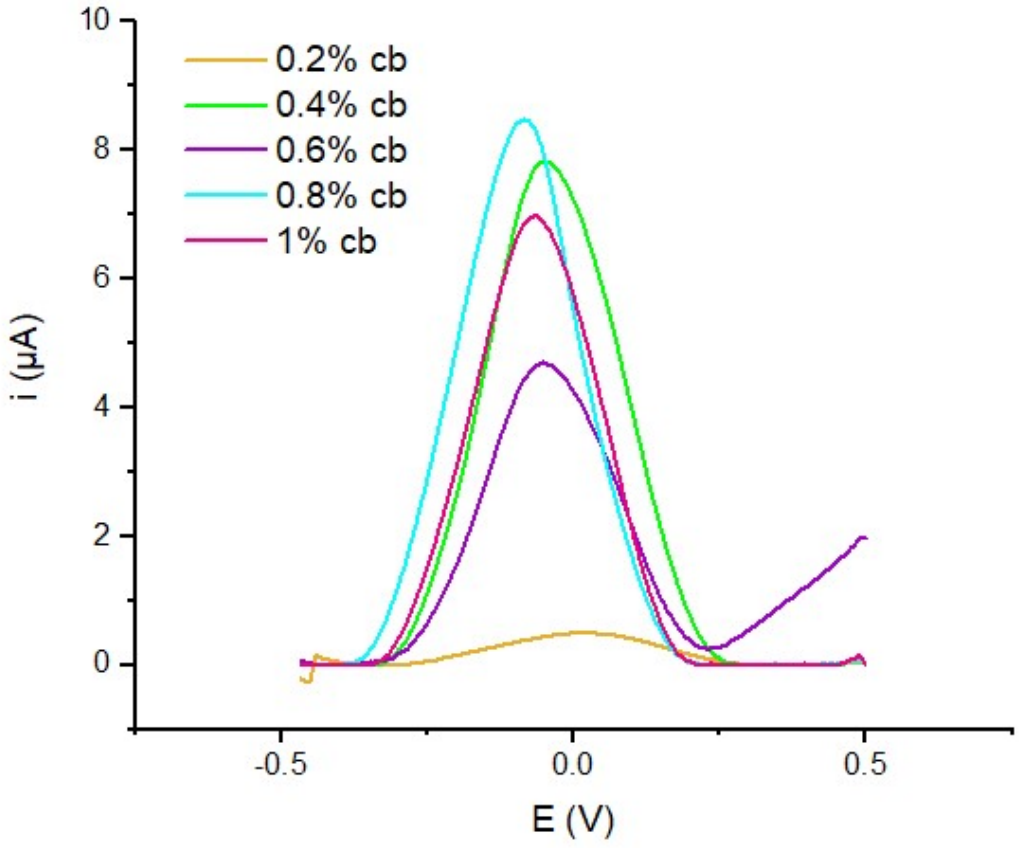

Figure 5.8: DPV responses vs. Ag wire for CB-modified GC electrodes in 100 µg/mL GN

In this case, 0.2 % and 0.6 % CB resins behaved as expected, displaying the lowest peaks. Again, 0.8 % and 1 % CB resins displayed similar responses to each other. The 0.4 % CB resin gave a higher peak than was expected; however, since the responses did not vary much from each other, this was not considered to be an abnormal result. Although little could be gleaned from the DPV results, the GC electrode modified with 0.8 % CB gave the highest peak. This in addition to its performance in $Fe(C_5H_5)_2$ led to the 0.8 % CB/PEGDA resin being selected for further investigation.

It is important to acknowledge certain limitations of this study, which may be addressed in future research. For example, a limited number of electrodes were available for analysis, with the presented data collated from just one electrode of each

%CB. This was largely due to issues with the Thinky ARE-250 conditioning planetary mixer. Sufficient mixing of CB resins is vital for conductivity; without it, modified sensors were unable to function, as the modification layer acted to insulate the surface of the GC electrode. Ideally, at least six electrodes of each %CB would be studied, and their responses averaged. In future, more thorough investigation may lead to the selection of a different optimal %CB resin; however, due to time constraints, the resin which performed best within the scope of this study was selected for further analysis.

5.4 Conclusion

The development of an effective electrochemical sensing platform relies on careful design and consideration of manufacturing methods. Here, the first steps of this process are described. The evolution of electrode assembly designs involved the addition of a recess to allow for the deposition of a small volume of solution, which could eliminate the need for a glass cell, an important step towards point-of-care diagnostics. A circumferential CE was also proposed, which would improve electron transfer. However, as discussed, miniaturisation and the introduction of microfluidics could hold the key to further improving sensor design.

DLP was successfully utilised for printing electrodes, with printing materials switched during pauses in the build process. This enabled conductive layers to be printed on top of structural layers and proved to be a rapid and low-cost method of manufacture. However, mass manufacture of these electrodes would further reduce production time and cost, as well as help to overcome the limitations of in-house, small batch printing.

Following the assessment of electrodes printed with MWCNTs in Chapter 4, initial steps were taken towards the exploration of CB as an alternative printing material. The

response of the CB-modified GC electrodes to $Fe(C_5H_5)_2$, as well as their ability to detect GN, suggest that CB-based resins could be successfully utilised in future 3D printed electrochemical sensors. However, it is important that these resins are investigated more thoroughly before such manufacture is considered.

5.5 References

1. H. Gong, M. Beauchamp, S. Perry, A. T. Woolley and G. P. Nordin, *RSC Advances*, 2015, **5**, 106621-106632.
2. B. Tiller, A. Reid, B. Zhu, J. Guerreiro, R. Domingo-Roca, J. Curt Jackson and J. F. C. Windmill, *Materials & Design*, 2019, **165**, 107593.
3. F. A. Alatraktchi, M. Dimaki, N. Støvring, H. K. Johansen, S. Molin and W. E. Svendsen, *Analytical Biochemistry*, 2020, **593**, 113586.
4. F. Alatraktchi, *PLoS One*, 2018, **13**.
5. F. A. Alatraktchi, H. K. Johansen, S. Molin and W. E. Svendsen, *Nanomedicine (Lond)*, 2016, **11**, 2185-2195.
6. F. Arduini, F. Di Nardo, A. Amine, L. Micheli, G. Palleschi and D. Moscone, *Electroanalysis*, 2012, **24**, 743-751.
7. S. Cinti, N. Colozza, I. Cacciotti, D. Moscone, M. Polomoshnov, E. Sowade, R. R. Baumann and F. Arduini, *Sensors and Actuators B: Chemical*, 2018, **265**, 155-160.
8. J. C. Liao, M. Mastali, V. Gau, M. A. Suchard, A. K. Møller, D. A. Bruckner, J. T. Babbitt, Y. Li, J. Gornbein, E. M. Landaw, E. R. McCabe, B. M. Churchill and D. A. Haake, *Journal of Clinical Microbiology*, 2006, **44**, 561-570.
9. M. Portaccio, D. Di Tuoro, F. Arduini, D. Moscone, M. Cammarota, D. G. Mita and M. Lepore, *Electrochimica Acta*, 2013, **109**, 340-347.
10. J. I. A. Rashid, V. Kannan, M. H. Ahmad, A. A. Mon, S. Taufik, A. Miskon, K. K. Ong and N. A. Yusof, *Materials Science and Engineering: C*, 2021, **120**, 111625.
11. H. J. Sismaet, A. Banerjee, S. McNish, Y. Choi, M. Torralba, S. Lucas, A. Chan, V. K. Shanmugam and E. D. Goluch, *Wound Repair and Regeneration*, 2016, **24**, 366-372.
12. A. Butterworth, D. K. Corrigan and A. C. Ward, *Analytical Methods*, 2019, **11**, 1958-1965.
13. T. A. Webster and E. D. Goluch, *Lab Chip*, 2012, **12**, 5195-5201.
14. W. E. Morf and N. F. de Rooij, *Sensors and Actuators A: Physical*, 1995, **51**, 89-95.
15. W. E. Morf and N. F. de Rooij, *Sensors and Actuators B: Chemical*, 1997, **44**, 538-541.
16. S. G. Weber, *Analytical Chemistry*, 1989, **61**, 295-302.
17. B. Wolfrum, M. Zevenbergen and S. Lemay, *Analytical Chemistry*, 2008, **80**, 972-977.
18. M. A. G. Zevenbergen, D. Krapf, M. R. Zuiddam and S. G. Lemay, *Nano Letters*, 2007, **7**, 384-388.
19. M. A. G. Zevenbergen, P. S. Singh, E. D. Goluch, B. L. Wolfrum and S. G. Lemay, *Nano Letters*, 2011, **11**, 2881-2886.
20. B. Teixeira, H. Rodulfo, N. Carreño, M. Guzmán, E. Salazar and M. De Donato, *Revista do Instituto de Medicina Tropical de Sao Paulo*, 2016, **58**, 13-13.

21. G. Rukholm, C. Mugabe, A. O. Azghani and A. Omri, *International Journal of Antimicrobial Agents*, 2006, **27**, 247-252.
22. N. L. Martin and T. J. Beveridge, *Antimicrobial agents and chemotherapy*, 1986, **29**, 1079-1087.
23. B. J. Chaves and P. Tadi, Gentamicin, https://www.ncbi.nlm.nih.gov/books/NBK557550/).

CHAPTER SIX

CHARACTERISING THE RESPONSE OF CB-MODIFIED GC ELECTRODES TO THE AMINOGLYCOSIDE ANTIBIOTIC GENTAMICIN

6.1 Overview

The facile manufacture of 3D printed electrochemical sensors has been previously described. Sensor development depends in part on the assessment of novel conductive printing resins. Carbon black has excellent conductive properties and fast electron transfer kinetics and was successfully incorporated into a photopolymerisable resin for the modification of glassy carbon electrodes. Gentamicin was selected for electrochemical investigation, being a common antibiotic for the treatment of *P. aeruginosa* infections. CB-modified GC electrodes for the detection of clinically relevant concentrations of gentamicin were investigated and compared to the response of a commercially available glassy carbon electrode. Electrodes achieved detection of gentamicin across the therapeutic range. Despite this, the results presented herein are preliminary, with further investigation into the electrochemical performance of CB-based resin required.

6.2 Introduction

Gentamicin (GN) is an aminoglycoside antibiotic which is commonly used for the treatment of *P. aeruginosa*-derived HCAIs. [1-4] Though effective in inhibiting bacterial growth, [5] GN can also cause serious side effects if administered outwith a tight safety margin, such as hearing loss and nephrotoxicity. [6] Its rapid detection is valuable for monitoring its local release from beads or spacers, and quantification of its systemic concentration is useful for patient monitoring. [7, 8]

Typically, GN is detected via microbiological assays, [5, 9-11] or immunoassays [5, 6, 9, 12-15] such as enzyme linked immunosorbent assay (ELISA). [6] Despite their simplicity and cost-effectiveness, microbiological assays require significant incubation and can suffer limited reproducibility. [9] Immunoassays provide higher accuracy and better

specificity, and sample pretreatment is less complicated. [5, 9] Both microbiological assays and immunoassays risk antibiotic interference. [9] High-performance liquid chromatography (HPLC) can also be used for sensitive GN detection. However, additional steps such as post-column derivatisation and fluorescence detection may be required. [6, 16]

The electrochemical detection of GN is an area of research that is yet to be explored in depth. Ghinami *et al.* have described the use of an electrochemical detector set up with an amperometric waveform for GN detection. The purpose of the study was to develop a simple detection method which complied with the European Pharmacopoeia (EP) analytical method, which involved integrated pulsed amperometric detection (IPAD). [17] However, voltammetric detection of GN is not widely reported. Techniques such as differential pulse voltammetry (DPV) allow for rapid analyte detection and may be advantageous as a facile technique for GN detection.

Carbon black (CB) has potential as a conductive additive for use in photopolymerisable resins, which can be utilised in 3D printing. It displays excellent conductivity, and its low cost renders it an accessible choice for rapid prototyping. [18, 19] CB was incorporated into poly(ethylene glycol) diacrylate (PEGDA) and used to modify the surface of commercial GC electrodes.

This study explores the effectiveness of CB-modified GC electrodes compared to an unmodified GC electrode in detecting GN. This was considered a valuable first step in assessing the suitability of the CB/PEGDA resin for use in 3D printed electrochemical sensing platforms.

6.3 Results and Discussion

6.3.1. Electrochemical characterisation

The first step towards investigating the performance of the CB-modified GC electrodes was to test them in $Fe(C_5H_5)_2$, a standard redox compound, as shown in Figure 6.1.

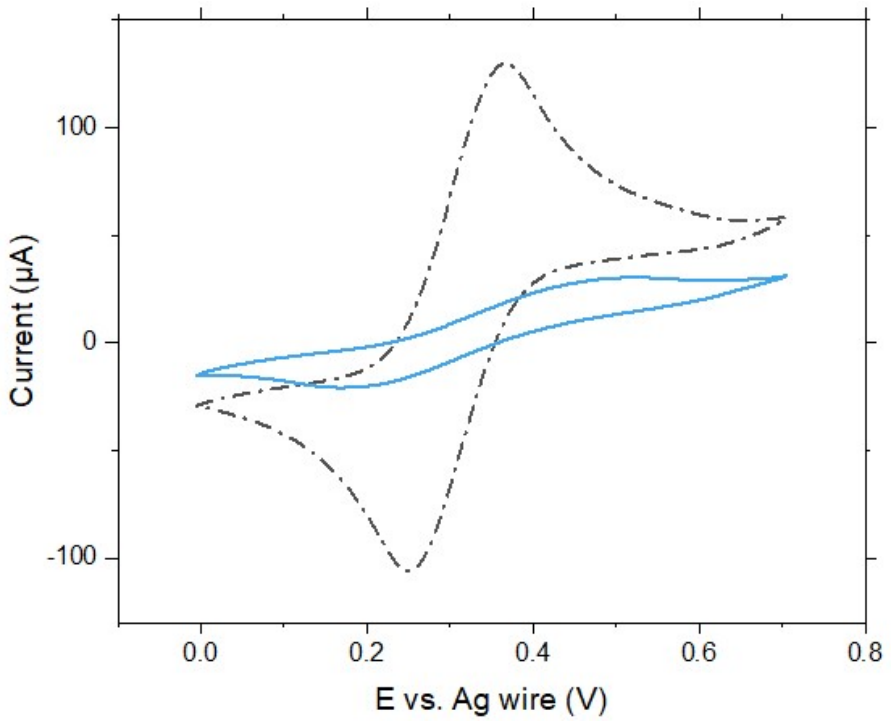

Figure 6.1: Cyclic voltammogram of 5 mM [Fe(C5H5)2] in 0.1 M LiClO4 in ACN for a GC (black) and CB-modified GC (blue) electrode over the potential range 0 ≤ E vs Ag wire ≤.0.7 V at a scan rate of 0.1 V s^{-1}.

In this case, the unmodified GC electrode adheres to the Nernst equation (Equation 4.1), exhibiting reversible behaviour as expected, though the peak separation is approximately 100 mV, which is slightly higher than that achieved in Chapter 3. This may be due to the utilisation of a pseudoreference (Ag wire) electrode, which is not ideally nonpolarisable. [20]

Peak separation was larger for the CB-modified GC electrode, with a sizeable decrease in i_p. This is postulated to be due to the inhibitory effects of the PEGDA-based resin, which may act to slow electron transfer kinetics. [21] The cyclic voltammogram appears to suggest a quasi-reversible response, similar to that which would be displayed by an insufficiently polished GC electrode. [22] This supports the hypothesis that the electrode modification is hindering the electrochemical activity of the GC electrode.

It should also be noted that any future printing with this resin would involve much smaller electrode areas, which would further reduce the i_p. Future work would therefore involve increasing electrode sensitivity as much as possible. Since the CB-modified GC electrode performed adequately in $Fe(C_5H_5)_2$, it was deemed acceptable to assess its response to clinically relevant concentrations of GN.

6.3.2. GN detection

As DPV has not been widely studied as a method of detecting GN, it was first necessary to establish a potential range on which to focus. As displayed in Figure 6.2, reduction potentials were observed at approximately -0.1 V and -0.075 V for the GC and CB-modified GC electrodes respectively. Due to time constraints, it was not possible to optimise all parameters; however, clear reduction peaks were observed across all scans.

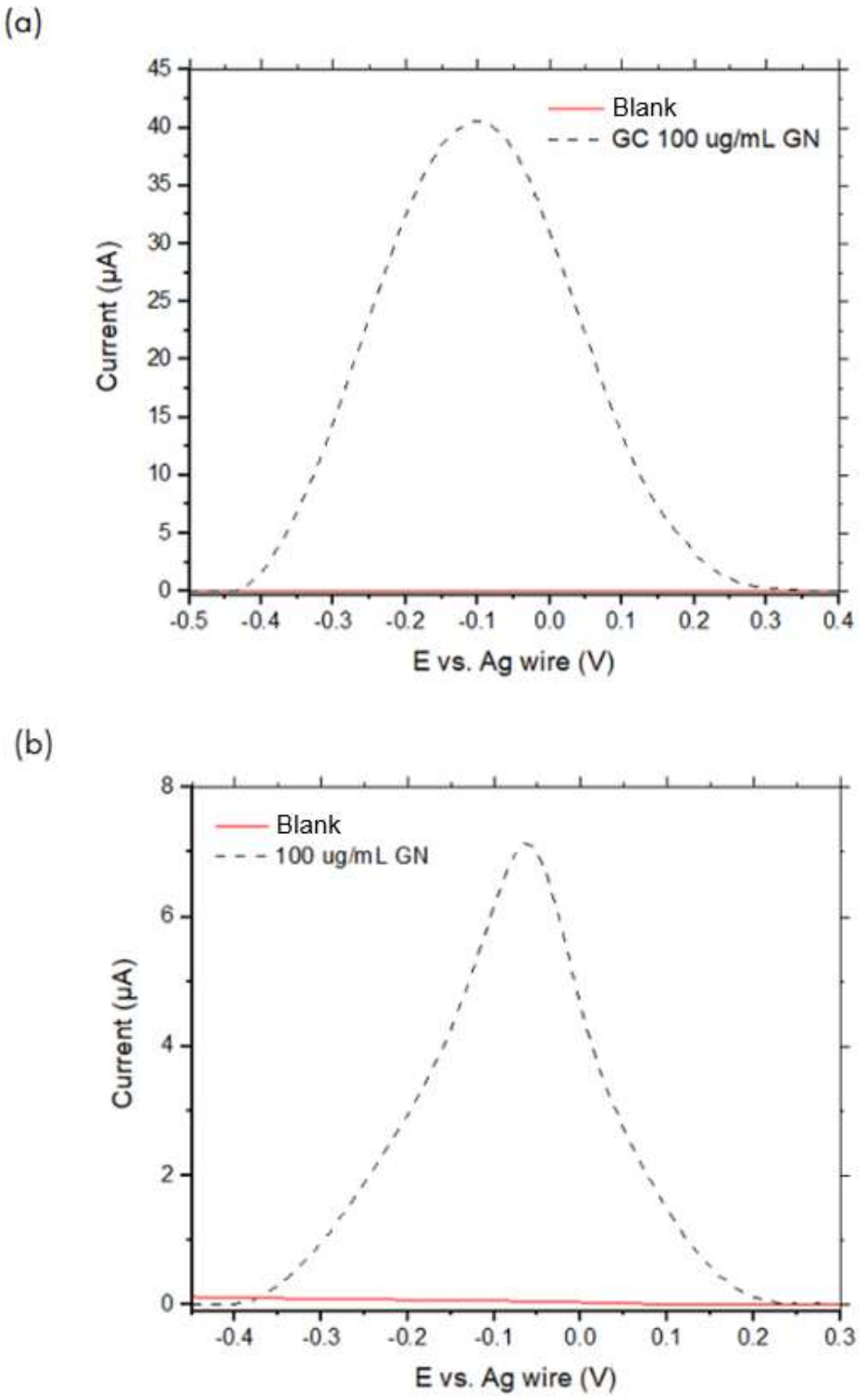

Figure 6.2: DPV responses for controls in 0.1 M PBS (red) and response from 100 µg/mL GN in 0.1 M PBS (black) for (a) GC electrode and (b) CB-modified GC electrode recorded at a scan rate of 0.1 Vs^{-1}.

These potentials are similar, with a virtually negligible positive shift observed in the case of the CB-modified GC electrode. An important consideration is that PyoC phenazine transformations are likely to occur within this potential window. [23] Thus, the possibility of interference is introduced, should electrode development involve simultaneous detection of multiple analytes. It may be necessary in this case to monitor another aminoglycoside antibiotic, such as streptomycin (STR), which has displayed oxidation peaks at circa 0.54 V vs. Ag wire. [24] Despite this, both electrode responses to GN are identifiable compared to the baseline, which indicates that both are capable of detecting the drug. Though there may be future issues with interference, it was still deemed to be valuable to research GN detection across a clinically relevant range.

6.3.3. Analytical Performance

The DPV response of the GC and CB-modified GC electrodes to increasing concentrations of GN is displayed in Figure 6.3, with insets showing peak intensity against [GN]. Electrodes were tested over the concentration range $0 \leq [GN] \leq 200$ µg/mL, in accordance with European Pharmacopoeia (EP) and U.S. Pharmacopeia (USP) methods. [25]

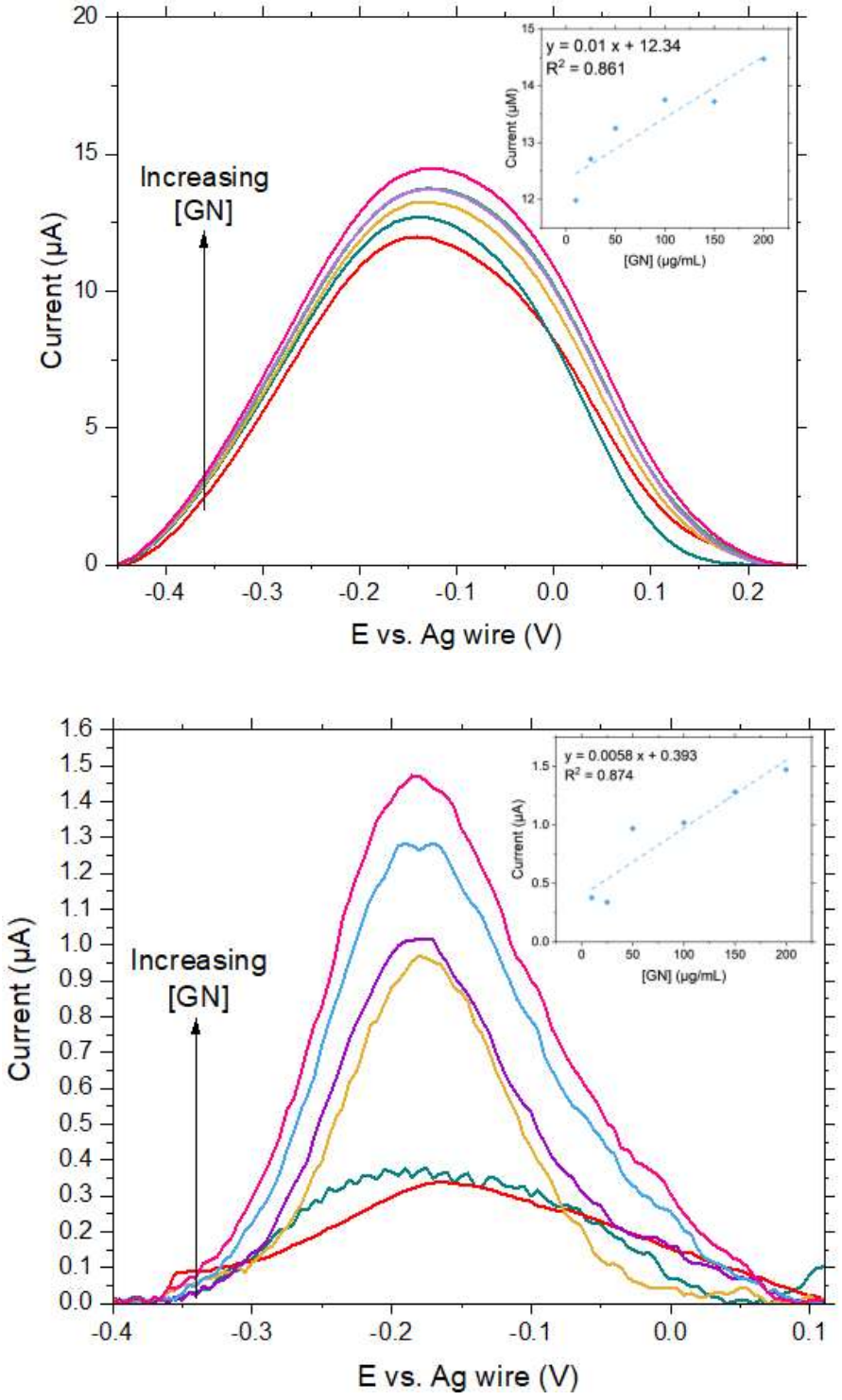

Figure 6.3: DPV responses for (a) GC electrode and (b) CB-modified GC electrode obtained for 0 to 200 µg/mL GN in 0.1 M PBS at a scan rate of 0.1 V s-1 insets show the corresponding linear relationship of this response with [GN].

Notable here are the slopes of the linear regression graphs, which have a relatively low m value where $y = mx + c$. For this type of analysis, a much higher value would be expected (See Figure 3.4(a)). These lesser slopes are postulated to be due to GN being less redox active at this pH. Dokuzparmak *et al.* [26] studied the detection of amphetamine type stimulants (ATS) via an electrochemiluminescence (ECL) strategy. It was noted that the overall efficiency of the reaction, as well as the ECL intensity, was strongly affected by the pH of the sample, [27-29] which affects the dominant form of the molecule. It is possible that the GN sample exhibits suboptimal electrochemical activity due to its pH level. It would be beneficial to study this theory in more depth with a comprehensive pH study, although this was beyond the scope of the current work.

The linear regression curves displayed in the inset of each graph display the line of best fit as determined by data analysis software (Origin). However, it is important to note that the response of the electrodes to GN are not truly linear. The trend displayed in Figure 6.3 (a) suggests an upward curve, whilst in Figure 6.3 (b), the presence of two linear curves is suggested. Further work is required to determine if these trends are accurate and consider their implications. Though linearity was not achieved, the results suggest that the CB/PEGDA resin has potential as a printing material for future electrochemical sensors.

6.3.4. Repeatability

Intraelectrode repeatability

Electrodes were examined for their ability to produce consistent readings over multiple scans. One GC and one CB-modified GC electrode were tested six times in 150 µg/mL GN, resulting in RSD values of 0.802 % and 14.56 % respectively.

Table 6.1: Relative standard deviation for a GC electrode across six scans in 150 µg/mL GN.

	Scan 1	Scan 2	Scan 3	Scan 4	Scan 5	Scan 6
i_p (µA)	**13.610**	**13.586**	**13.613**	**13.642**	**13.620**	**13.903**
$\bar{i}_p$ (µA)	**13.587**					
SD	**0.109**					
RSD (%)	**0.802**					

Table 6.2: Relative standard deviation for a CB-modified GC electrode across six scans in 150 µg/mL GN.

	Scan 1	Scan 2	Scan 3	Scan 4	Scan 5	Scan 6
i_p (µA)	**1.500**	**1.385**	**1.310**	**1.208**	**1.106**	**0.949**
$\bar{i}_p$ (µA)	**1.243**					
SD	**0.181**					
RSD (%)	**14.56**					

This marks an ~18-fold increase in RSD between the GC electrode and the CB-modified GC electrode. It is clear that the modification layer adversely affects repeatability, and that the CB-modified electrode response is inconsistent across multiple scans.

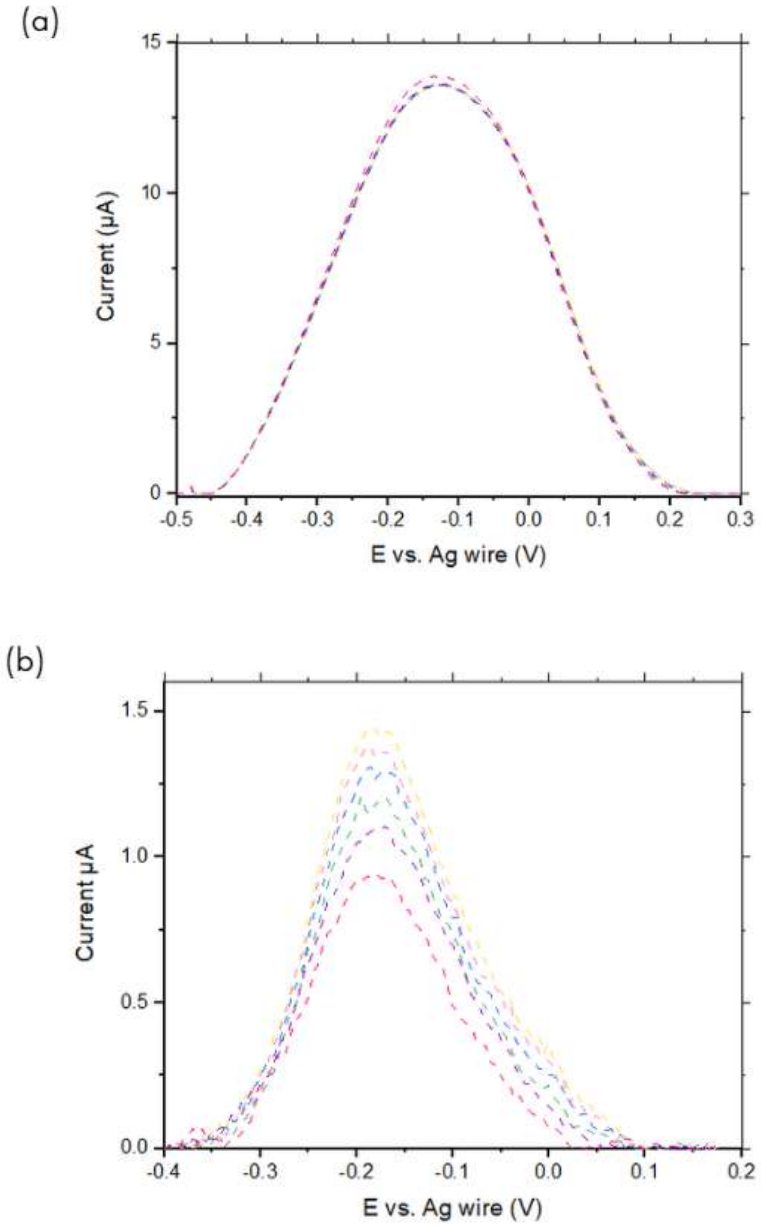

Figure 6.4: The response of (a) a GC electrode and (b) a CB-modified GC electrode across six scans in 150 µg/mL.

GC electrodes owe their excellent function and repeatability in part to their uniformity and high conductivity. As with the MWCNT electrodes discussed in Chapter 3, the CB-modified electrodes are likely subject to poor homogeneity and sheltering of electrochemically active carbon particles by PEGDA. The conductive path may differ between scans, and since the electrodes cannot be polished, there is no simple way to ensure a consistent response. Improving upon this will be a vital area of future work, possibly involving adaption of the conductive resin. Pretreatment steps could also help to overcome the issue, although the ideal goal is to produce a sensing platform using facile manufacturing, without any need for pretreatment.

Long-term repeatability

Electrodes were also tested over six days to assess their long-term stability. As displayed in Table 6.3, the RSD value for one CB-modified GC electrode was high with a value of 38.26 %. In comparison, the RSD value for the GC electrode was 5.85 %.

Table 6.3: Relative standard deviation for one CB-modified GC electrode tested in triplicate over 6 days in 150 µg/mL GN.

	Day 1	Day 2	Day 3	Day 4	Day 5	Day 6
i_{p1} (µA)	**0.782**	**1.418**	**1.122**	**0.567**	**1.333**	**0.513**
i_{p2} (µA)	**0.948**	**1.461**	**1.217**	**0.505**	**1.414**	**0.539**
i_{p3} (µA)	**1.078**	**1.606**	**1.406**	**0.540**	**1.725**	**0.581**
$\bar{i}_p$ (µA)	**0.936**	**1.495**	**1.248**	**0.537**	**1.490**	**0.544**
SD	**0.121**	**0.080**	**0.118**	**0.025**	**0.169**	**0.028**
					RSD (%)	**38.26**

The RSD value achieved for the modified electrode highlights a key issue - although printed electrodes would ideally be disposable, poor long-term repeatability calls into question the shelf-life of the product. Given that results will be used to inform healthcare, it is vital that electrodes are stable over time and that readings are consistent and reliable. The issue of ensuring homogeneity of conductive printing resins is central to this project and will prove to be one of the biggest obstacles regarding future work. Mass manufacturing may help to improve repeatability, but the feasibility of printing electrodes using stereolithographic techniques will need to be assessed in much greater detail.

6.3.5. Biological Samples

Given that the CB-modified electrodes were able to detect GN in ideal matrices, their response to biological matrices was also deemed important to assess. GN was spiked into human pooled serum and analysed directly, without any sample purification. Blank serum was initially analysed, with the response used as a baseline against which spiked serum scans would be compared. Serum was then spiked with 50 µg/mL and 100 µg/mL GN for analysis. However, no notable difference was observed between the baseline response and the spiked serum responses for either electrode, as illustrated in Figure 6.5.

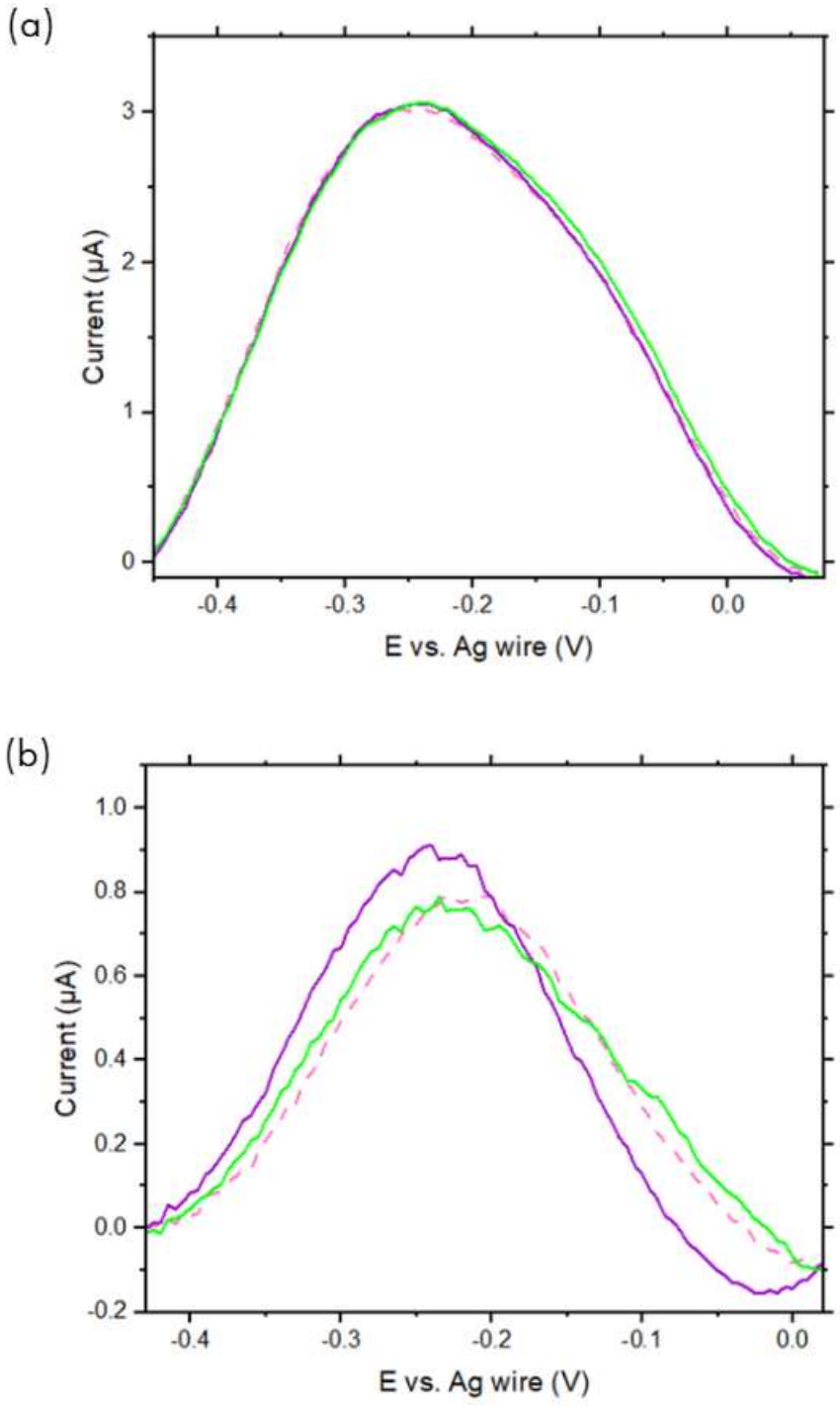

Figure 6.5: Average responses of 50 µg/mL (purple) GN and 100 µg/mL (green) GN within human pooled serum for a (a) GC electrode and (b) CB-modified GC electrode at a scan rate of 0.1 V s^{-1}. The blank response is shown in pink.

This indicates that neither electrode was able to successfully detect GN within a biological environment. The limited redox activity of GN in combination with the complexity of the serum matrix is the most likely reason for this. Sample purification could help to overcome this issue, as could adjusting the pH of the GN. Due to time limitations, detection in biological samples could not be further investigated; however, this will be an important area of future work. It is vital that manufactured electrodes can detect target analytes in clinical samples, to ensure their success in patient monitoring and diagnosis.

It is important to acknowledge the various limitations of this study. Issues with the THINKY mixer often rendered CB/PEGDA resins completely insulating, so it was not possible to produce six electrodes which were able to give a response. Thus, all results discussed in this chapter are based on one electrode only, and it was not possible to study interelectrode repeatability. Clearly this is an inadequate assessment of the feasibility of CB-based resins for the manufacture of electrochemical sensors. This study will need to be repeated in future with at least six functioning electrodes, to produce statistically relevant results. Another issue is the limited redox activity of GN. As discussed, it may be beneficial to adapt the pH of the drug, or to assess the response of CB-modified GC electrodes to another antibiotic such as STR.

6.4 Conclusion

Assessing the electrochemical performance of CB-based resin is an important step towards the development of a 3D printed electrochemical sensor. A photopolymerisable resin was developed which incorporated CB and was simple and economical to produce. The response of the CB-modified electrode to $Fe(C_5H_5)_2$ was

adequate, and it was able to achieve a response over a clinically relevant GN concentration range. However, long term and intraelectrode repeatability studies highlighted issues with the reliability of the modified electrode, with RSD values of 14.56 % and 38.26 % respectively. The resin likely suffers from many of the same drawbacks as the MWCNT printing resin discussed in Chapter 3; working towards improving these issues will be vital for improving both the repeatability and the sensitivity of the final product.

This study establishes the methodology for producing CB-modified electrodes and outlines the voltammetric procedures that are required for their characterisation. Its limitations have been discussed and it is clear that future work would involve repeating this study with a statistically relevant number of electrodes or assessing the performance of fully printed electrodes which utilise a CB-based conductive resin. It may also be advantageous to determine the analytical performance of the electrodes using a more redox active drug, which would enable a more complete investigation.

6.5 References

1. B. Teixeira, H. Rodulfo, N. Carreño, M. Guzmán, E. Salazar and M. De Donato, *Revista do Instituto de Medicina Tropical de Sao Paulo*, 2016, **58**, 13-13.
2. G. Rukholm, C. Mugabe, A. O. Azghani and A. Omri, *International Journal of Antimicrobial Agents*, 2006, **27**, 247-252.
3. N. L. Martin and T. J. Beveridge, *Antimicrobial Agents and Chemotherapy*, 1986, **29**, 1079-1087.
4. B. J. Chaves and P. Tadi, Gentamicin, https://www.ncbi.nlm.nih.gov/books/NBK557550/).
5. Y. Chen, X. Li, L. He, S. Tang and X. Xiao, *Journal of AOAC International*, 2010, **93**, 335-342.
6. Q. Liu, H. Mu, C. Sun and J. Duan, *RSC Advances*, 2016, **6**, 14483-14489.
7. J. C. E. Odekerken, D. M. W. Logister, L. Assabre, J. J. C. Arts, G. H. I. M. Walenkamp and T. J. M. Welting, *SpringerPlus*, 2015, **4**, 614-614.
8. H. Wahlig, E. Dingeldein, R. Bergmann and K. Reuss, *The Journal of Bone and Joint Surgery*, 1978, **60-b**, 270-275.
9. J. M. Fernández-Ramos, A. M. García-Campaña, F. Alés-Barrero and J. M. Bosque-Sendra, *Talanta*, 2006, **69**, 763-768.
10. M. E. Lund, D. J. Blazevic and J. M. Matsen, *Antimicrobial Agents and Chemotherapy*, 1973, **4**, 569-573.
11. C. H. Lantz, D. J. Lawrie, F. G. Witebsky and J. D. MacLowry, *Journal of Clinical Microbiology*, 1980, **12**, 583-589.
12. J. M. Andrews and R. Wise, *Journal of Antimicrobial Chemotherapy*, 1984, **14**, 509-520.
13. W. Haasnoot and R. Verheijen, *Food and Agricultural Immunology*, 2001, **13**, 131-134.
14. N. Pastor-Navarro, A. Maquieira and R. Puchades, *Analytical and Bioanalytical Chemistry*, 2009, **395**, 907-920.
15. T. Le, H. He, X. Niu, Y. Chen and J. Xu, *Food and Agricultural Immunology*, 2013, **24**, 467-480.
16. A. Posyniak, J. Zmudzki and J. Niedzielska, *Journal of Chromatography A*, 2001, **914**, 59-66.
17. C. Ghinami, V. Giuliani, A. Menarini, F. Abballe, S. Travaini and T. Ladisa, *Journal of Chromatography A*, 2007, **1139**, 53-56.
18. T. A. Silva and O. Fatibello-Filho, *Analytical Methods*, 2017, **9**, 4680-4687.
19. F. Arduini, S. Cinti, V. Mazzaracchio, V. Scognamiglio, A. Amine and D. Moscone, *Biosensors and Bioelectronics*, 2020, **156**, 112033.
20. G. Inzelt, in *Handbook of Reference Electrodes*, eds. G. Inzelt, A. Lewenstam and F. Scholz, Springer Berlin Heidelberg, Berlin, Heidelberg, 2013, pp. 331-332.
21. T. Pajkossy and S. Vesztergom, *Electrochimica Acta*, 2019, **297**, 1121-1129.
22. D. J. Graham, Electrochemical Reversibility, https://sop4cv.com/chapters/ElectrochemicalReversibility.html, (accessed 14/4/22).

23. D. Sharp, P. Gladstone, R. B. Smith, S. Forsythe and J. Davis, *Bioelectrochemistry*, 2010, **77**, 114-119.
24. S. Akbarzadeh, H. Khajesharifi and M. Thompson, *Biosensors (Basel)*, 2020, **10**.
25. Antec, *Application Note Aminoglycosides Antibiotics*.
26. E. Dokuzparmak, K. Brown and L. Dennany, *Analyst*, 2021, **146**, 3336-3345.
27. K. Brown, C. Jacquet, J. Biscay, P. Allan and L. Dennany, *Analyst*, 2020, **145**, 4295-4304.
28. J. McGeehan and L. Dennany, *Forensic Science International*, 2016, **264**, 1-6.
29. L. Dennany, E. J. O'Reilly, T. E. Keyes and R. J. Forster, *Electrochemistry Communications*, 2006, **8**, 1588-1594.

CHAPTER SEVEN

CONCLUSIONS AND FUTURE WORK

Conclusions

P. aeruginosa is a prevalent and opportunistic pathogen which often causes nosocomial infection. Such infections can be particularly aggressive, resulting in significant morbidity and mortality. Electrochemical detection of *P. aeruginosa* is a rapidly growing area of research. Simple instrumentation and minimal sample volumes may be used to produce results with high sensitivity. Of particular note are studies which explore novel sensor design, materials selection, and print surfaces, all of which may be exploited within a clinical environment. Sensors may also be used in tandem with portable, handheld potentiostats, thus facilitating point-of-care bacterial detection. As the area continues to grow and new fabrication techniques come to light, proposed sensor designs will become even more facile and cost effective, rendering them more accessible and applicable to clinical use.

PyoC is deemed to be an attractive *P. aeruginosa* biomarker, since it is exclusively secreted by the bacterium, and significantly contributes to its pathogenesis via its redox activity. Though extremely disruptive to the host, this activity allows for the electrochemical detection of PyoC, via various voltammetric methods including CV and DPV. For these reasons, PyoC was selected for use throughout this study, to test the specificity and sensitivity of our 3D printed sensing platforms. Also, of interest was the aminoglycoside antibiotic gentamicin (GN), commonly utilised for the treatment of *P. aeruginosa* infections. Its facile electrochemical detection within a clinical setting would be highly beneficial for patient monitoring and safety.

Our initial study characterised novel electrode chips comprising WE and CE, whose conductive layers were fabricated using a 0.1 % S1 1 % (w/w) MWCNT-PEGDA resin. These electrodes displayed a linear response across a clinically relevant range of $0 \leq [PyoC] \leq 100$ μM, with a LOD of 1 μM. Inter-electrode repeatability results were poor, displaying a relative deviation of 18. 5% across six electrodes. PyoC detection was also proved to be possible within spiked serum samples, with acceptable percentage recoveries of 92-95 %. The main limitation of this study was a lack of understanding regarding how MWCNTs behave within a polymer matrix, and how effectively they can be printed. It was postulated that poor connections between MWCNTs led to lower sensor conductivity and thus less sensitive analyte detection. Though there are well-established protocols for improving CNT alignment, this was deemed to be beyond the scope of our laboratory facilities. Despite issues with MWCNT performance, this was a valuable, proof-of-concept study, which introduced a novel method of sensor manufacture.

In order to move forward with new and improved designs, it was important to select another conductive material to incorporate into the printing resin. The advantages of using carbon materials for sensor manufacture are manifold, and of particular interest was carbon black, (CB). Already a material of interest for biosensor applications, due to its excellent chemical, mechanical and physical properties, CB was selected for further study. Compared to MWCNT, CB is a cheaper option, and can be incorporated more readily into resins. Initial CB characterisation involved the surface modification of commercial GC electrodes (Ø = 3 mm) with CB-PEGDA resins, at concentrations of 0.2 % to 1 % (w/w). Their initial characterisation in ferrocene ($Fe(C_5H_5)_2$) and GN

lead to the selection of the 0.8% CB resin as an optimal material for electrode modification.

This resin was studied in more detail in Chapter 5. Though this study was not without limitations, it was confirmed that CB-modified GC electrodes were capable of detecting clinically relevant concentrations of GN. Linearity was achieved across this range, with intraelectrode and long-term repeatability studies producing RSD values of 14.56 % and 38.26 % respectively. It was postulated that the CB resin suffered from many of the same issues as the MWCNT resin, with the insulating PEGDA environment somewhat hindering electrochemical activity. It is clear that further development of conductive resins will be vital for improving electrode performance.

Many factors must be considered regarding the design of the sensing platform. Electrode placement and geometry is vital to performance, with facile sample deposition a main goal. User friendliness, size, scalability, and disposability were considered whilst developing a model that could be 3D printed with relative ease. Aside from exploring CB as a new conductive material, later iterations of the platform design included a circumferential counter electrode (CE) to facilitate homogenous electron transfer, and a recess into which small sample volumes could be deposited.

The development of an effective sensor would greatly contribute towards reducing instances of antimicrobial resistance (AMR). This particular body of work has established the feasibility of utilising additive manufacturing techniques to produce the early iterations of such a device. Our initial batch of electrodes, which were printed using a PEGDA-MWCNT composite, demonstrated effective PyoC detection across a clinically relevant range. In moving away from the use of MWCNTs towards an

elementary CB study, it was also proven that CB has potential as a conductive additive regarding photopolymerisable resins. Currently, 3D printed conductive elements tend to be fabricated using extraction techniques. It follows that any number of conductive elements may be explored for this purpose, potentially broadening digital light processing (DLP) applications to a great extent.

Future work

Beyond this work, there are countless ways in which the device can be developed and improved. Sensor design was explored to an extent, but it would be beneficial to spend time optimising the size and geometry of each electrode. This would involve printing the working electrode (WE) and CE in isolation, for testing with commercial electrodes, and selecting which designs result in the highest sensitivity. Another important aspect would be introducing a pseudoreference, by adding Ag paint to a conductive track. This would render the device wholly self-contained and would eliminate the need for costly commercial electrodes. The testing process could be further simplified by utilising a recessed design, which would allow for minimal sample volumes to be deposited onto the electrodes. In circumventing the need to use a glass cell, this would prove to be a significant step towards a truly point-of-care device, as would introducing the use of a handheld potentiostat. Devices such as SimpleStat could be used in conjunction with our electrode chip to test samples rapidly within a clinical environment, an essential step towards early detection of nosocomial infection.

Another valuable area of research would involve expanding our repertoire of photopolymerisable printing resins. The simple nature of DLP would enable rapid prototyping, and thus testing, of electrodes, to determine which conductive additives

elicit the most desirable electrode characteristics. Combinations of different additives could also be explored, and their ratios varied, to further optimise the resin. Different conductive resins could be layered on top of one another, allowing for facile 'surface modification' of one resin with another. Investigating how these materials interact with each other could benefit future sensor designs.

Though this study focussed on detecting *P. aeruginosa* via PyoC, the sensing platform could be adapted to enable the detection of a range of pathogens, provided their electrochemical detection windows do not overlap. The ability to detect two or more prominent nosocomial pathogens at a time would be invaluable in terms of saving time and money and limiting the sample volumes required from patients. Sensitive testing would enable early infection diagnosis, with early prompt treatment reducing the length of hospital stays for patients. Another valuable use for the sensing platform would be to monitor the response of a pathogen to treatment, again providing that their detection windows are discrete. In this sense, electrode chips could also facilitate large scale drug studies. However, it should be noted that widespread use of 3D printed sensing platforms would require extensive research into scalability, with manufacturing methods being revised for mass production. From here, there are any number of further modifications that could be made to the electrodes, to improve their performance and/or alter their function. These include surface modification, microfluidics, the incorporation of biorecognition elements, or altering the design to create an electrode array. The study and development of facile and sensitive 3D printed electrode systems for point-of-care diagnostics would not only be invaluable for patient welfare but would also inform new additive manufacturing techniques for the development of technologies within other industries. This body of work demonstrates

the feasibility of utilising additive manufacturing methods to manufacture electrochemical sensors for the detection of analytes such as PyoC, as well as exploring the effectiveness of novel conductive printing resins and highlighting key areas for expansion.